A SURVEY OF HALO RR LYRAE STARS

Thesis by

Abhijit Saha

In Partial Fulfillment of the Requirements

for the Degree of

Doctor of Philosophy

California Institute of Technology

Pasadena, California

1984

(Submitted September 30, 1983)

To my parents

ACKNOWLEDGEMENTS

My sojourn at Caltech has been a most memorable and enriching experience. I have benefited greatly from my association with the faculty and fellow graduate students of the department, and have been inspired by the scientific dedication and integrity around me.

Bev Oke, who guided my first steps into astronomical research and also through this thesis, has always been a source of inspiration. His aid, particularly with the spectroscopic observations at the big eye, has made this thesis possible. I am indebted also for the countless valuable discussions I have had with him, which have always helped to encourage me. I take great pleasure in thanking him.

I am grateful to Jim Gunn, Robert Kraft and Allan Sandage, who were all instrumental in getting me started on this particular project. I also thank Wal Sargent and Peter Goldreich for their interest in both my work and my well-being.

Observing at Palomar has been most enjoyable. I thank the observatory staff, particularly Roger Higson and Skip Staples. In this regard, thanks are due to the late Peter Young and to Charlie Kowal who introduced me to observing. Larry Blakee must get special mention.

I owe a large debt to the CIT/JPL astronomy computing facility, and to those who have made it possible. Without it, this thesis would have been impossible. My thanks to Todd Boroson, John Biretta, Keith Horne, James Fillmore, Tim Pearson, Jeff Pier, Bill Sebok, Keith

Shortridge, John Tonry and Barbara Zimmerman for help with computer software.

I thank the department powers that be for arranging financial support during my tenure here. One of the unique features of this department has been the free reign given to graduate students, where they are left alone to pursue their projects independently. I greatly value having had this opportunity, and hope that this marvelous tradition will continue.

It is difficult to encapsulate one's appreciation of the fellow denizen's of Robinson's underground (fellow graduate students, post-docs, some Santa Barbarians, and others). Every one of them has been unique in his own way, and I treasure my cameraderie with them. Special mention must be made of Graham Berriman, Todd Boroson, Alex Filippenko, Richard Gomer, Fred Harris, John Hoessel, Keith Horne, David Hough, Matthew Malkan, Dave Monet, Georg Pauls, Alain Porter, Russell Redman, Mike Rich, Raghvendra Sahai, Don Schneider, Bill Sebok, Richard Simon and Richard Wade. Their companionship has been memorable, and I look forward to continuing my association with them.

ABSTRACT

A survey of RR Lyrae stars has been conducted in selected regions of the Galactic halo, using the 48 inch Schmidt telescope at Palomar. 29 RR Lyrae stars were found in three fields (each is 42 square degrees) centered at $l = 180^{\circ}$, $b = 24^{\circ}$; $l = 180^{\circ}$, $b = 30^{\circ}$ and $l = 110^{\circ}$, $b = -30^{\circ}$. The faint limit for finding RR Lyraes is $19^{m}.5$ in B, and the faintest RR Lyrae stars that were found are at Galactocentric distances of over 40 kpc. The majority of the stars are 20 to 30 kpc from the Galactic center, and typically around 18^{m} in B. Apart from a very few globular clusters, these stars are the most distant known probes of the outer halo.

Photoelectric photometry done with the 60 inch telescope at Palomar has been used to obtain accurate light curves and ephemerides for all the survey RR Lyraes stars. Spectrophotometry at minimum light has been used to estimate reddening and interstellar extinction. Distances to the individual RR Lyrae stars have been derived using the information thus obtained.

The space densities of RR Lyrae stars has been traced out to a Galactocentric distance R of 33 kpc. The data are combined with that obtained by others in the Galactic bulge and in the relatively nearby halo, which gives an overall picture of the run of space densities over a very wide range of R.

Spectra of many of these objects have been taken with the double spectrograph on the 200 inch telescope at Palomar. Chemical abundances and radial velocities have been derived from them. Center of mass velocities have typically been obtained to an accuracy of 35 km s^{-1}.

There is no discernible abundance gradient in the halo from 10 to 40 kpc, but there is a very wide range of abundances. Two RR Lyrae stars have been found which have metallicities that are unprecedentedly high ([Fe/H] ~ -0.5]) for this region of the halo. If the results are confirmed, this will imply that there is a sizeable population of moderately metal rich stars in the outer halo.

From the radial velocities, the systemic and random motions of the system of RR Lyrae stars in the distant halo have been studied. The velocity dispersion along the axis that points to the Galactic center is found to be 105 ± 17 km s^{-1}. The mass of the Galaxy within 25 kpc has been estimated at 3.9 (+3.4 or -2.2) x $10^{11} M_{\odot}$, assuming isotropic orbits and spherical potential at 25 kpc. This confirms that the Galactic mass continues to increase out to 25 kpc.

TABLE OF CONTENTS

INTRODUCTION

The question of how galaxies formed and evolved is among the foremost problems that challenge modern astronomy. From our severely constrained perspective of the universe, we are left with the task of picking out those clues which will tell us exactly what galaxies are and how they have come to be. We are still at the stage where we have a very limited data base, and each new discovery leads to more questions than to answers. Even so, our knowledge of our own and of other galaxies has grown by leaps and bounds in the last two decades.

In a galaxy such as ours, the disk is the most striking feature. Most of the stars are to be found here. Halos, in comparison are faint, and at first sight seemingly uninteresting. However, there is mounting evidence to show that a large fraction of a galaxy's total mass resides in the halo. It is therefore necessary to develop a proper understanding of halos, for it is likely that some of the clues we seek are hidden here.

Rotation curves of our own and of other disk galaxies are seen to remain flat out to tens of kpc from the center (Rubin et. al. 1980), indicating that the mass distribution in galaxies extends beyond their detectable luminous boundaries. In elliptical and spherical galaxies the same conclusion is drawn from the observed run of velocity dispersions, which remain flat with increasing galactocentric distance. The masses derived from the velocities of binary galaxies

around each other point in the same direction, i.e. that galaxies are larger in extent and more massive than we had previously believed.

Clearly then, a more detailed look at the halos of galaxies is warranted. In particular we would like to know more about the kinds of stars that populate this realm; about their age, abundance, and kinematical properties. The low luminosities of the halos of other galaxies thwarts our attempts to study them. Our location in the disk hinders the study of our own Galaxy: we are surrounded by disk stars, which far outnumber the halo stars that we can see in any direction of the sky to any given limiting magnitude. Globular clusters are members of the halo, and they have been used as probes (Hartwick and Sargent 1978, Searle and Zinn 1978). However, the number of such clusters is limited, and they are not necessarily representatives of field halo stars. High velocity subdwarfs, which are field halo stars, have told us much of what we know about this region of the Galaxy (Eggen, Lynden Bell and Sandage 1962), but these are all stars that are close to the sun, and hence limited to a small region in the proximity of the disk. We would prefer to study halo stars "in situ", i.e. several kpc away from the disk.

We would like to pick out faint but intrinsically bright objects along appropriate directions in order to probe the distant halo. The red giants would be the ideal objects, but distinguishing distant red giants from the plethora of nearby red dwarfs requires moderate dispersion spectroscopy, and the observation time required is preposterously large. Multi-color surveys to pick out blue early type

stars are contaminated by nearby subdwarfs and white dwarfs. Objective prism surveys do remove the ambiguities in searches for blue stars and have been used: Pier (1982) has studied A and B type stars obtained from an objective prism survey by Preston and Shectman (1979). The drawback with objective prism surveys is that they do not go faint enough.

RR Lyrae stars have proved to be very valuable probes of the Galactic halo. They are horizontal branch stars, not as bright as the giants, but readily detectable from their characteristic light variation, and are perhaps the best calibrated distance indicators. The kinematics of the brighter field RR Lyrae stars, many of which are members of the halo, have been studied by Woolley (1978). The Lick Astrograph survey (Kinman et. al. 1982 and references therein) has made major headway in identifying faint RR Lyrae stars in several selected regions of the Galaxy, down to 18^m in B. Butler et. al. (1982) (and references therein) have investigated the abundance distribution in the halo as gleaned from the spectroscopy of these stars. It is only recently that it has become possible to measure radial velocities of RR Lyrae stars as faint as 19^m with sufficient accuracy to study their kinematics.

This thesis is an attempt to push the search for RR Lyrae stars to yet fainter magnitudes, and hence to regions even farther out in the halo. Use of the Palomar 48 inch Schmidt telescope and of newer, more suitable photographic emulsions has made this possible. This survey can find RR Lyrae stars out to 50 kpc from the Galactic center,

twice the distance reached by the Lick Astrograph survey. Using these stars we are able to probe the extent, abundance content, and kinematical properties (and hence the mass distribution) of the distant halo.

The thesis is divided into five chapters. Chapter 1 deals with the plate material of the survey and the techniques used for discovering RR Lyrae and other short period variable stars. The selection effects inherent in the survey are examined. Chapter 2 describes the photometric measurements, derivation of periods, and construction of light curves for the variable stars found in this survey. Chapter 3 discusses the spectroscopy and spectrophotometry of the RR Lyrae stars thus found, from which chemical abundances, radial velocities and interstellar extinctions are derived. Chapter 4 examines the space distribution of RR Lyrae stars as a function of position in the Galaxy. Abundance distribution as inferred from this sample of stars is also discussed. The kinematics of the RR Lyrae stars is analysed in Chapter 5, and the mass of the Galaxy within 25 kpc is obtained. The implications of these results with regard to the nature and extent of the halo are discussed. The final concluding section summarizes the results from this survey.

REFERENCES

Butler, D., Kemper, E., Kraft, R. P., and Sumtzeff, N. B. 1982, A.J. 87, 353.

Eggen, O. J., Lynden Bell, D., and Sandage, A. R. 1962, Ap.J, 136, 748.

Hartwick, F. D. A., and Sargent, W. L. W. 1978, Ap.J, 221, 512.

Kinman, T. D., Mahaffey, C. T., and Wirtanen, C. A. (1982). A. J., 87, 314.

Pier, J. R. (1982). Ph. D. Thesis, California Institute of Technology

Preston, G. W., and Shectman, S. A. 1979, Annual Report of the Director, Hale Observatories, (Carnegie Institute of Washington, Washington, D.C.)

Rubin, V., Ford, W. K., and Thonnard, N. 1980, Ap.J., 238, 471.

Searle, L., and Zinn, R. 1978, Ap.J., 225, 357.

Woolley, R. 1978, M.N.R.A.S., 184, 311.

CHAPTER 1

DETECTION OF SHORT PERIOD VARIABLE STARS

1.1 OBSERVATIONS

The plates for the survey were taken with the 48-inch Schmidt telescope at Palomar mountain. 14"X14" plates with Kodak IIIaJ emulsion were used with a Kodak Wratten 4 filter. This combination allows a bandpass from 4600Å to 5400Å, and corresponds to the 'g' filter in the Thuan and Gunn (1976) photometric system. Since this passband is in a region where there are no significant night sky emission lines, and since the emulsion has fine grain and high contrast, the deepest plates are possible with this combination. Each plate covers an area of approximately 6.6°x6.6°. There is no vignetting within the central 12 inch diameter circle on the plate.

The plates were sensitized by baking them in Forming gas at 65°C for 2 to 2.5 hours (depending on the batch), and after exposure, were processed for 5 minutes in Kodak D-19 developer at 19°C. The time required for a sky limited exposure with a Wratten 4 filter is then about 2.5 hours, and when the seeing is 3 arc-seconds or better, stellar images to 22^{m} can be detected.

For the purposes of the survey, a faint limit of 20^{m} was considered adequate. Four separate 30 min. exposures of any particular field were taken on the same plate, and the telescope was moved about 12 arc-seconds between exposures. In this way, for every star in the field, there are 4 identical images on the plate arranged in a line. As long as the average spacing between objects in the field is not smaller than half a minute of arc, there is no difficulty in identifying separate sets of four images that all belong to the

same star. The time between successive exposures was typically 1.5 to 2 hours. It is possible to remove the plate-holder from the telescope and re-insert it without appreciable change in the positioning of the plate, provided the plate itself is not removed from the plate-holder. Thus while waiting for the 1.5 to 2 hours to elapse between successive exposures on the same plate, it was possible to take out the plate-holder, and expose plates of other fields by using different plate-holders for each plate. It was possible, through this cycle, to obtain 4-image plates for 3 different fields on the same night, thus making maximum use of the telescope.

This multiple-image technique emulates the methods described by Kinman (1972). Its advantage is in reducing the labor involved in manually comparing different exposures, as well as in cutting down the cost of plate material used by a factor of four (in this case). When a plate is scanned, the four images of each star are compared to check for variability. In scanning one plate, six pairs of images are compared, as opposed to one pair when two single image plates are blinked. Although the blink process is more efficient and easier to perform manually, this factor of six gain appreciably reduces the total labor performed.

Table 1.1 is the list of fields for which plates were taken.

1.2 DETECTION OF VARIABLE STARS

The plates described above were scanned by eye. The faint limit on the plates is approximately 20^m. Due to the high contrast of IIIaJ emulsions, the images are saturated at about 16.5^m. Small differences in magnitude are more easily recognized when the images are unsaturated. For brighter objects, where the images are saturated, brightness is judged by the size of the image rather than by the density, and so the sensitivity to a change in brightness is poorer in this domain. A change of 0.3^m can be readily detected (by visual inspection) for objects between 16.5^m and 19.5^m, but for objects brighter than 16.5^m, the change must be much larger before it can be detected with confidence. The discussions regarding completeness of the survey will be restricted to the magnitude interval 16.5^m to 19.5^m. Some variable objects were found at brighter magnitudes, and if so they were noted. At these bright magnitudes, only objects with appreciably higher amplitudes of light variation could be found, and the selection effects are very complicated.

Several plates of each field were scanned. Work has been completed for fields FII, FIII and FIV (see Table 1.1). From the way the plates were taken and images compared, only objects whose brightnesses change over durations of a few hours would be detected. Thus only objects with periods of a day or smaller were expected. In each of the above fields about 30 variable stars were found, but it was not immediately known which were RR Lyrae stars, and which were other types of short period variables. To be able to make this

distinction, it is necessary to obtain light curves for the objects.

An obvious approach is to photoelectrically measure and define standard stars in each field, and then use these to calibrate iris-photometer measurements made on the plate and thus measure magnitudes of the variable stars. However, severe difficulties were encountered in attempting such measurements. The Schmidt telescope makes images at f/2.5. Even slight errors in positioning the plates (due to defects in the plate-holder, inaccuracy in focussing, etc.) means that images in one part of the plate are focussed slightly differently from those in another part of the same plate. Since the resulting image characteristics are quite different in different parts of the field, and since the plate response is of course non-linear, the iris-photometry calibrations change from one section of the plate to another. Ironically, this effect is more pronounced on finer grain emulsions which resolve the change in image contours, than on coarser grain emulsions that do not "see" this effect. The non-uniformity of the IIIaJ emulsion over the entire plate surface is another likely contributor to the calibration errors. Within the unvignetted region of the plate, only a region with a 2 inch radius can be calibrated, and a different set of standards is required for each such section of the plate.

Since the aim was to separate the RR Lyrae stars from the rest, it was realized that the periods and light-curve asymmetry can be obtained without tying to a magnitude scale. About 10 stars around each variable star were chosen so that their magnitudes span the range

of variability of the object under study, and the brightness of the variable could be placed relative to these surrounding stars. These arbitrary "magnitude" measurements could then be used to derive periods using the technique of Lafler and Kinman (1965).

The pseudo light curves so obtained, do contain the period and asymmetry information. Light curves that showed asymmetry were immediately spotted as pulsating variables (all type ab RR Lyrae stars are asymmetric), and were picked out for further study with photoelectric techniques. Those that showed two unequal "dips" and symmetric light curves were identified as eclipsing variables. It is not possible to distinguish between c-type RR Lyraes and eclipsing stars which have only one discernible eclipse (or two equal eclipses), except when the periods are too short or too long for them to be RR Lyrae stars. These ambiguous cases were also selected for further study.

1.3 COMPLETENESS OF THE SAMPLE

In a survey of this kind, it is very important to pay close attention to selection effects and incompleteness. In the present case there are mainly three factors that produce incompleteness in the sample. They are discussed one by one.

Firstly, there are limitations due to the "dynamic range" of the detector. As mentioned before, a change of 0.3^m can be detected if the object lies in the magnitude interval 16.5 to 19.5 during at least one of the observed pnases. This discussion will be restricted to objects that have amplitudes $\geq 0.4^m$ and lie, during some part of their light cycle, in the above stated magnitude interval. The amplitude criterion is sufficient to include RR Lyrae stars of all Bailey types.

The second factor will be called "detectability". The procedure followed in scanning the plates, as described in the preceding section, effectively checks for objects that have changed in brightness over a few hours. Objects that have periods less than 90 minutes fall out of the scope of this discussion. An object which does not change by at least 0.3^m during any 6 hour interval (or less) is also outside the domain of this discussion. Thus Cepheids and other relatively longer period variables are excluded, but RR Lyrae stars and many short period binary stars fall within the purview of the following analysis. Although RR Lyrae stars have periods of up to 0.8 days, there is always a section of their light curve, particularly during the rapid rise to maximum light, which satisfies the last criterion. Similarly, objects with eclipses that are at least 0.3^m deep and have durations shorter than 12 hours, are included in this analysis. Without any loss of generality, we can, for the present discussion, assign the phase "ϕ" at which this criterion of rapid change of intensity is satisfied, to be equal to zero. If the first and last images on any given plate were taken at times t and t' respectively, then an object that passed through $\phi=0$ between t and t'

is expected to be "detectable" on that plate. There are periodicities associated with the plate observations: chiefly the night to night period of one day and the lunation period of one month. By working according to a pre-determined schedule, some of the effects of these can be minimized. However, even the best laid plans are subject to the interference of weather conditions.

Thirdly, there are the human errors associated with the plate scanning itself. These are the hardest to describe objectively, but an ex post facto analysis is given below. From this analysis, it is possible to derive the "efficiency" of the scanning. The efficiency index η measures the fraction of objects that were detected on any given plate, as opposed to the number of "detectable" objects on that plate. η is estimated by cross comparing the results of scanning several plates of the same field and the derivation is as follows.

Let N_i be the number of detectable objects on the i^{th} plate of any field. Let n_i be the number of objects actually detected in that field. Let β_{ij} be the scanning efficiency that will be derived for plate i by comparing against plate j of the same field. We then have:

$$n_i = \beta_{ij} N_i \tag{1.1}$$

Let n_{ij} denote the number of objects detected on both plates i and j, and let $n_{i\bar{j}}$ denote the number of objects found on plate i but not on plate j. Thus:

$$n_{ij} = \beta_{ij}\beta_{ji}N_{ij},$$

where N_{ij} is the number of objects that are detectable on both plates.

Also, $n_{i\bar{j}} = \beta_{ij}(1-\beta_{ji})N_{ij}$

and $n_{j\bar{i}} = \beta_{ji}(1-\beta_{ij})N_{ij}$ (1.2)

It follows that

$$\beta_{ij} = n_{ij}/(n_{j\bar{i}} + n_{ij}) \quad (1.3)$$

The various plates of each field were compared after scanning to find the quantities n_{ij} and $n_{i\bar{j}}$ for all i and j, and the β_{ij}'s were calculated according to equation 1.3. The final adopted value η_i for the efficiency with which the ith plate was scanned was taken to be the weighted (by n_{ij}) average (over j) of β_{ij}:

$$\eta_i = \frac{1}{M}\sum_j n_{ij}\beta_{ij} \quad (1.4)$$

where $M = \sum_j n_{ij}$

and where $i \neq j$. Table 1.2 shows the values of η_i's that were found for the plates of the 3 different fields.

It was stated earlier that an object is considered to be "detectable" if it passes through phase $\phi=0$ during the time spanned by the four exposures on that plate. Consider an object with period P which has $\phi=\phi_0$ at some fiducial time (before any plates were taken) t=0. Consider a plate on which the first exposure was at time t_1 and the last exposure was at time t_2. According to the stipulated criterion, the object is detectable on the plate if there is some t such that

$$t_1 \leq t \leq t_2$$
$$\text{and} \quad t = (K-\phi_0)P$$
$$\text{(where K is an integer)} \tag{1.5}$$

By testing if the criterion in equation 1.5 is satisfied, it can be determined if an object with period P and initial phase ϕ_0 is detectable on a given plate. For a given period P and initial phase ϕ_0, define

$$\rho_i = \eta_i \qquad \text{if the object is detectable, and}$$
$$\rho_i = 0.0 \qquad \text{if not detectable} \tag{1.6}$$

The probability that this object is not detected on any of the N plates is then given by

$$\bar{p}(P,\phi_0) = \prod_{i=1}^{N} (1-\rho_i) \tag{1.7}$$

where $p(P,\phi_0)$ is the probability of finding an object with period P and initial phase ϕ_0 By assuming that all values of ϕ_0 (between 0 and 1) are equally likely, the probability p(P) with which an object with period P is detected on the N plate can be calculated as follows :

$$p(P) = \int [1-\bar{p}(P,\phi_0)]d\phi_0 \qquad (1.8)$$

The calculations pertaining to equations 1.5 to 1.8 were performed numerically.

Fig. 1.1(a) is a plot of p(P) vs. P for a plate that spans 6 hours on one night, and where η has been taken to be 0.8. Fig. 1.1(b) shows the improved probability of discovery when two such plates taken on adjacent nights are considered. Fig. 1.1(c) is a plot of the same where plates from 6 consecutive nights are taken together. Note how the selection effects due to periodicity in the period range of the RR Lyrae stars is reduced as the number of nights is increased. Note also the difficulty of detecting variables with periods at or around one-third day, half a day, two-thirds of a day, etc. Fig. 1.2 illustrates the discovery probabilities for the plates that were actually examined. Results for each of the 3 fields studied are shown. These plots show more rapid variation with P because the plates were not taken on consecutive nights (because weather or seeing conditions would not permit). The larger the number of days that elapse between successive observations, the more "grassy" the plot appears.

This method of a posteriori analysis is the most realistic representation of selection effects arising from periodicity in the data.

1.4 COORDINATE MEASUREMENT

To ascertain the coordinates of the variables that were detected, X and Y positions of the objects were found using the comparator ("X-Y machine") at the offices of the Mt. Wilson and Las Campanas Observatories. Position standards were chosen from the SAO catalogue. Existing computer software were used to perform the necessary calculations. The positions of all the stars for which photometric light curves have been obtained are listed in Table 1.3, and the corresponding finding charts are in Fig. 1.3.

REFERENCES

Kinman, T. D. 1972, Q.J.R.A.S. 13, 258

Lafler, J., and Kinman, T. D. 1965, Ap.J. Supp. 11, 216

Thuan, T. X., and Gunn, J. E. 1976, Pub.A.S.P. 88, 543

TABLE 1.1

Positions of Field Centers

Field Name	Guide Star Coordinates (1950) (Plate center) α h m s	δ ° ′ ″	Galactic Coordinates l (degrees)	b (degrees)
FI	6 57 24.1	37 11 59	179.7	17.7
FII	7 28 32.2	39 0 11	180.0	24.1
FIII	7 58 24.9	40 17 6	180.2	30.0
FIV	23 56 15.9	32 6 13	110.2	-29.2
FV	9 48 50.7	-13 29 32	250.3	30.2
FVI	3 56 55.9	10 11 23	180.1	-31.0
FVII	8 31 43.7	41 54 34	179.5	36.4

TABLE 1.2

Plates Scanned

Field	Plate No.	Julian Date of 1st exposure	Julian Date of last exposure	Scanning efficiency 'η'
	1	2444258.697	2444258.870	0.71
	2	2444260.647	2444260.801	0.71
	3	2444261.782	2444261.887	0.77
FII	4	2444582.808	2444582.961	0.81
	5	2444583.911	2444583.935	0.81
	6	2444639.652	2444639.934	0.72
	7	2444992.646	2444992.949	0.74
	1	2444639.681	2444639.959	0.84
FIII	2	2444640.676	2444640.966	0.84
	3	2444947.830	2444948.035	0.77
	1	2444582.613	2444582.779	0.70
	2	2444910.629	2444910.849	0.86
FIV	3	2445200.752	2445200.979	0.65
	4	2445199.796	2445199.980	0.79

TABLE 1.3

Coordinates of Variable Stars

FIELD II (Epoch 1950.0)

OBJECT	α h ′ ″	δ ° ′ ″	OBJECT	α h m s	δ ° ′ ″
II V1	07 41 53.1	+40 38 05	II V2	07 31 04.4	+40 43 31
II V3	07 37 22.1	+39 25 51	II V4	07 23 44.7	+38 54 15
II V5	07 13 23.3	+38 38 56	II V6	07 26 48.0	+38 28 11
II V104	07 28 28.5	+39 14 11	II V208	07 32 14.4	+39 22 07
II V303	07 28 06.5	+40 11 34	II V306	07 23 41.0	+36 44 51
II V401	07 42 16.0	+40 29 51	II V407	07 14 44.2	+40 36 41
II V501	07 41 23.7	+40 19 59	II V502	07 37 06.0	+41 18 36
II V504	07 22 45.5	+40 58 53	II V601	07 22 33.1	+38 18 59

FIELD III (Epoch 1950.0)

OBJECT	α h ′ ″	δ ° ′ ″	OBJECT	α h m s	δ ° ′ ″
III V101	08 00 13.1	+42 39 15	III V102	07 53 55.7	+43 20 34
III V103	07 56 25.0	+39 24 44	III V201	07 47 02.1	+37 49 37
III V202	07 50 41.0	+42 56 59	III V203	07 46 08.4	+41 50 32
III V204	07 51 20.8	+39 02 15	III V206	08 06 11.4	+42 42 23
III V208	07 57 06.2	+40 47 42	III V302	08 01 09.7	+42 37 34

FIELD IV (Epoch 1950.0)

OBJECT	α h ′ ″	δ ° ′ ″	OBJECT	α h m s	δ ° ′ ″
IV V101	00 05 58.4	+29 08 58	IV V103	23 59 41.3	+29 47 55
IV V104	23 53 12.2	+28 53 11	IV V105	23 42 06.2	+29 53 31
IV V106	23 44 25.7	+29 34 23	IV V107	23 54 13.6	+31 23 40
IV V108	00 04 23.5	+31 45 26	IV V122	00 08 04.0	+33 50 16
IV V201	00 04 21.3	+31 11 17	IV V301	00 08 57.3	+30 34 42
IV V401	00 03 33.0	+29 02 12			

FIGURE CAPTIONS

Fig. 1.1

The diagrams show the probability of discovery (assuming a scanning efficiency of 0.8 for each plate) as a function of period. 1(a) shows the result of scanning a single plate where the four exposures span a total time interval of six hours on one night. 1(b) shows the result when two such plates from two consecutive nights (i.e. 24 hours apart) are scanned, and 1(c) shows the result of scanning six such plates taken on six consecutive nights.

Fig. 1.2

These plots show the probability of discovery as a function of period in the three fields that were scanned. The actual times of exposure have been used to estimate the probabilities according to the arguments given in section 3.

Fig. 1.3

Finding charts for the variable stars listed in Table 1.3. North is up and East is to the left. The scale is approximately 13" per mm.

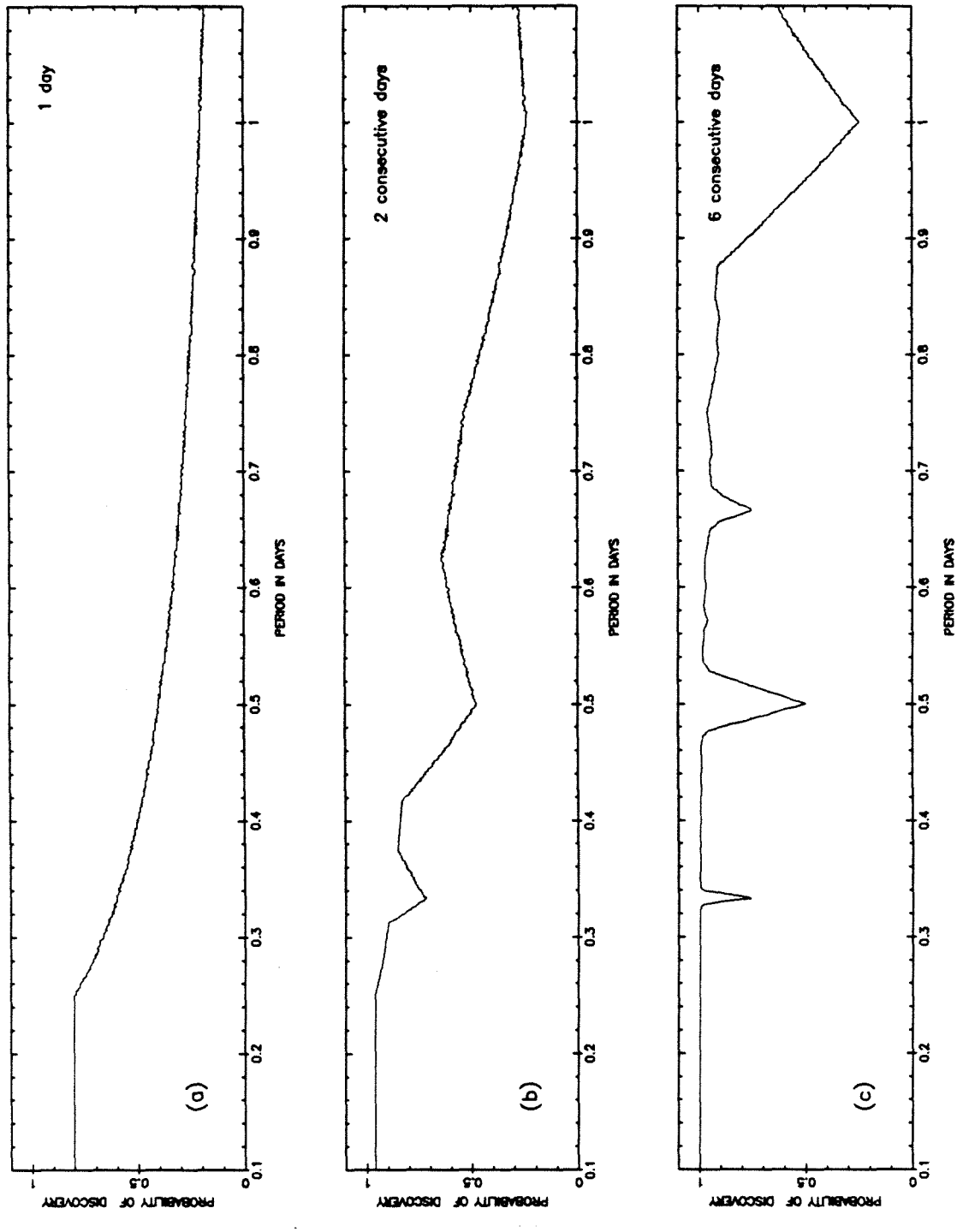
1 day
(a)
2 consecutive days
(b)
6 consecutive days
(c)
PROBABILITY OF DISCOVERY
PERIOD IN DAYS
0
0.5
1
0.1
0.2
0.3
0.4
0.5
0.6
0.7
0.8
0.9
1

Fig. 1.1

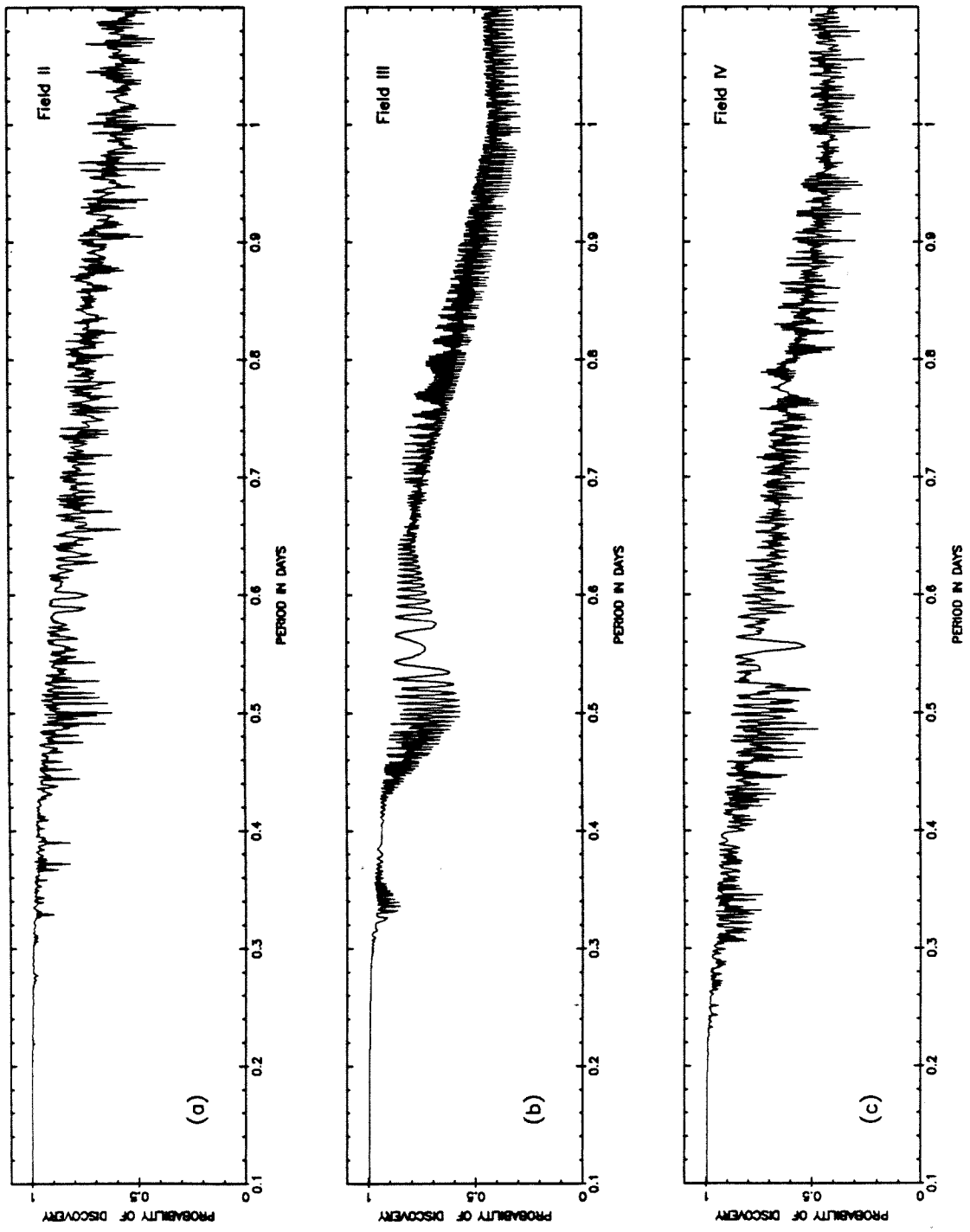
Field II
(a)
Field III
(b)
Field IV
(c)
PROBABILITY OF DISCOVERY
PERIOD IN DAYS
0
0.1
0.2
0.3
0.4
0.5
0.6
0.7
0.8
0.9
1
0.5

Fig. 1.2

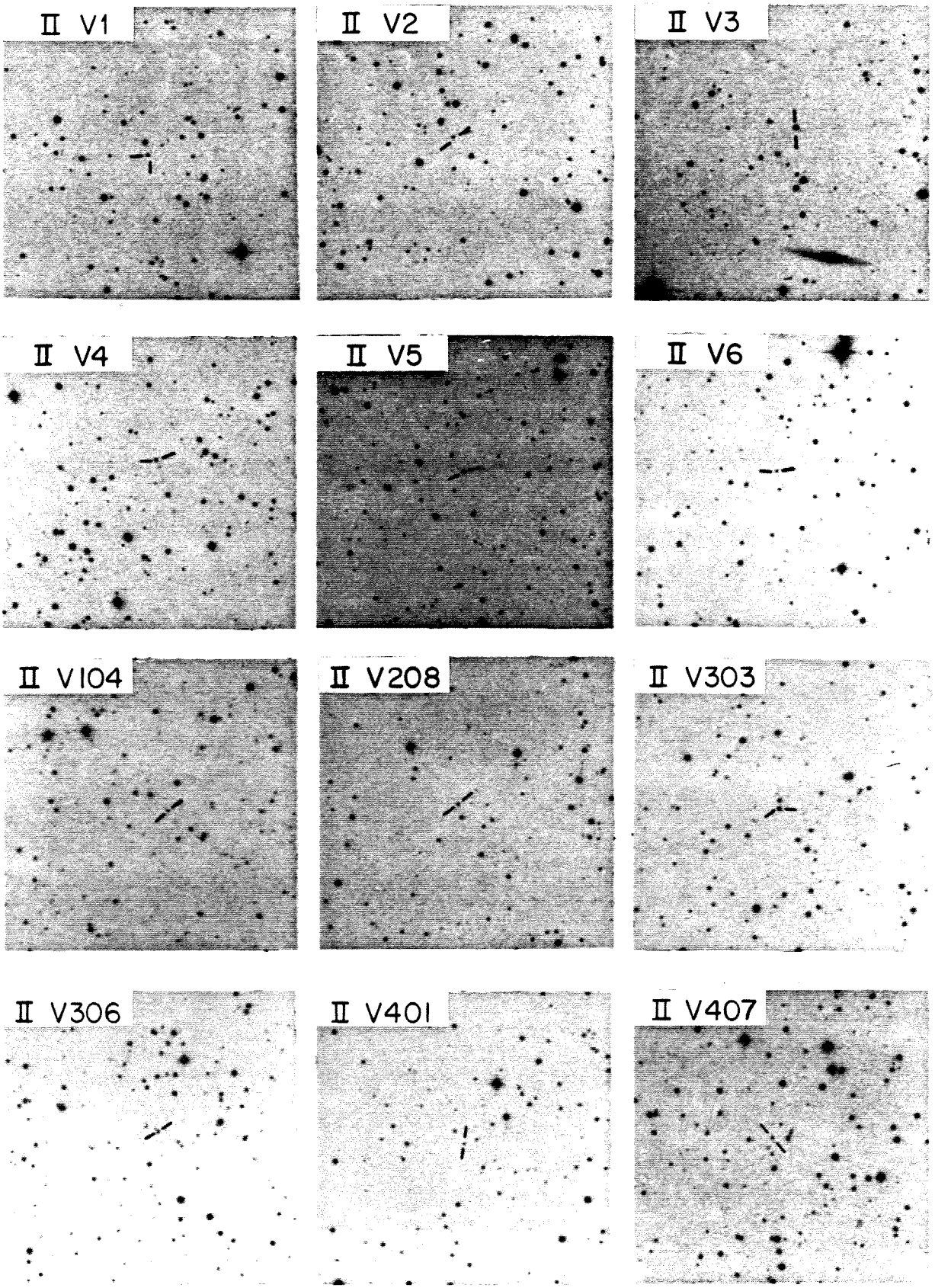
II V1
II V2
II V3
II V4
II V5
II V6
II V104
II V208
II V303
II V306
II V401
II V407

Fig. 1.3

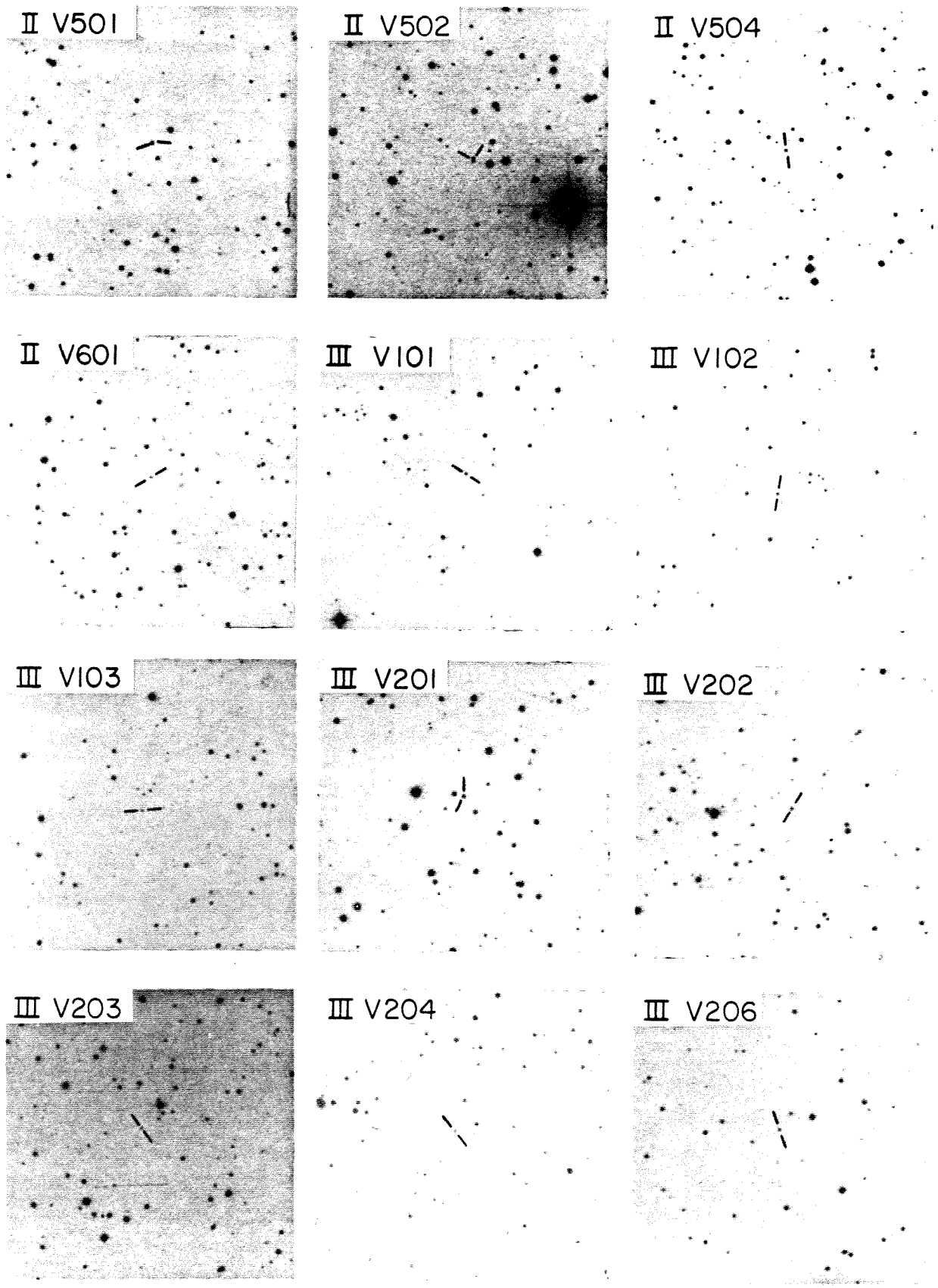
II V501
II V502
II V504
II V601
III V101
III V102
III V103
III V201
III V202
III V203
III V204
III V206

Fig. 1.3 contd.

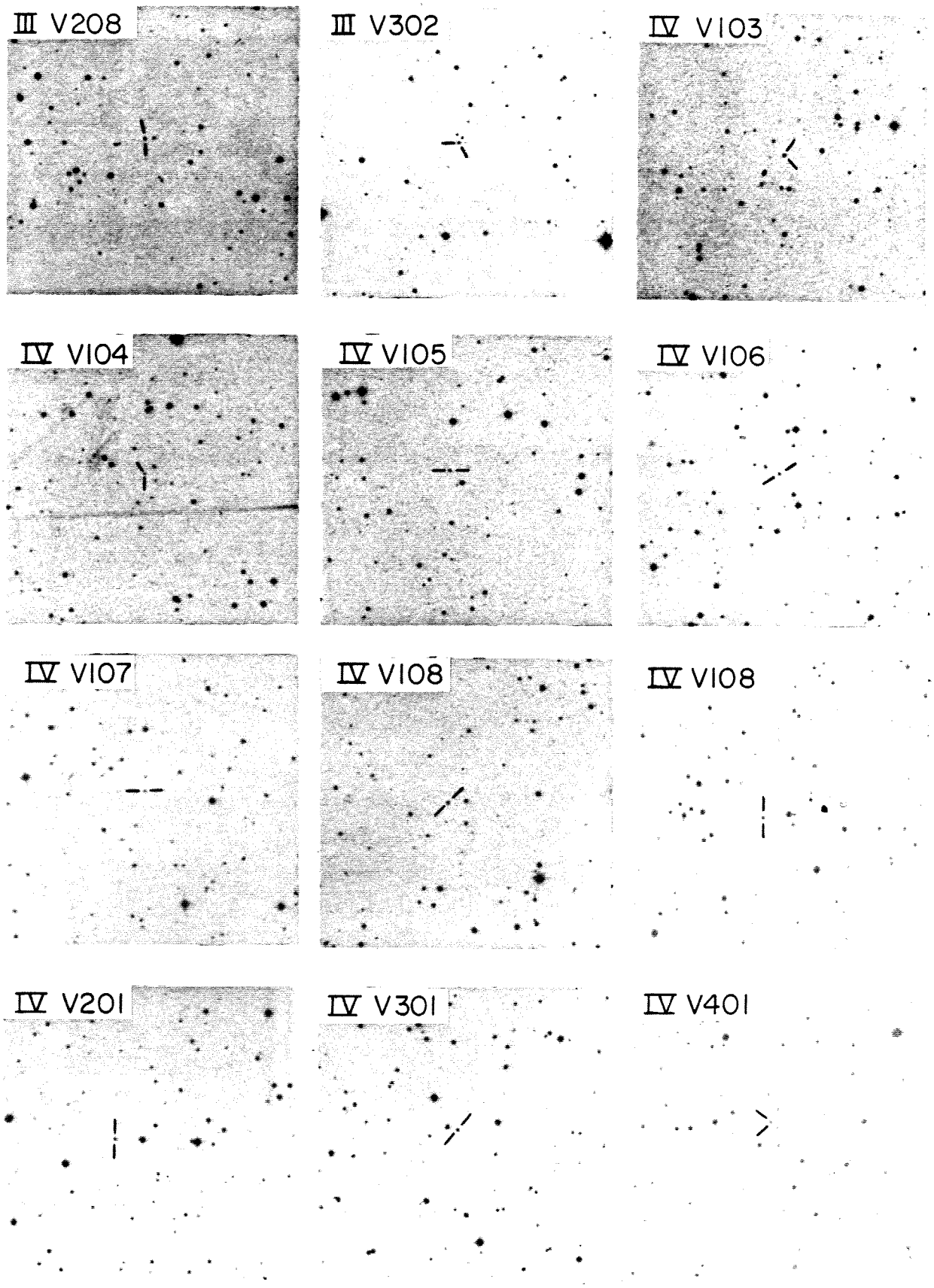
III V208
III V302
IV V103
IV V104
IV V105
IV V106
IV V107
IV V108
IV V108
IV V201
IV V301
IV V401

Fig. 1.3 contd.

CHAPTER 2

PHOTOMETRY OF RR LYRAE CANDIDATES AND PERIOD DETERMINATION

2.1 OBSERVATIONS

Photoelectric photometry of the variable stars that are listed in Table 1.3 (Chapter 1) was done with the SIT Vidicon direct camera at the Cassegrain focus of the 60" telescope at Palomar mountain. The purpose was to obtain reliable light curves in 'B' for the RR Lyrae stars. The light curves so obtained are then compatible with the available literature on other RR Lyrae stars, both in the field and in globular clusters. Also, light curves obtained from photoelectric photometry help to discriminate between W UMa stars and the c-type RR Lyrae stars, and all the doubtful cases could be tested in this way.

There are distinct advantages in using an area photometer over a one or two channel photometer when measuring faint stars. At 18th and 19th magnitude, sky subtraction must be done very accurately. If the object being measured has magnitude 'm', then the sky patch that is used for sky subtraction must not be contaminated by an object brighter than 'm+5' if systematic errors are to be kept to within a few percent. This means that the observer must be able to see several magnitudes fainter than the object under study. Since crowding effects get progressively worse as one goes fainter, this problem merits greater attention at the faint magnitudes involved here. By the time a SIT camera picture is well enough exposed to get good photon statistics on the object, it is possible to detect objects several magnitudes fainter, so that they can be avoided when choosing a suitable sky patch. Secondly, with an area photometer it is

possible to do 'differential photometry' i.e. a star adjacent to the object of interest, which lies in the field of the camera (in this case a 3'x3' field) can be used as a comparison standard. The error in a single measurement of an object when calibrated against a standard star in another part of the sky, is much larger than the error incurred in comparing two objects adjacent to each other which are measured simultaneously. Of course, the comparison object in the field has to be calibrated against a suitable standard to make the zero point adjustment, but here we take the average of several observations, which decreases the random errors. For constructing light curves, where each individual observation is to be used as a data point, the scatter is considerably reduced by using such a technique. Further, at the time that the project was begun, there was no available TV viewer, so that acquiring the faint objects on an aperture of a conventional photometer was impossible, to say nothing of choosing an appropriate sky patch for sky subtraction.

The SIT tube or the camera has an S20 photocathode. However, the construction of the SIT camera precludes the use of liquid $CuSO_4$ cells, so the standard 'B' filter described by Sandage and Smith (1963) could not be used. A modified 'B' filter, using Schott BG38 as the red leak eliminating element was specially constructed. The thicknesses of the other elements, namely Schott BG12 and GG385 were also altered to compensate for the response changes that the BG38 introduces within the passband. The filter has 1mm BG12, 2mm GG385, and 3mm BG38.

Whenever possible, observations were made so that the comparison object for differential photometry was in the same picture as the object. In the few cases where this was not possible, the closest feasible local comparison object was exposed either immediately before or after the object. The photometric standards of Thuan and Gunn (1976) were observed on the nights when photometric conditions were pristine, so that the local comparison standards (LCS) could be calibrated.

2.2 REDUCTION

The pictures obtained in this way were reduced using a program by W. L. Sebok to obtain instrumental magnitudes for the objects, the LCS and the photometric standards. Sky and object 'apertures' were simulated in software, and the device response was assumed to be linear. The sky 'aperture' was an annulus around the object being measured, and the object 'aperture' was a circle centred on the object. The mean or median of the pixel values in the sky 'aperture' was subtracted from every picture in the pixel; this proved to be a reasonably good sky subtraction. A yet better criterion is to adjust the sky level (by adding to or subtracting from data numbers in each pixel) until the object's 'growth curve' (i.e. the run of instrumental magnitude measured in the object aperture as a function of aperture radius) is flat for an object aperture diameter of around 20 to 30 seconds of arc. Sky subtraction was performed separately for each object being measured. Sometimes due to crowding and contamination by

neighboring objects it was not possible to follow the above prescription of choosing sky and object apertures; in these cases, what appeared to be the most feasible alternatives were used.

It was found that the pixel to pixel response variations in the field of the SIT camera were very small. No change in actual response was detected over the field of the camera down to the 3 percent level. On the other hand, the pin-cushion distortion of the field is quite large, i.e. a pixel at an edge of the picture sees a smaller solid angle of the sky than a pixel near the centre of the field. Thus the point spread profile of a star image is wider at the edge of the field than at the centre, but the total number of counts of two equally bright stars is the same in the two places. This means that a conventional 'flat field' (an exposure of a uniformly illuminated surface viz. the top of the dome) cannot be used to flatten the field when doing stellar photometry, because such a process would make the stars at the edge of the field appear brighter than the stars in the middle.

By repeatedly exposing a 15^m test star all over the field, it was found that instrumental magnitudes for this object could be reproduced to within 3 percent without using a flat field correction, and that there was no correlation of the instrumental magnitudes obtained in this manner with position in the field. When the fields were flattened in the standard manner, however, position dependent variations of up to 25 percent were seen. This proves that the non-flatness of the field is primarily due to field distortion and

that the effects due to response variations are negligible. In the light of this test, it was decided not to apply any flat field 'corrections'. This means though, that sky gradients (since sky is a uniform surface brightness source) that appear due to the pin-cushion distortion are left uncorrected. By subtracting the sky separately around each star that is measured, it is possible to circumvent this problem.

The magnitudes of the LCS were calibrated against the Thuan and Gunn (1976) standards. The atmospheric extinction was derived for each night using observations of the standard stars at different airmasses. Color corrections were not applied, since an adequate number of observations in other colors were not possible. The error introduced by ignoring color corrections does not exceed $0^m.02$ for the airmasses at which observations were made. Once the brightness of the LCS were established, they were used to convert the magnitude differences between object and LCS to actual magnitudes for the object.

There remains the question of whether the device is truly linear as assumed in the reductions. This is particularly important since 9th and 10th magnitude standards were used to calibrate magnitudes as faint as 20. Some of the stars in and around the globular cluster M3, whose UBV magnitudes are known from Sandage (1970), were observed with the SIT camera. These test stars were chosen to as faint as $19^m.4$ in B. Repeated observations were made to keep the internal random errors in the measurement of each star to within $0^m.03$. The

mean values thus obtained agree with those given by Sandage (1970) within a standard deviation error of $0.^{m}06$ and show no systematic difference. No trend that could indicate non-linearity was found.

2.3 PERIODS AND LIGHT CURVES

Table 2.1 shows the results of the photometric measurements. The first column shows the mean time of exposure in heliocentric Julian dates (HJD), and the second column shows the 'B' magnitude measured in the way described above. The last entry for each object which shows HJD = 0.0, gives the magnitude of the local comparison star.

The observations obtained in the above manner were used to obtain periods and epochs for the variable stars. The method of Lafler and Kinman (1965) was used. In some cases it is very difficult to distinguish between the true period and an alias period because of the periodicity in the observations themselves. In such cases, the dispute could often be solved by looking at the possible periods obtained from the iris photometry of the plates (as described in Chapter 1). Despite all the care and precaution, it is not possible to guarantee that spurious periods do not occur. Only what appear to be the most likely values('best' periods), are quoted in Table 2.2. The first column of Table 2.2 lists the object name, the second column gives the best determination of its period. The third column is the accuracy to which the 'best' period was determined. The fourth

column gives the normalized value of the discriminant 'Θ' (after Lafler and Kinman (1965)). A lower value of Θ indicates a better determination of the light curve (smaller errors in photometry and/or better sampling in phase) and a greater likelihood that spurious periods have been eliminated. Although the exact interpretation of Θ as a light curve quality indicator is complicated and depends on the light curve shape itself, generally a value less than .30 is quite adequate. The fifth column gives the mean B magnitude '⟨B⟩'. If the N individual measurements of B for any object are denoted by B_i, ⟨B⟩ is given by:

$$\langle B \rangle = \log \sum_{i=1}^{N} 0.5(\phi_{i+1}-\phi_{i-1})10^{B_i} \qquad (2.1)$$

where ϕ_i is the phase of the ith observation in order of increasing ϕ, and where we set $\phi_0=\phi_N$ and $\phi_{N+1}=\phi_1$. Thus ⟨B⟩ indicates a mean flux. The sixth column of Table 2.2 gives the epoch (heliocentric Julian date) of phase zero. According to convention, for eclipsing stars the phase is zero at the time of minimum light (i.e. at the bottom of the deeper eclipse), and for pulsating stars it is at the time of maximum light. The last column indicates what type of variable the object was classified as. For eclipsing stars (E), the phase is taken to be zero at minimum light. For RR Lyrae stars, the phase is zero at maximum light.

The light curves obtained from the photometry with the SIT camera are presented in Fig. 2.1. For the RR Lyrae stars, the phase at maximum light has been set to zero. No attempt has been made to set the phase zero point for the eclipsing stars. Apart from obtaining reliable periods so that follow up spectroscopy can be done at the appropriate phase, the light curves in B make it possible to investigate these stars on the lines of Sandage et. al. (1981) and Sandage (1981(a),(b),1982(a),(b)), who have studied the absolute magnitudes and chemical compositions of RR Lyrae stars on the basis of the light curve morphology alone.

2.4 THE ECLIPSING VARIABLES

It is worth a digression at this point, to draw attention to the eclipsing variables that have been found. A few of these have been studied photoelectrically, and the results have been stated here, although it has not been possible to look at the majority of them in any detail (there are twice as many of them per field as RR Lyrae stars). The light curves and periods of the ones that have been studied here indicate that a large fraction of these are W UMa type contact binaries. Some of them are as faint as 18.5^{m}, and so are apparently several kpc from the disk and are probabaly halo objects. Mochnaki (1981 and priv. comm.) has shown that absolute magnitudes of W Uma type stars can be derived to an accuracy of 0.3 magnitudes without requiring a complete radial velocity curve. Spectroscopic observations at a few strategic phases allow the center of mass

velocity to be determined. These are therefore potential probes of the Galactic halo.

REFERENCES

Lafler, J., and Kinman, T. D. 1965, Ap.J. Suppl., 11, 216.

Mochnaki, S. W. 1981, Ap.J. 245, 650.

Sandage, A. (1970), Ap.J., 162, 841.

Sandage, A. 1981(a), Ap.J. (Letters) 244, L23.

Sandage, A. 1981(b), Ap.J. 248, 161.

Sandage, A. 1982(a), Ap.J. 252, 553.

Sandage, A. 1982(b), Ap.J. 252, 574.

Sandage, A., Katem, B., and Sandage, M. 1981, Ap.J. Suppl., 46, 41.

Sandage, A., and Smith, L. W. 1963, Ap.J., 137, 105-.

Thuan, T. X., and Gunn, J. E. 1976, Pub. A.S.P., 88, 543.

FIGURE CAPTIONS

Fig. 2.1

The light curves in B obtained with SIT Vidicon photometry are presented. Periods and mean magnitudes are quoted for each object.

TABLE 2.1

SIT camera data for light curves

HJD	B	HJD	B	HJD	B
		II V1			
2444547.981	18.16	2444548.856	17.72	2444548.952	17.88
2444549.015	18.47	2444549.834	17.99	2444549.886	18.20
2444549.933	17.92	2444550.861	18.03	2444550.927	18.12
2444550.977	18.01	2444551.841	17.99	2444551.934	17.81
2444552.005	18.22	2444552.823	17.78	2444552.963	18.16
2444609.690	18.06	2444609.694	18.23	2444609.854	18.64
2444609.896	18.03	2444609.899	17.90	2444609.974	18.68
2444636.725	17.92	2444636.830	18.13	2444636.966	17.93
0.000	15.84(±.03)				
		II V2			
2444547.983	18.25	2444548.861	17.95	2444548.954	18.33
2444549.020	17.92	2444549.841	18.43	2444549.888	18.33
2444549.936	18.07	2444550.865	18.12	2444550.930	18.62
2444550.980	18.11	2444551.848	18.78	2444551.937	18.14
2444552.008	18.21	2444552.833	17.83	2444552.904	18.67
2444552.967	17.99	2444609.694	18.53	2444609.769	18.32
2444609.858	18.54	2444609.902	18.14	2444609.906	18.05
2444609.977	18.92	2444609.981	18.88	2444636.728	18.76
2444636.732	18.98	2444636.834	18.36	2444636.839	18.37
2444636.970	18.32	0.000	16.11(±.02)		
		II V3			
2444547.986	15.03	2444549.021	14.83	2444549.843	15.03
2444549.891	15.03	2444549.938	15.17	2444550.866	14.83
2444550.937	15.02	2444550.986	15.00	2444551.852	13.93
2444551.939	14.20	2444552.011	14.45	2444552.836	15.11
2444552.907	14.93	2444609.701	14.30	2444609.772	14.61
2444609.861	14.93	2444609.910	15.09	2444609.912	14.99
2444609.985	15.10	2444636.734	14.97	2444636.841	14.92
2444636.973	14.08	0.000	16.28(±.03)		
		II V4			
2444548.866	17.11	2444548.960	16.75	2444549.846	17.12
2444549.894	16.96	2444549.940	16.63	2444550.869	17.19
2444550.937	16.67	2444550.989	16.65	2444551.854	16.76
2444551.942	16.79	2444552.015	16.67	2444552.839	16.66
2444552.909	16.91	2444552.971	16.78	2444609.718	16.80
2444609.774	17.64	2444609.865	16.66	2444609.914	17.08
2444609.917	17.11	2444609.990	16.84	2444636.845	17.17

2444636.739	16.62	2444636.977	17.11	2444636.743	16.62
0.000	15.76(±.03)				

II V5

2444548.869	16.60	2444548.962	16.62	2444549.026	17.42
2444549.849	16.59	2444549.897	16.54	2444549.943	16.54
2444550.872	16.60	2444550.949	16.46	2444550.991	16.60
2444551.875	16.94	2444551.945	18.72	2444552.018	16.93
2444552.843	16.70	2444552.912	16.62	2444552.973	16.62
2444609.720	16.69	2444609.722	16.69	2444609.776	16.53
2444609.779	16.56	2444609.867	16.55	2444609.869	16.60
2444609.920	16.65	2444609.923	16.61	2444609.992	16.63
2444636.847	16.61	2444636.746	16.61	2444636.978	16.59
0.000	17.10(±.02)				

II V6

2444548.870	18.29	2444636.745	18.19	2444636.847	17.79
2444636.979	17.82	2444609.720	18.31	2444609.724	18.16
2444609.777	18.42	2444609.867	17.24	2444609.921	17.57
2444609.927	17.58	2444609.991	17.89	2444552.850	18.15
2444552.915	18.36	2444552.973	17.29	2444551.880	17.32
2444551.945	17.59	2444552.018	17.86	2444550.873	17.84
2444550.950	18.17	2444550.995	18.16	2444549.852	18.22
2444549.897	18.30	2444549.943	18.29	2444548.963	18.29
2444549.027	17.37	2444994.824	18.26	2444994.830	18.34
2445322.757	17.49	2445322.761	17.44	2445355.912	18.40
2445355.920	18.34	2445355.929	18.06	2445355.934	17.78
2445355.939	17.70	2445355.947	17.61	2445355.952	17.48
2445355.962	17.36	2445355.967	17.34	2445355.971	17.17
2445355.975	17.21	2445355.980	17.30	0.000	18.20(±.04)

II V104

2445323.779	17.72	2445323.784	17.74	2445323.866	16.99
2445323.946	16.83	2445324.016	17.27	2445324.764	17.84
2445324.944	17.59	2445324.991	16.47	2445325.019	16.51
2445327.878	17.03	2445354.865	16.79	2445355.761	17.71
2445355.803	17.60	2445355.857	17.66	2445355.892	17.49
2445349.780	17.79	2445349.697	17.71	0.000	16.88(±.02)

II V208

2445323.791	16.91	2445323.872	17.15	2445323.950	17.34
2445324.021	17.34	2445324.767	16.67	2445324.949	17.03
2445324.992	17.19	2445325.024	17.28	2445327.887	17.41
2445328.053	17.06	2445349.679	16.55	2445349.688	16.50
2445349.704	16.58	2445349.783	16.94	2445354.872	17.27
2445354.876	17.34	2445355.779	16.54	2445355.797	16.60
2445355.799	16.61	2445355.862	16.79	2445355.896	17.13
0.000	16.55(±.02)				

II V303

2444548.885	16.26	2444548.973	15.86	2444549.042	15.77
2444549.868	15.63	2444549.907	15.66	2444549.957	16.27
2444550.884	16.32	2444550.962	15.66	2444551.004	16.39
2444551.888	15.69	2444551.957	16.29	2444552.028	15.69
2444552.863	15.99	2444552.926	15.80	2444552.984	15.82
2444609.758	16.47	2444609.759	16.46	2444609.849	15.78
2444609.890	16.35	2444609.894	16.16	2444609.968	15.66
2444609.970	15.70	2444610.015	16.41	2444636.710	16.09
2444636.818	15.75	2444636.956	15.75	0.000	16.27(±.02)

II V306

2444636.697	17.42	2444636.807	17.89	2444636.945	17.95
2444912.879	17.48	2444912.944	17.72	2444912.995	17.83
2444960.727	17.70	2444960.821	17.84	2444960.892	17.66
2444961.726	17.77	2444961.813	17.68	2444961.878	17.79
2444961.966	16.58	2444962.027	17.06	2444962.876	17.64
2444962.948	16.59	2444963.021	17.12	2444994.647	17.80
2444994.753	17.85	2444994.843	17.77	2444994.937	16.53
2444995.620	17.68	2444995.749	17.83	2444995.812	17.79
2444995.909	16.42	2444995.965	16.83	0.000	17.88(±.03)

II V401

2444908.886	17.28	2444908.953	17.17	2444909.001	17.44
2444960.734	18.04	2444960.825	18.20	2444960.937	18.16
2444961.730	18.01	2444961.817	18.17	2444961.882	18.25
2444961.969	18.24	2444962.053	16.79	2444962.880	18.21
2444962.953	18.22	2444963.054	16.84	2444994.652	18.22
2444994.758	18.21	2444994.848	17.14	2444994.942	17.64
2444995.624	18.39	2444995.744	18.34	2444995.821	16.89
2444995.915	17.57	0.000	18.02(±.05)		

II V407

2444912.893	17.72	2444912.961	18.39	2444913.008	17.76
2444960.740	18.05	2444960.837	17.75	2444961.735	18.42
2444961.821	17.69	2444961.887	18.10	2444961.975	17.80
2444962.885	17.95	2444962.959	17.69	2444994.658	18.18
2444994.763	17.84	2444994.853	17.84	2444994.946	18.15
2444995.630	17.99	2444995.739	17.74	2444995.825	17.84
2444995.917	18.22	2445026.687	17.73	2445026.692	17.68
2445026.698	17.64	2445026.702	17.76	0.000	18.11(±.06)

II V501

2444912.902	16.30	2444912.965	16.59	2444913.011	16.81
2444960.755	16.82	2444960.843	16.22	2444961.739	16.13
2444961.825	16.55	2444961.891	16.82	2444961.978	16.18
2444962.892	16.22	2444962.962	16.59	2444962.966	16.62

2444994.662	16.86	2444994.770	16.15	2444994.857	16.58
2444994.951	16.83	2444995.633	16.17	2444995.734	16.66
2444995.767	16.84	2444995.829	16.68	2444995.921	16.18
0.000	16.48(±.01)				

II V502

2444960.753	19.20	2444960.851	18.18	2444961.833	17.92
2444961.896	18.38	2444961.983	19.01	2444962.033	19.07
2444962.897	18.34	2444962.976	18.80	2444963.032	19.07
2444994.670	18.82	2444961.746	19.23	2444994.955	19.15
2444995.638	18.70	2444995.727	19.04	2444995.777	19.18
2444995.831	19.10	2444995.925	19.18	2444995.971	19.11
2445026.707	18.07	2445026.721	17.77	2445026.750	18.01
2445026.788	18.28	2445026.794	18.44	2445026.830	18.61
2445026.880	18.83	2445027.658	19.21	2445027.692	19.05
2445028.639	19.15	2445028.782	18.20	2445028.835	18.57
2445322.770	19.05	2445349.717	18.07	2445349.738	17.89
2445349.750	18.06	0.000	18.23(±.04)		

II V504

2444912.871	16.76	2444912.930	17.00	2444912.934	17.00
2444912.991	17.35	2444960.717	16.73	2444960.817	17.11
2444960.887	17.38	2444961.758	17.26	2444961.838	17.29
2444961.901	16.74	2444961.988	16.92	2444962.764	17.30
2444962.768	17.14	2444962.903	16.85	2444962.982	17.31
2444994.623	16.93	2444994.626	16.91	2444994.629	16.79
2444994.740	17.40	2444994.839	16.74	2444994.931	16.96
2444995.616	17.38	2444995.752	16.76	2444995.809	16.75
2444995.902	17.28	0.000	16.78(±.04)		

II V601

2445322.797	17.95	2445322.801	18.03	2445322.866	17.98
2445322.953	18.13	2445322.996	18.10	2445323.064	17.79
2445323.772	17.58	2445323.863	17.82	2445323.906	18.05
2445323.966	18.13	2445324.030	18.09	2445324.771	17.38
2445324.953	17.95	2445324.997	17.98	2445325.032	18.08
2445327.898	18.01	2445354.897	18.15	2445355.769	17.75
2445355.811	17.82	2445355.774	17.76	2445355.870	17.97
2445355.899	18.02	2445355.984	18.15	0.000	18.51(±.03)

III V101

2445026.798	17.56	2445026.801	17.37	2445026.857	17.40
2445028.645	17.63	2445028.700	17.56	2445028.788	17.18
2445028.848	15.79	2445028.906	16.56	2445285.906	17.34
2445286.905	17.21	2445286.935	17.13	2445286.985	16.54
2445287.023	16.43	2445287.878	17.24	2445287.880	17.12
2445287.923	16.65	2445287.976	16.40	2445288.020	16.55
2445322.786	17.16	2445322.872	17.23	2445322.999	17.03

2445323.008	16.95	2445323.827	17.24	2445323.877	17.35
2445323.914	17.41	2445323.974	16.64	2445323.976	16.63
2445324.959	15.82	2445325.002	16.14	0.000	17.70(±.02)

III V102

2445026.806	17.03	2445026.808	17.09	2445026.860	17.10
2445028.648	17.04	2445028.706	17.02	2445028.791	16.86
2445028.851	15.77	2445285.898	15.93	2445285.901	15.97
2445285.947	16.11	2445285.984	16.38	2445286.908	16.30
2445286.938	16.51	2445286.990	16.69	2445287.026	16.87
2445287.884	16.54	2445287.926	16.76	2445287.978	16.88
2445288.023	16.96	2445322.805	16.92	2445322.875	16.99
2445322.964	16.93	2445314.015	16.93	2445323.829	17.03
2445323.880	16.97	2445323.918	17.00	2445323.981	15.92
2445323.983	15.86	2445324.972	15.94	2445325.009	16.25
0.000	16.69(±.01)				

III V103

2444960.766	19.40	2444960.858	18.75	2444961.768	19.11
2444961.844	18.06	2444961.931	18.78	2444961.993	19.16
2444962.040	19.32	2444962.986	19.29	2444962.909	18.90
2444963.039	19.33	2444994.680	19.12	2444994.784	19.31
2444994.878	19.30	2444994.970	18.15	2444995.648	19.35
2444995.718	19.22	2444995.792	19.23	2444995.843	19.01
2444995.933	18.31	2444995.985	18.72	2445026.732	18.50
2445026.737	18.41	2445026.742	18.44	2445026.812	19.08
2445026.864	19.11	2445026.899	19.10	2445027.667	18.51
2445027.711	18.83	2445028.653	18.82	2445028.714	19.04
2445287.892	18.35	2445287.933	18.47	2445287.983	18.66
2445287.892	18.55	2445287.933	18.56	2445287.983	18.75
2445322.746	19.37	2445322.880	18.46	2445323.021	18.90
2445323.850	18.49	2445323.856	18.54	2445323.886	18.73
2445323.922	18.91	2445323.988	19.15	2445355.992	18.53
2445356.011	18.76	0.000	18.61(±.02)		

III V201

2444960.783	16.74	2444960.785	16.67	2444960.871	16.82
2444961.774	16.76	2444961.851	16.87	2444961.936	16.81
2444962.000	16.57	2444962.914	16.91	2444962.991	15.63
2444994.685	16.01	2444994.789	16.62	2444994.881	16.90
2444994.964	16.98	2444995.653	16.02	2444995.713	16.40
2444995.849	16.80	2444995.940	16.90	2445026.643	16.74
2445026.675	15.40	2445026.678	15.43	2445026.681	15.41
2445026.867	16.54	2445027.626	16.28	2445027.628	16.10
2445027.639	15.70	2445027.642	15.54	2445027.653	15.41
2445027.683	15.55	2445027.716	15.89	2445028.635	15.36
2445028.658	15.58	2445355.833	15.87	2445355.855	16.17
2445355.845	16.09	0.000	16.17(±.01)		

III V202

2445026.819	16.46	2445026.821	16.49	2445026.870	16.64
2445028.660	16.75	2445028.720	17.01	2445028.758	16.90
2445028.800	16.95	2445028.863	16.89	2445028.866	16.86
2445285.925	17.10	2445285.951	16.95	2445285.956	16.88
2445285.988	16.34	2445285.999	16.12	2445286.912	16.91
2445286.941	16.93	2445286.993	16.94	2445287.028	16.93
2445287.897	16.46	2445287.937	16.60	2445287.987	16.71
2445288.026	16.80	2445322.888	16.15	2445322.890	16.15
2445322.914	15.99	2445322.916	16.02	2445322.919	16.04
2445322.972	16.35	2445323.026	16.58	2445323.931	17.02
2445323.993	16.97	0.000	17.33(±.02)		

III V203

2444960.777	18.53	2444960.866	18.65	2444961.780	18.32
2444961.856	18.52	2444961.941	18.55	2444962.005	18.55
2444962.046	18.56	2444962.920	17.67	2444962.996	18.04
2444963.006	18.26	2444994.689	17.83	2444994.794	18.20
2444994.886	18.50	2444994.978	18.49	2444995.657	18.66
2444995.710	18.60	2444995.853	17.82	2444995.944	17.60
2444995.993	17.91	2445026.747	18.66	2445026.824	18.71
2445026.874	18.52	2445027.679	17.51	2445027.705	17.71
2445028.663	18.64	2445028.761	18.50	2445028.803	18.67
2445028.899	17.83	2445287.956	18.53	2445287.995	18.64
2445288.030	18.68	2445322.809	18.63	2445322.928	18.51
2445323.033	17.97	2445323.816	17.99	2445323.820	17.96
2445323.911	18.23	2445323.996	18.47	2445325.038	17.71
0.000	17.94(±.01)				

III V204

2444961.860	17.29	2444961.946	17.03	2444962.010	16.34
2444962.925	17.27	2444963.002	17.37	2444994.694	16.86
2444994.798	16.54	2444994.890	17.01	2444994.983	17.20
2444995.661	17.30	2444995.705	17.29	2444995.858	16.30
2444995.949	16.74	2445026.762	17.20	2445026.837	17.32
2445028.765	17.05	2445028.806	17.19	2445028.810	17.26
2445028.869	17.34	2445028.668	16.70	2445286.921	17.21
2445286.948	17.19	2445286.999	17.24	2445287.031	17.28
2445287.905	16.97	2445287.939	17.11	2445287.998	17.24
2445322.824	16.75	2445323.794	16.62	2445323.811	16.24
0.000	16.42(±.02)				

III V206

2444961.797	16.49	2444961.863	16.90	2444961.949	17.44
2445692.013	17.61	2444962.928	17.07	2444963.006	17.50
2444994.698	17.91	2444994.801	16.79	2444994.892	17.39
2444994.994	17.82	2444994.701	17.76	2444995.664	17.79
2444995.702	17.83	2444995.865	16.94	2444995.952	17.39

2445026.765	17.08	2445026.840	17.47	2445028.671	17.84
2445028.768	16.50	2445028.812	16.80	2445028.873	17.23
2445285.916	17.83	2445285.920	17.70	2445285.961	17.80
2445286.010	17.74	2445286.944	17.71	2445286.914	17.68
2445287.003	17.83	2445287.037	17.64	2445287.901	17.41
2445287.949	17.61	2445288.003	17.73	2445322.827	16.65
2445322.912	17.21	2445322.978	17.42	2445323.039	17.70
2445323.799	17.78	2445323.891	16.78	2445323.935	17.01
2445324.000	17.40	0.000	16.60(±.01)		

III V208

2444960.793	17.36	2444960.875	17.59	2444961.802	17.56
2444961.869	17.21	2444961.953	16.77	2444962.018	17.07
2444962.931	16.80	2444963.010	17.16	2444994.710	17.35
2444994.804	17.43	2444994.999	17.31	2444995.671	17.38
2444995.699	17.48	2444995.872	16.93	2444995.957	17.19
2444996.005	17.67	2445026.772	17.40	2445026.843	17.33
2445026.889	16.88	2445028.673	17.51	2445028.773	16.94
2445028.814	16.81	2445285.930	16.98	2445285.967	17.08
2445286.005	17.34	2445286.927	17.23	2445287.007	17.50
2445287.042	17.30	2445287.911	17.39	2445287.960	17.41
2445288.008	17.04	2445288.038	16.85	2445322.833	17.29
2445322.893	16.82	2445322.980	17.01	2445322.988	17.01
2445323.047	17.36	2445323.801	17.01	2445323.894	16.94
2445323.938	17.01	2445324.003	17.48	2445324.006	17.48
2445324.033	17.53	2445324.978	17.56	2445325.015	17.40
0.000	18.61(±.02)				

III V302

2444961.720	17.15	2444961.807	17.40	2444961.873	17.46
2444961.957	17.41	2444962.022	17.63	2444962.936	17.34
2444963.015	17.46	2444994.714	17.31	2444994.808	17.45
2444994.903	17.48	2444995.005	17.45	2444995.680	16.68
2444995.694	16.75	2444995.878	17.35	2444995.962	17.51
2445026.778	17.53	2445026.846	17.40	2445028.680	16.88
2445028.775	17.29	2445028.820	17.37	2445028.889	17.48
2445285.936	17.51	2445285.978	17.55	2445286.016	16.76
2445286.955	17.46	2445286.975	17.47	2445287.014	17.53
2445287.047	17.54	2445287.916	17.20	2445287.966	17.29
2445288.013	17.46	2445322.858	17.31	2445322.907	16.31
2445322.910	16.35	2445322.992	16.84	2445324.010	16.62
0.000	18.24(±.02)				

IV V103

2444856.681	16.72	2444856.684	16.67	2444856.758	16.79
2444856.833	16.63	2444856.887	16.59	2444856.944	16.70
2444856.989	16.26	2444857.726	16.15	2444857.760	16.25
2444857.840	16.50	2444857.899	16.54	2444857.956	16.61
2444858.007	16.75	2444858.897	15.93	2444858.945	15.97

2444858.995	16.09	2444883.689	16.81	2444883.741	16.72
2444883.849	16.73	2444883.959	16.15	2444883.964	15.96
2444884.660	16.14	2444912.630	16.60	2444912.697	16.38
2444912.765	15.84	2444912.795	15.97	2444912.813	16.02
2444912.857	16.23	2444914.631	16.09	2444914.672	16.28
2444914.703	16.35	2444960.670	16.31	2444960.680	16.41
2444960.696	16.47	2444961.618	16.58	2444961.628	16.65
2444961.639	16.73	2444961.655	16.73	2444961.702	16.08
2444961.710	16.01	2445322.638	16.68	2445323.599	15.96
2445323.602	16.01	2445323.604	16.01	2445323.606	16.03
0.000	17.90(±.02)				

IV V104

2444856.692	17.46	2444856.760	18.01	2444856.891	18.32
2444856.948	18.42	2444857.695	17.25	2444857.903	18.40
2444857.960	18.47	2444883.750	18.27	2444883.746	18.16
2444884.693	17.84	2445285.639	17.36	2445285.642	17.36
2445285.732	17.68	2445285.799	18.05	2445285.841	18.14
2445286.633	18.10	2445286.686	17.36	2445286.753	17.74
2445287.708	17.44	2445287.756	17.53	2445287.801	17.74
2445287.825	17.76	2445288.614	18.47	2445349.641	18.33
0.000	17.35(±.02)				

IV V105

2444856.953	18.63	2444857.001	17.80	2444857.909	18.55
2444857.967	18.53	2444883.757	18.47	2444883.861	18.53
2444883.960	18.64	2444884.687	17.78	2445285.652	18.42
2445285.740	17.34	2445285.808	17.62	2445286.641	18.39
2445286.693	18.51	2445287.713	18.49	2445287.762	18.33
2445322.629	18.15	2445322.634	18.13	2445323.590	17.69
2445323.595	17.54	2445323.652	17.91	2445324.601	17.66
2445324.637	17.48	2445324.672	17.73	2445324.708	17.88
0.000	15.96(±.02)				

IV V106

2444856.710	17.55	2444856.772	16.27	2444856.848	16.67
2444856.901	17.18	2444856.958	17.41	2444856.992	17.50
2444857.699	17.14	2444857.781	16.64	2444857.783	16.69
2444857.858	16.85	2444857.915	17.32	2444857.970	17.52
2444858.010	17.78	2444858.865	17.46	2444858.912	17.45
2444858.961	17.60	2444858.992	17.68	2444883.696	16.86
2444883.700	16.81	2444883.776	17.26	2444883.864	17.68
2444883.947	17.80	2444884.663	16.77	2444884.723	17.33
2444884.727	17.32	2444912.636	17.74	2444912.639	17.57
2444912.702	17.49	2444912.705	17.45	2444912.772	17.68
2444912.802	17.54	2444912.823	16.72	2444912.827	16.56
2444912.830	16.43	2444912.834	16.30	2444912.838	16.21
2444912.841	16.28	2444912.843	16.30	2444914.646	17.70
2444914.679	17.31	2444914.686	17.39	2444914.711	17.55

2444914.718	17.63	2444958.641	17.72	2444958.658	17.73
2445322.645	16.75	2445322.648	16.80	2445323.609	16.81
2445323.612	16.77	0.000	17.31(±.03)		

IV V107

2444856.714	18.08	2444856.780	18.09	2444856.851	18.07
2444856.905	18.08	2444856.962	18.14	2444857.917	18.14
2444857.974	17.86	2444858.970	17.94	2444858.988	18.02
2444883.780	18.04	2444883.784	18.11	2444883.869	18.13
2444883.952	17.92	2444884.671	17.62	2445285.658	17.97
2445285.744	18.16	2445285.813	17.42	2445286.654	17.96
2445286.697	18.14	2445286.759	18.09	2445287.720	17.90
2445287.767	17.95	2445287.806	18.09	2445322.619	17.47
2445322.622	17.47	2445323.659	17.37	2445323.661	17.36
2445323.664	17.21	2445323.667	17.26	2445323.684	17.28
2445323.690	17.35	2445323.703	17.27	2445323.705	17.26
0.000	18.21(±.03)				

IV V108

2444856.716	16.96	2444856.719	16.82	2444856.783	17.00
2444856.855	16.54	2444856.909	16.52	2444856.966	16.81
2444857.794	16.83	2444857.865	17.13	2444857.921	16.94
2444857.978	16.49	2444858.871	16.81	2444858.919	16.91
2444858.974	17.09	2444883.703	16.77	2444883.706	16.89
2444883.789	17.05	2444883.791	17.11	2444883.873	16.48
2444884.668	16.53	2444912.644	17.06	2444912.646	17.15
2444912.649	17.11	2444912.653	17.15	2444912.656	17.17
2444912.659	17.14	2444912.662	17.12	2444912.664	17.13
2444912.668	17.11	2444912.671	17.08	2444912.673	17.14
2444912.676	17.11	2444912.678	17.01	2444912.689	17.00
2444912.717	16.69	2444912.720	16.66	2444912.722	16.60
2444912.726	16.56	2444912.732	16.56	2444912.737	16.50
2444912.742	16.49	2444912.748	16.51	2444912.754	16.53
2444912.757	16.46	2444912.806	16.69	2444912.853	16.87
2444914.650	16.50	2444914.653	16.52	2444914.698	16.49
0.000	16.26(±.01)				

IV V122

2444856.793	15.53	2444856.869	15.36	2444856.923	15.37
2444856.976	16.10	2444856.979	16.07	2444857.884	15.34
2444857.932	15.68	2444857.997	15.29	2444858.017	15.31
2444858.835	15.43	2444858.880	15.35	2444858.930	16.10
2444858.984	15.35	2444883.679	15.42	2444883.682	15.42
2444883.684	15.32	2444883.708	15.36	2444883.813	15.43
2444883.916	15.74	2444883.920	15.74	2444884.651	15.40
2444912.709	15.34	2444912.712	15.38	2444912.714	15.34
2444912.778	16.04	2444912.791	15.95	2444912.810	15.57
2444912.866	15.43	2444914.616	15.53	2444914.618	15.55
2444914.655	15.40	2444914.661	15.38	2444914.665	15.35

2444914.666	15.36	2444914.668	15.39	2444914.700	15.46
2444914.721	15.87	2444914.725	16.01	2444914.727	15.95
2444914.730	16.05	2444914.732	15.98	2444914.734	16.04
2444914.736	16.01	2444962.626	15.38	2444962.634	15.37
2444962.637	15.36	2444962.641	15.34	2444962.644	15.29
2444962.651	15.29	2444958.616	15.33	2444958.627	15.37
0.000	16.74(±.03)				

IV V201

2445285.623	17.40	2445285.627	17.42	2445285.719	17.52
2445285.722	17.32	2445285.779	16.69	2445285.826	16.13
2445286.614	17.39	2445286.617	17.31	2445286.679	17.03
2445286.738	16.29	2445286.744	16.20	2445286.783	16.56
2445287.702	16.52	2445287.742	16.89	2445287.793	17.12
2445287.815	17.19	2445288.603	16.36	2445288.606	16.42
2445288.649	16.78	2445322.607	17.29	2445322.613	17.22
2445322.732	17.42	2445323.656	17.41	2445324.626	17.51
2445324.639	17.50	2445324.672	16.91	2445324.678	16.58
2445324.713	16.03	2445324.717	15.97	0.000	16.77(±.02)

IV V301

2445285.665	16.52	2445285.748	16.73	2445285.822	16.95
2445285.817	16.88	2445286.658	17.10	2445286.706	17.00
2445286.774	16.26	2445286.777	16.33	2445286.780	16.29
2445287.724	16.87	2445287.771	16.89	2445287.812	16.96
2445287.835	17.00	2445288.642	16.25	2445322.654	16.59
2445322.657	16.55	2445322.651	16.62	2445322.717	16.16
2445322.721	16.17	2445323.616	16.78	2445313.620	16.82
2445324.622	16.28	2445324.646	16.42	2445324.711	16.57
2445324.713	16.58	2445349.613	16.72	0.000	17.85(±.03)

IV V401

2445285.631	16.89	2445285.636	16.92	2445285.727	17.08
2445285.788	16.42	2445285.792	16.19	2445285.795	16.01
2445285.830	15.55	2445286.621	16.86	2445286.625	16.92
2445286.683	16.89	2445286.749	16.25	2445286.792	15.56
2445286.704	17.15	2445287.704	17.15	2445287.747	15.39
2445287.749	15.42	2445287.751	15.45	2445287.797	15.91
2445287.820	16.15	2445288.609	16.96	2445288.691	15.42
2445322.663	16.82	2445322.670	16.87	2445322.725	16.70
2445323.622	16.81	2445323.624	16.91	2445323.696	16.44
2445323.711	15.83	2445323.714	15.79	2445323.716	15.69
2445324.608	16.99	2445324.640	16.80	2445324.690	15.71
2445324.699	15.71	2445349.603	16.82	2445349.646	15.54
2445349.650	15.56	2445349.658	15.67	0.000	17.82(±.02)

TABLE 2.2

OBJECT	P(days)	ΔP(days)	θ	⟨B⟩	EPOCH(HJD)	TYPE
II V1	.119699	.0000033	0.58	18.12	2444609.974	E
II V2	.1324162	.000032	0.24	18.28	2444636.732	E
II V3	.620710	.000059	0.47	14.61	2444636.973	RRab
II V4	.340350	.000009	0.67	16.89	2444609.774	E
II V5	.5759	.0008	1.11	16.77	2444551.945	E
II V6	.5631099	.0000014	0.11	17.93	2445355.971	RRab
II V104	.553320	.0000026	0.26	17.26	2445324.991	RRab
II V208	.55299	.00007	0.19	17.02	2445349.688	RRab
II V303	.267010	.000006	0.47	15.88	2444609.758	E
II V306	.49227	.00014	0.33	17.32	2444995.909	RRab
II V401	.49662	.00008	0.24	17.73	2444994.848	RRab
II V407	.1401464	.0000023	0.32	17.89	2444961.736	?
II V501	.282456	.000053	0.24	16.47	2444961.740	RRc
II V502	.5031095	.000001	0.17	18.74	2445026.722	RRab
II V504	.304879	.00002	0.24	17.01	2444960.717	RRc
II V601	.54160	.000015	0.42	17.80	2445324.771	RRab
III V101	.474526	.000005	0.27	16.86	2445028.848	RRab
III V102	.464796	.000052	0.19	16.51	2445028.851	RRab
III V103	.46647	.00003	0.27	18.93	2444961.845	RRab
III V201	.486080	.000015	0.07	16.33	2445028.635	RRab
III V202	.58538	.000018	0.17	16.64	2445322.914	RRab
III V203	.63533	.00004	0.17	18.21	2445027.679	RRab
III V204	.554944	.00005	0.16	16.94	2445323.812	RRab
III V206	.523248	.000005	0.26	17.39	2444961.797	RRab
III V208	.313887	.000004	0.20	17.12	2444961.953	RRc
III V302	.558502	.000022	0.17	17.11	2445322.907	RRab
IV V103	.612208	.000020	0.14	16.40	2444912.765	RRab
IV V104	.517510	.000021	0.23	17.99	2444857.695	RRab
IV V105	.539885	.00004	0.23	18.05	2445285.741	RRab
IV V106	.47918	.00005	0.12	17.13	2444912.838	RRab
IV V107*	.573247	.00002	0.11	17.81	2445323.665	RRab
IV V108	.272611	.00001	0.09	16.77	2444912.758	RRc
IV V122	.1622245	.000008	0.11	15.50	2444856.979	E
IV V201	.457328	.000016	0.15	16.96	2445324.713	RRab
IV V301*	.619330	.000030	0.203	16.68	2445322.717	RRab
IV V401	.479850	.000084	0.14	16.36	2445287.750	RRab

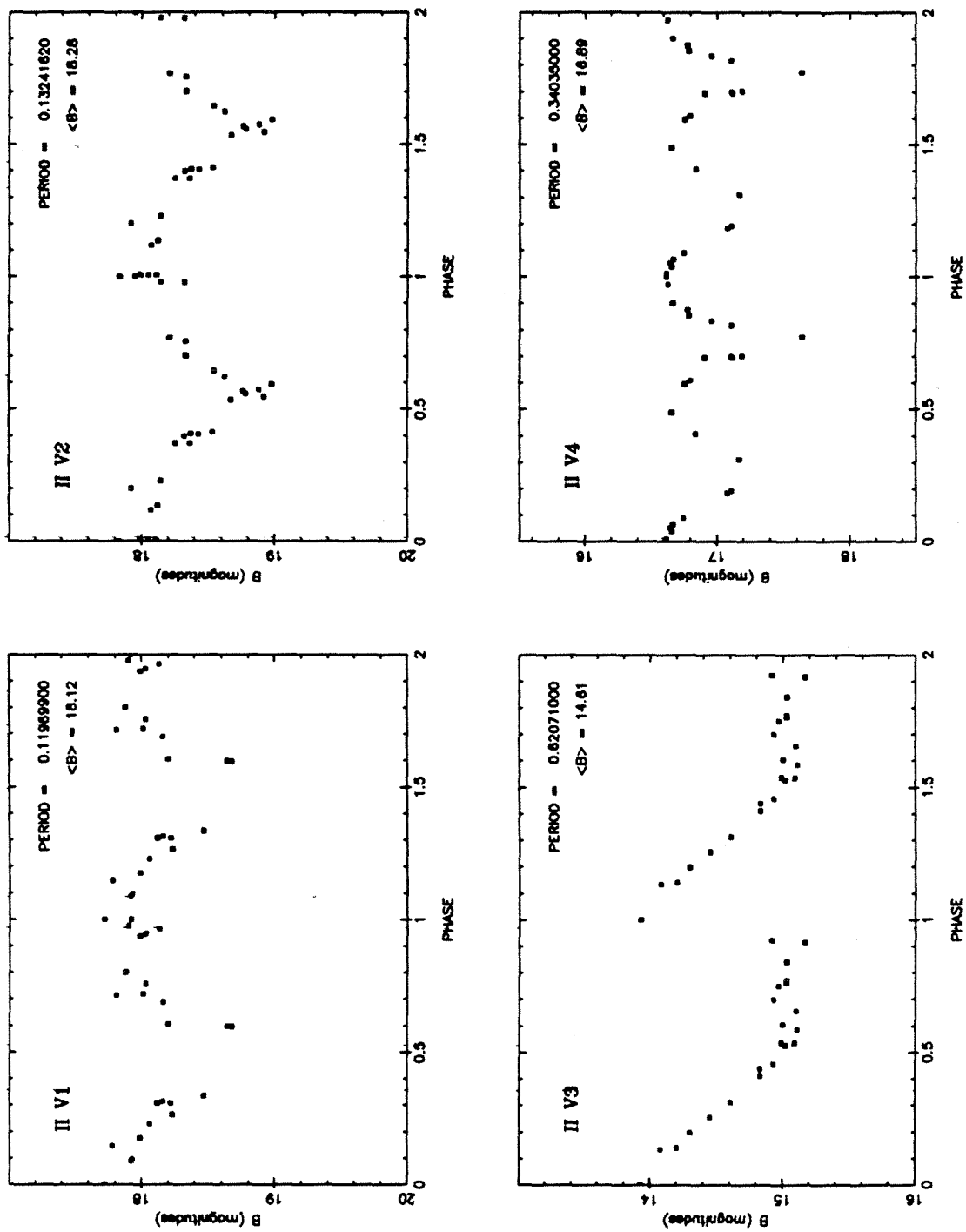
II V2
PERIOD = 0.13241620
<B> = 18.26
II V4
PERIOD = 0.34039000
<B> = 16.89
II V1
PERIOD = 0.11969900
<B> = 18.12
II V3
PERIOD = 0.62071000
<B> = 14.61
B (magnitudes)
PHASE

Fig 2.1

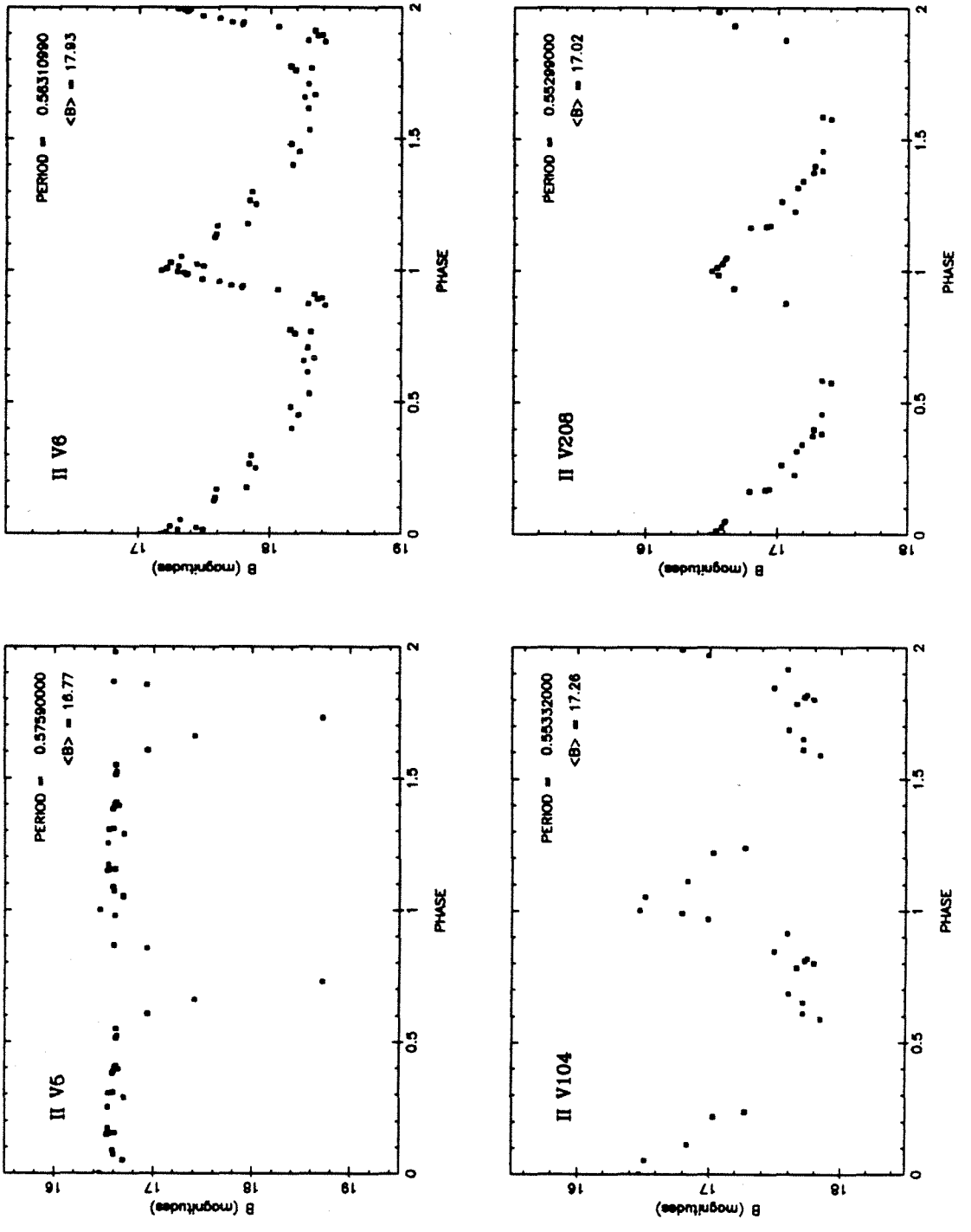
II V6
PERIOD = 0.56310990
<B> = 17.93
II V208
PERIOD = 0.55299000
<B> = 17.02
II V5
PERIOD = 0.57590000
<B> = 16.77
II V104
PERIOD = 0.55332000
<B> = 17.26
B (magnitudes)
PHASE

Fig 2.1 contd.

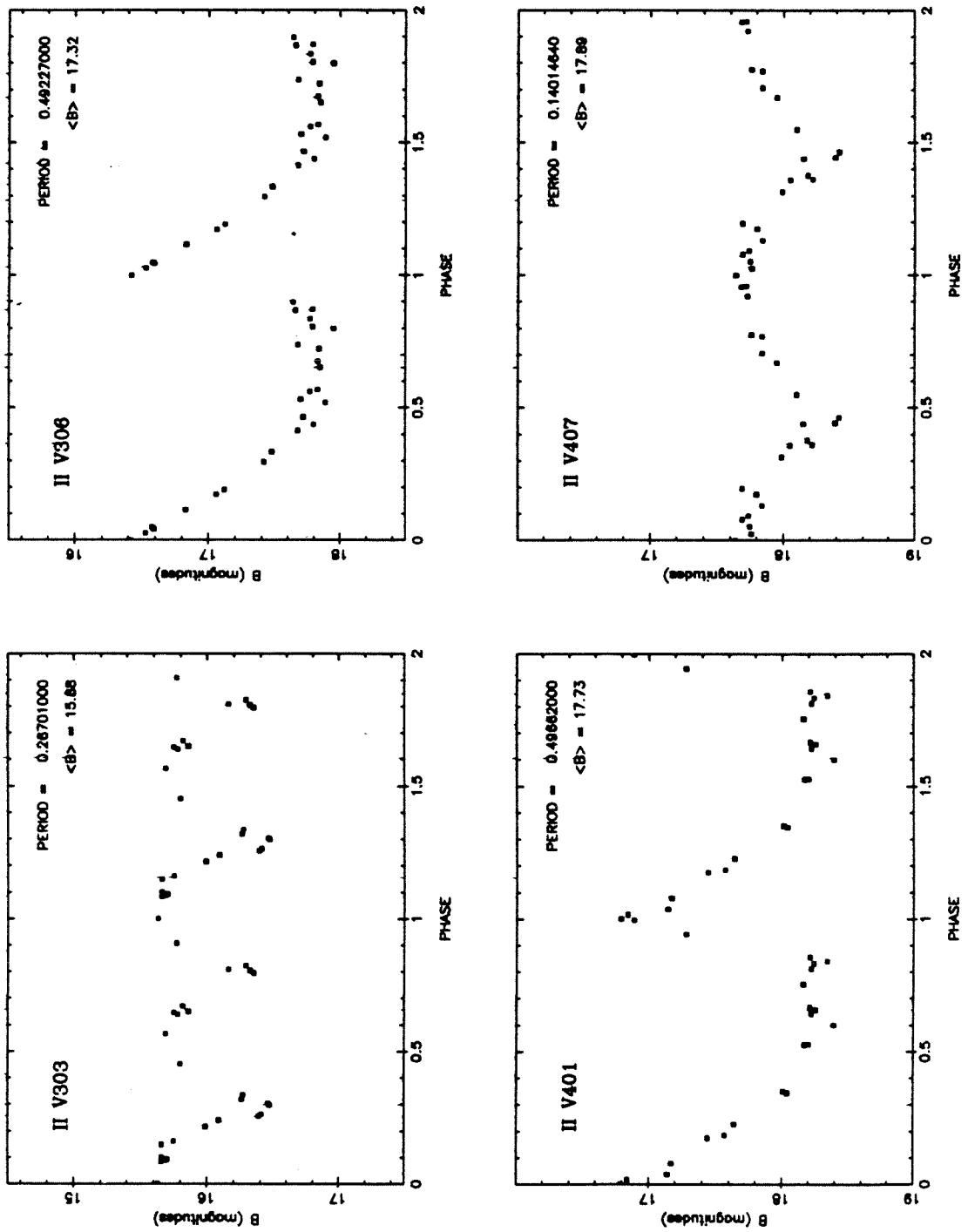
II V306
PERIOD = 0.49227000
<B> = 17.32
II V407
PERIOD = 0.14014640
<B> = 17.89
II V303
PERIOD = 0.26701000
<B> = 15.88
II V401
PERIOD = 0.49862000
<B> = 17.73
B (magnitudes)
PHASE

Fig 2.1 contd.

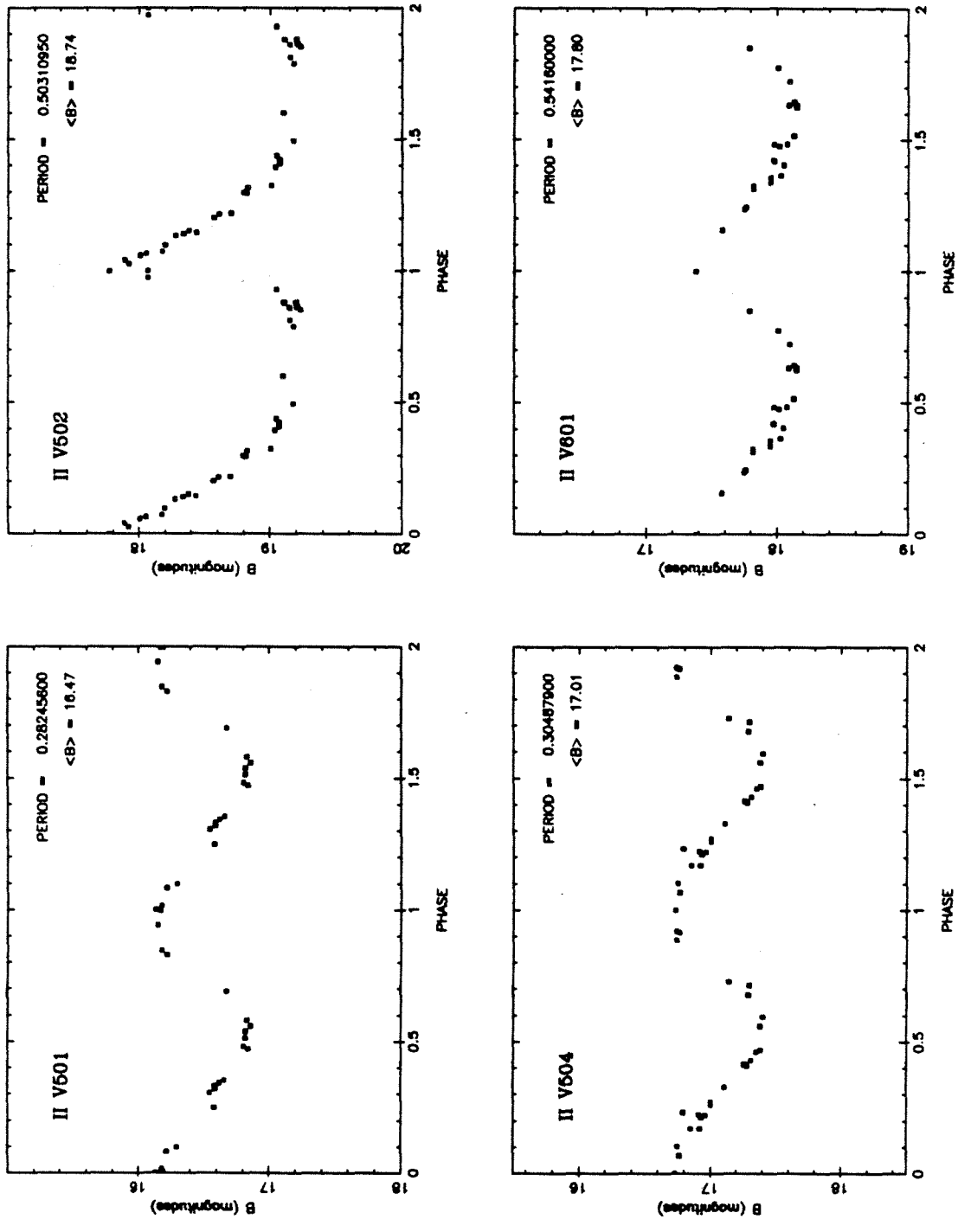
II V502
PERIOD = 0.50310950
<B> = 18.74
II V601
PERIOD = 0.54160000
<B> = 17.80
II V601
PERIOD = 0.28245600
<B> = 16.47
II V504
PERIOD = 0.30457900
<B> = 17.01
B (magnitudes)
PHASE

Fig 2.1 contd.

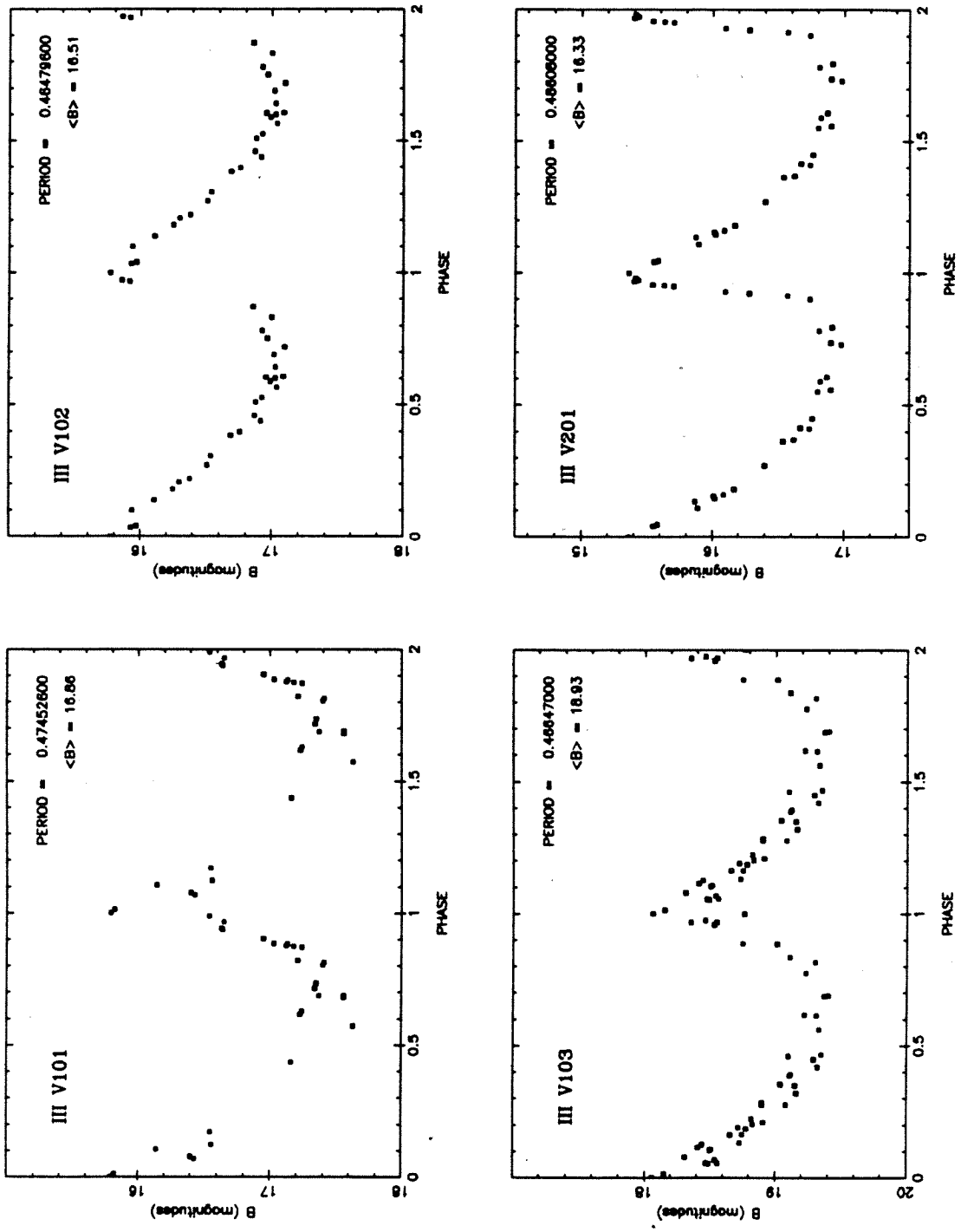
III V102
PERIOD = 0.46479600
<B> = 16.51
III V201
PERIOD = 0.48608000
<B> = 16.33
III V101
PERIOD = 0.47452600
<B> = 16.86
III V103
PERIOD = 0.46647000
<B> = 18.93
B (magnitudes)
PHASE

Fig 2.1 contd.

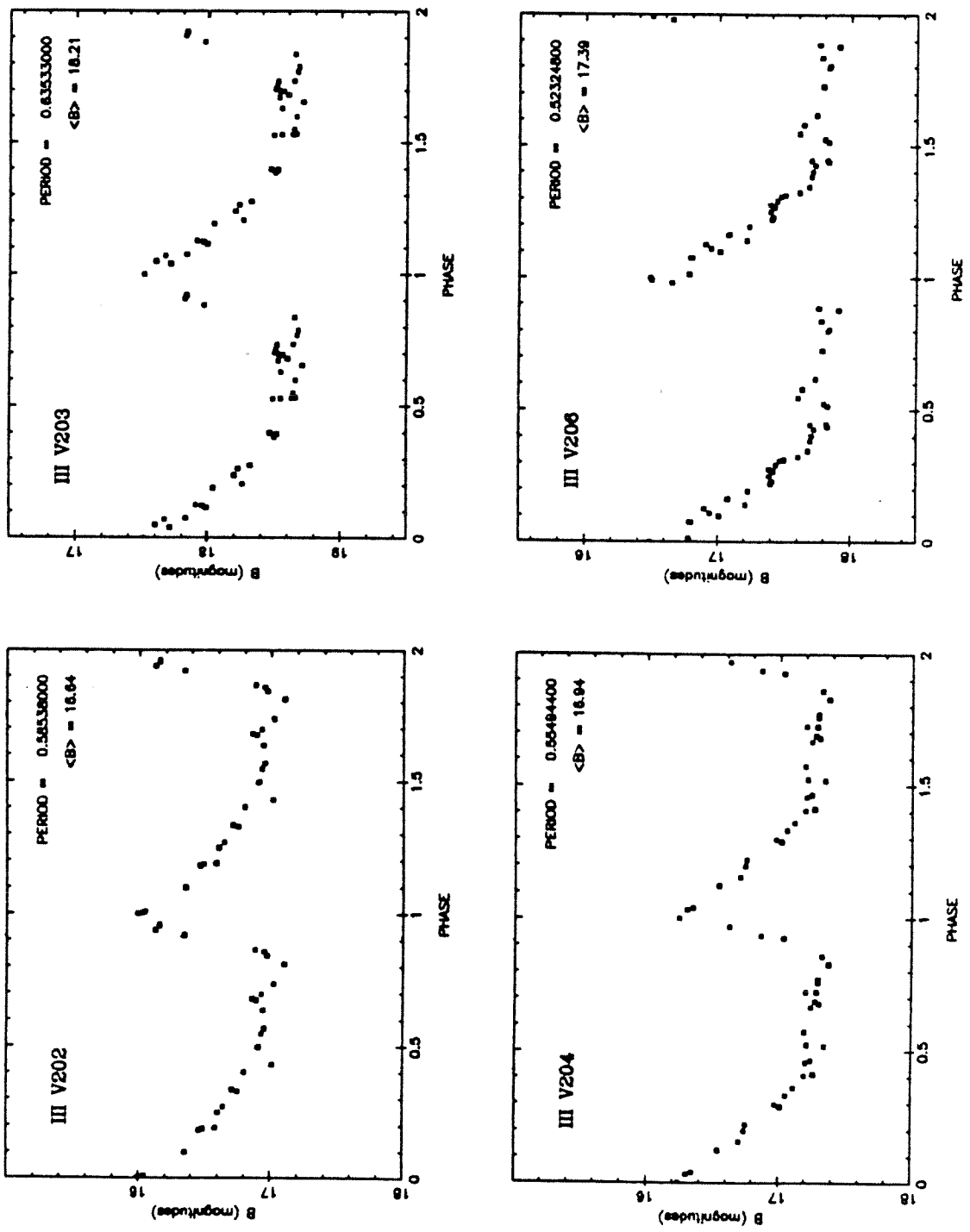
III V203
PERIOD = 0.63533000
<B> = 18.21
III V206
PERIOD = 0.52324800
<B> = 17.39
III V202
PERIOD = 0.58538000
<B> = 16.64
III V204
PERIOD = 0.58484400
<B> = 16.94
B (magnitudes)
PHASE

Fig 2.1 contd.

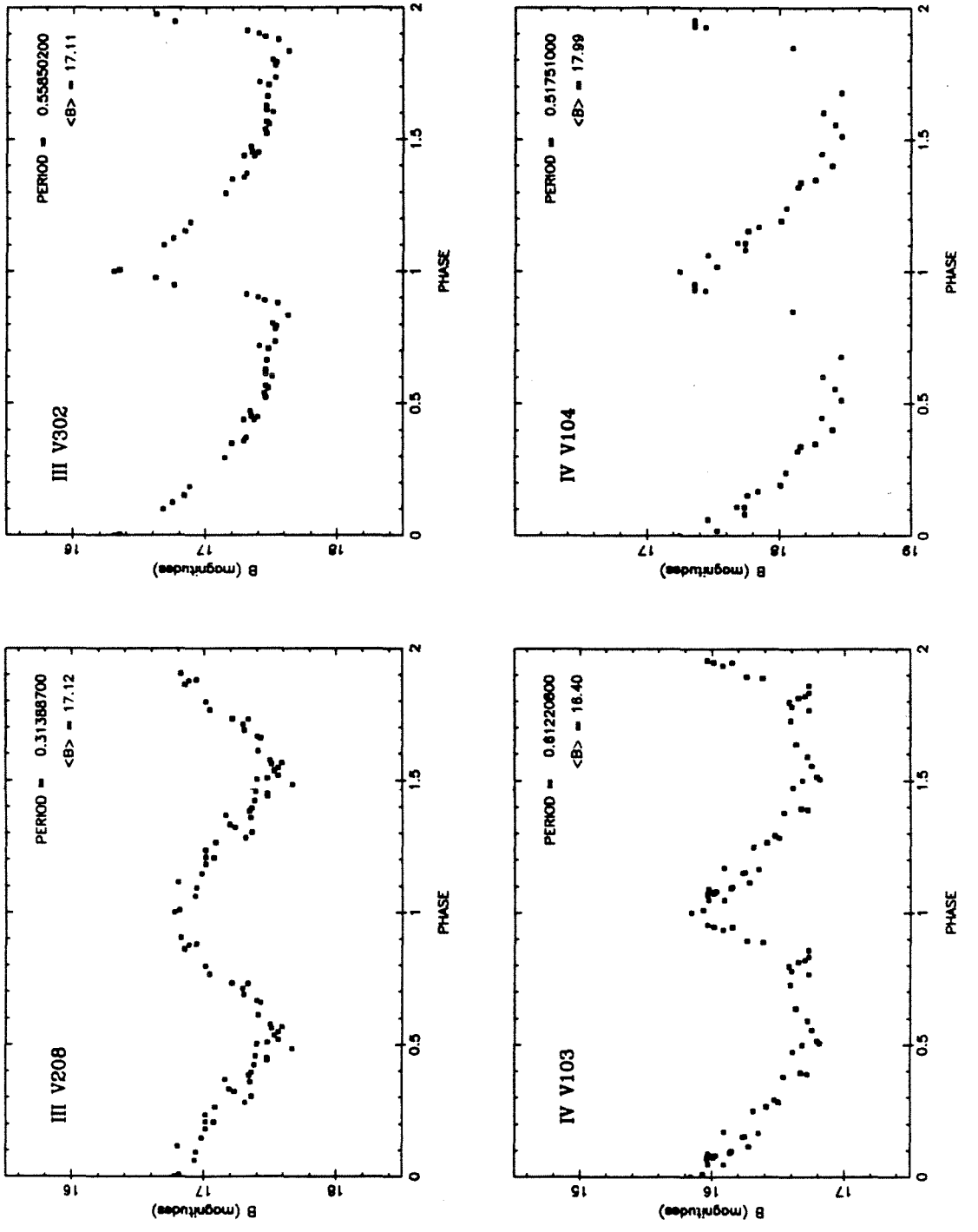
III V302
PERIOD = 0.55850200
<B> = 17.11
IV V104
PERIOD = 0.51751000
<B> = 17.99
III V208
PERIOD = 0.31388700
<B> = 17.12
IV V103
PERIOD = 0.61220600
<B> = 16.40
B (magnitudes)
PHASE

Fig 2.1 cont'd.

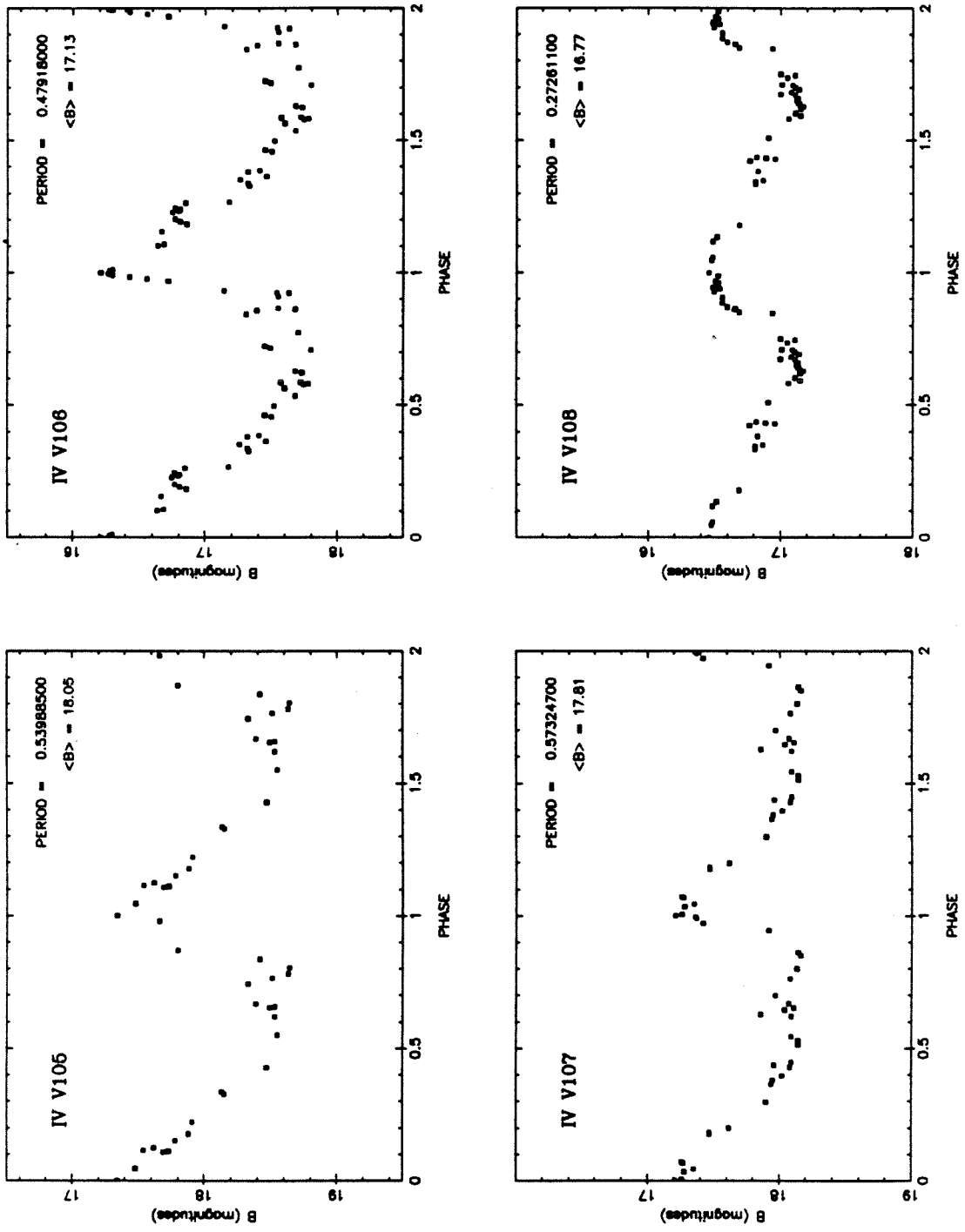
IV V108
PERIOD = 0.47918000
<B> = 17.13
IV V108
PERIOD = 0.27261100
<B> = 16.77
IV V106
PERIOD = 0.53988500
<B> = 18.05
IV V107
PERIOD = 0.57324700
<B> = 17.81
B (magnitudes)
PHASE

Fig 2.1 contd.

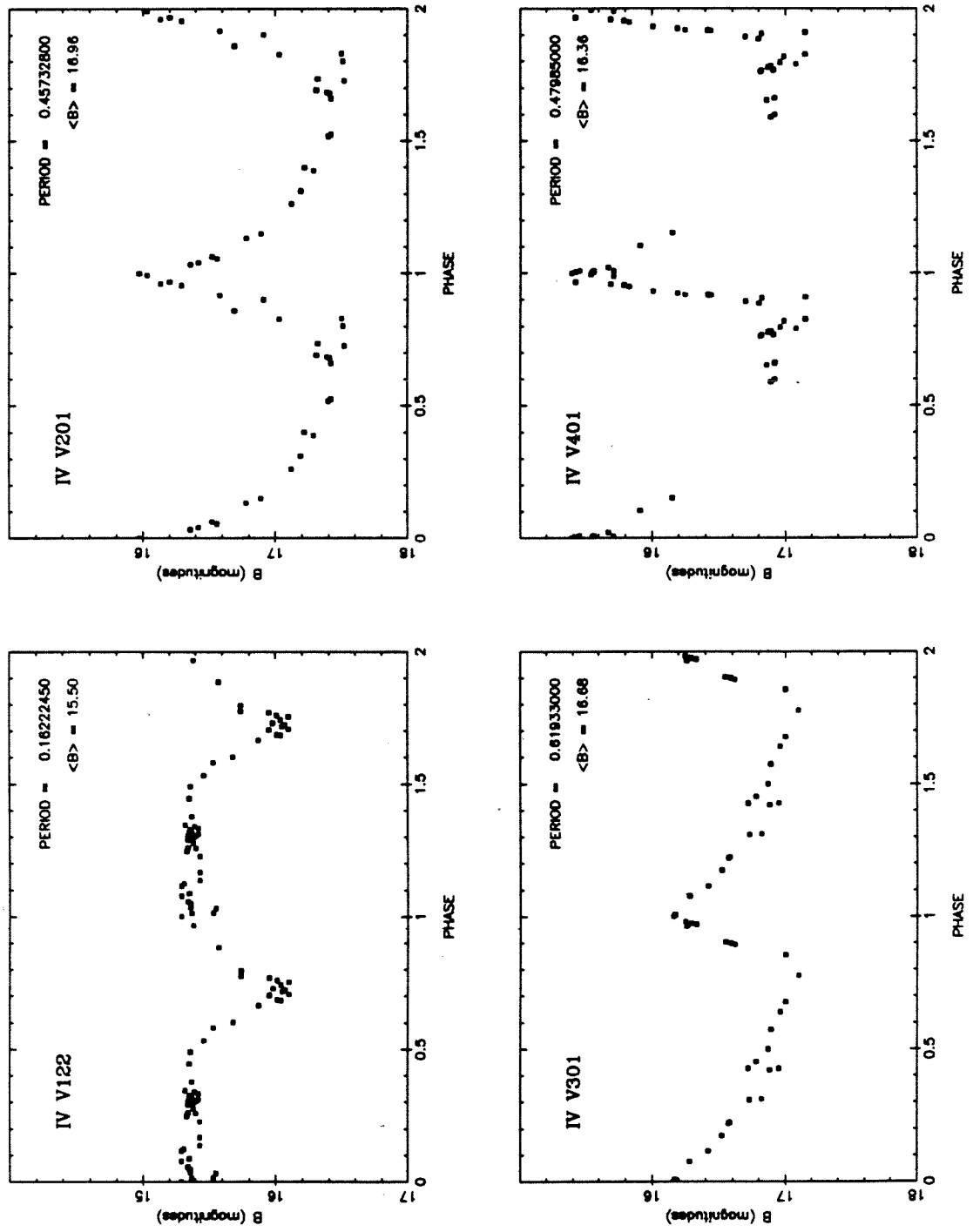
IV V201
PERIOD = 0.45732800
<B> = 16.96
IV V401
PERIOD = 0.47985000
<B> = 16.36
IV V122
PERIOD = 0.16222450
<B> = 15.50
IV V301
PERIOD = 0.61933000
<B> = 16.66
B (magnitudes)
PHASE

Fig 2.1 contd.

CHAPTER 3

SPECTROSCOPY AND SPECTROPHOTOMETRY

3.1 SPECTROSCOPIC OBSERVATIONS

Spectroscopy and spectrophotometry furnish information on chemical abundances, radial velocities and interstellar extinctions for the RR Lyrae stars under study.

Spectra of the RR Lyrae stars found by this survey were obtained in collaboration with Dr. J. B. Oke with the double spectrograph (Oke and Gunn 1982) at the cassegrain focus of the of the 200 inch telescope at Palomar mountain. The blue spectra, which are the ones of interest here, were taken with the RCA CCD. A 1 arc-second entrance slit and a 300 lines/mm grating were used. The spectra cover the range from about 3300Å to about 5300Å. The dispersion is 4.2Å per pixel. The optical resolution of the spectrograph is about 6Å in this setup, so that the spectra are undersampled. Spectra of laboratory sources were taken after each observation for wavelength calibration.

The spectra were taken to measure radial velocities and the Preston (1959) metallicity index ΔS as redefined by Butler (1975). Systematic errors in the measurement of radial velocities may be introduced because the comparison spectra and the object spectra have systematic differences. This may be caused if the entrance slit is nonuniformly illuminated by the comparison lamps or because of charge transfer irregularities that produce systematic differences between emission and absorption lines. To guard against such errors, spectra of the subdwarfs BD $+17^{o}$ 4708, BD $+26^{o}$ 2606, HD 84937 and HD 19445

were observed with the same setup. The spectral features of these stars are very similar to the RR Lyrae stars at minimum light, and can be used as templates in cross-correlation analyses or in otherwise adjusting for "zero-error" in radial velocity measurement. The radial velocities of these subdwarfs have been very well determined from coude spectroscopy (J. L. Greenstein, priv. comm.). To calibrate the ΔS scale, 20 bright field RR Lyrae stars, whose ΔS values on the Butler system are well determined, were observed (with the same setup) in the phase interval 0.4 to 0.85. In addition, some of these "ΔS standards" were also observed between phases 0.1 and 0.4, but the interval during which the light rises to maximum was avoided. These ΔS standards were chosen to span the entire gamut of metallicities.

The stars from this survey were observed in the phase interval 0.4 to 0.85. The ephemerides in Table 2.2 were used to compute phases. The ΔS system refers to objects during minimum light. Also, the CaII K line is strongest at minimum light and thus provides better leverage for the determination of metallicity. At the dispersions used here, velocity determinations can be made only from the hydrogen and CaII lines, since they are broader than the effective resolution, while the weaker metallic lines are not. It is well known that in the ab-type RR Lyrae stars the velocity amplitudes of the hydrogen and the CaII lines are in excess of 100 km/s. During the rise to maximum light there are line doubling phenomena seen in these stronger lines, and so velocities measured from the strong lines near maximum light can be quite ambiguous. All the above reasons demand that the spectra be taken at minimum light, i.e. in the phase interval 0.4 to 0.85,

when the atmospheres of the RR Lyrae stars are quiescent. The center of mass velocity (or γ-velocity) of an RR Lyrae star can be found by applying a phase dependent correction to the velocity obtained from the hydrogen or CaII lines. The procedure is described in detail in a later section.

Columns 1, 2 and 3 of Table 3.2 show the object name, Julian date at middle of exposure, and mean phase of the object for each observation of the survey RR Lyrae stars. Notice that some stars were observed at mean phases greater than 0.85 (because the ephemerides were not known well enough at the time of observation). These observations have been used for velocity and ΔS measurement only if the hydrogen lines appear to be as weak as they are expected to be in the 0.5 to 0.85 phase interval (i.e. the rise to maximum has not yet begun). The star III V202 has been observed a second time at phase 0.12. At this phase the CaII K line is too weak and the hydrogen lines are too strong so that they lie beyond the range of the ΔS calibration used here. However, a reasonable radial velocity can be obtained as long as the phase is not earlier than about 0.08.

Reduction to one dimensional spectra, wavelength fitting and flux calibration according to the system of Oke and Gunn (1983) was done using a reduction program by T. Boroson. Subsequent processing of these reduced spectra to obtain velocities and ΔS is discussed in the following sections.

3.2 MEASUREMENT OF LINE STRENGTHS

The metallicity parameter ΔS is derived from the relative strengths of the hydrogen lines and the CaII K line. At the resolutions that are commonly used to measure the strengths of these lines with the aim of finding ΔS, it is impossible to derive an equivalent width in the physical sense, (i.e. where it can be used in a curve of growth analysis). The best that one can hope to do is to establish an empirical method or line strength measurement which is a sensitive monotonic index of equivalent width.

The selection of continuum points is a major problem. The low dispersion spectra show no true continuum points. Furthermore, because or the undersampling, it is not possible to distinguish between the weaker metallic lines and the noise. Two criteria need consideration:

(1) it is required that there be no systematic differences between the selection of continuum points in spectra that have different signal to noise, and

(2) it is desirable to avoid systematic differences in continuum selection between spectra of stars with different metallicity (and hence different amounts of line blanketing).

If we wish to satisfy the first of these criteria, it has to be at the expense of the second one, since the spectra are undersampled and are at low dispersion where they do not show true continuum points. Metallicity effects in selecting the continuum are therefore inevitable, but can be kept to a minimum by choosing points in the

spectrum where the line-blanketing is minimal. The Procyon spectral atlas (Griffin 1979) was consulted to find wavelength intervals where the line blanketing is minimal for a late F-type star. The wavelength bands have been chosen so that the line blanketing does not change drastically if the band is moved 5Å to either side. This is to ensure that stars with different radial velocities are not treated differently. The systematic effects of continuum selection with metallicity are admittedly still present, but are small enough so that the hydrogen and CaII K line strengths are still a reliable measure of ΔS. The wavelength bands at which the continuum is defined are listed in Table 3.1. In each or these wavelength bands, the average intensity of all the data points (whose number varies from one part of the spectrum to another) in that band is taken to be the continuum intensity at the center of that wavelength band. A quartic spline that passes through all these "continuum" points is evaluated and used to rescale the spectrum so that all the "continuum" points are at the same ordinate, i.e. the spectrum is "flattened" using the spline.

After examining several possible ways of measuring line strengths, it was found that fitting a model profile to the lines using a non-linear least squares method and evaluating the equivalent width of the best fit profile is the most consistent way of measuring line strengths, although these measures are not to be confused with "true" or "physical" equivalent widths. This method has two major advantages: there is no systematic bias when measuring spectra that have different signal to noise (provided the continuum selection has no such bias), and it is possible to make better estimates of the

strengths of lines that are partially blended. The latter point is very important. In all but the most metal poor stars, the CaII K line wings blend into the wings of the H8 and the CaII H + Hε lines. By simultaneously fitting all three features, it is possible to make a better estimate of the CaII K line strength. Such a fit evaluates profile parameters separately for each of the lines. The area in each line can be calculated from these parameters. In principle this method should be able to fit an arbitrarily large number of lines at the same time. However, resolution and signal to noise limitations govern its use. For instance, it cannot be used to separate the CaII H and the Hε lines, which are quite hopelessly blended at the resolution used here. It has proved useful for the CaII K line and for Hγ whose blue wing is distorted by a weak feature in the nominal position of the G-band.

Various model profiles were examined for suitability. Gaussians are quite inadequate and Stark profiles fail in the centers of lines (they work better for hydrogen lines in A-type stars). Voigt functions, which have an extra parameter, make it possible to fit the wings and the centers of lines independently. These were found to be very suitable.

Even from a theoretical standpoint, Voigt profiles are among the best profiles to use. Most stellar lines are intrinsically very near to Voigt functions (of which the Gaussian and the Lorentzian are limiting cases). They are convolutions of a Gaussian and Lorentzian, and can be characterized by a Gaussian width σ and a Lorentzian width

γ. Further, if a Voigt function with width parameters (σ_1,γ_1) is convolved with a Voigt function with width parameters (σ_2,γ_2), the result is a Voigt function with width parameters (σ_3,γ_3) such that

$$\sigma_3^2 = \sigma_1^2 + \sigma_2^2$$
$$\text{and } \gamma_3 = \gamma_1 + \gamma_2 \qquad (3.1)$$

Other associated properties of Voigt functions discussed by Van de Hulst and Reesinck (1947) imply that the successive convolution of a symmetrical profile with other symmetrical profiles (the diffraction due to the spectrograph slit results in such a convolution) makes the resulting profile tend towards a Voigt profile, even if the broadening function at each step is not a Voigt profile.

Unfortunately, since the Voigt function cannot be calculated analytically, but must be evaluated by numerical integration, the computer time required for fitting such a function was found to be prohibitively large. Approximations to the Voigt function which use a pure Gaussian in the core of the line and a pure Lorentzian outside a critical width are also difficult to use. A transcendental equation must be solved to evaluate the critical width, and fitting such a function takes almost as long as fitting a real Voigt function. As a compromise between computing time and optimum functional form, a hybrid analytical function meant to mimic a Voigt function was used. Let the continuum (after flattening) be at a fiducial value F. Denote the wavelength by λ and the spectrum ordinate (intensity) by y. The model profile is given by:

$$y = F - A[\exp(-v^2) + .25\gamma\sigma^{-1}\pi^{-1.5}(v^2+f)^{-1}] \qquad (3.2)$$

where $v = (\lambda-\lambda_0)/\sigma$, A is a measure of the depth of the line, λ_0 is the central wavelength, σ is the Gaussian, γ is like the Lorentzian width in the Voigt function. 'f' is a parameter which is not fitted, but is set by hand, and is the same for all the lines and all the spectra that are measured. For the spectra in this study, a value of 1.0 for f was found to be suitable. Such a model profile behaves like a Gaussian in the center of the line (the second term within parenthesis in equation 3.2 is nearly constant), but behaves like a Lorentzian when $|\lambda-\lambda_0|$ is greater than σ. The spectra were flattened so that F was set equal to 1.0. Thus, the equivalent width W of a line described by the four parameters A, λ_0, σ, and γ is given by:

$$W = A\sigma\pi^{0.5}\left[1.0 + 0.5\gamma\sigma^{-1}\pi^{-2}\right] \qquad (3.3)$$

When fitting the profiles to the observed spectra, the function is evaluated at three points in each wavelength bin (at points 1/6, 1/2 and 5/6 of the way along each bin) and the average of these values is taken to be the value at the bin. This needs to be done for undersampled spectra since any given pixel may be seeing a non-linear variation of intensity versus wavelength across its width.

A computer program named "PLAY" was written by the author to perform the necessary operations with the one dimensional spectra. A non-linear least squares fitting routine by J. Tonry was incorporated in this program to perform the line fitting operations.

Fig. 3.1 displays some typical spectra. Note particularly the variation in the CaII K line strengths. Fig. 3.2 illustrates the multiple line fit of H8, CaII K and CaII H + Hε to the spectrum of one of the above stars (II V306).

3.3 DETERMINATION OF DELTA-S

The equivalent widths of Hδ, Hγ, Hβ and the CaII K line measured in the above manner carry the information needed to determine ΔS. ΔS is formally defined as 10[S(K)-S(Hydrogen)] where S(K) and S(Hydrogen) are the spectral types according to the K line and the hydrogen (Balmer) lines respectively (see Preston (1959) and Butler et.al. (1973)). Fig. 1 of Butler et. al. (1973) suggests that we may define S(K) and S(Hydrogen) as follows:

$$S(K) = a_0 + a_1 W(K) + a_2 W(K)^2 + a_3 W(K)^3 \qquad (3.4)$$

$$\text{and } S(Hy) = b_0 + b_1 W(Hy) + b_2 W(Hy)^2 + b_3 W(Hy)^3 \qquad (3.5)$$

where W(K) is the equivalent width of the CaII K line and W(Hy) is the average of the equivalent widths of Hδ, Hγ and Hβ. This implies that ΔS may be written as:

$$\Delta S = C_0+a_1W(K)+a_2W(K)^2+a_3W(K)^3-b_1W(H)-b_2W(H)^2-b_3W(H)^3 \qquad (3.6)$$

The equivalent widths of the pertinent lines in the bright RR Lyrae stars were measured. Their ΔS values on the Butler system are known (Kraft priv. comm.), and so the coefficients in the above equation could be determined by least squares regression. Once the coefficients were known, ΔS could be calculated for the objects of interest. The ΔS residuals in the fit using 19 stars (some of them were observed more than once, so there are 23 points) with known ΔS had a standard deviation of 1.1, which is as good as the internal consistency of the ΔS system. This shows that eqn. (3.6) is adequate.

Fig. 3.3 is a contour map of ΔS in the W(Hy) vs. W(K) plane. An interesting feature is that at low values of W(Hy), W(K) <u>decreases</u> with decrease in ΔS, quite contrary to what one expects. A possible explanation is that at these low temperatures (low values of W(Hy)), the line blanketing increases, thus depressing the apparent continuum relative to the true continuum. As a result, the measured quantity W(K) underestimates the true line strength of the CaII K line, thereby producing this effect in the calibrations. However, the calibrations are still unambiguous and acceptable for the present purpose, particularly so because the measured RR Lyraes lie along a relatively narrow vertical strip of the diagram. The c-type RR Lyraes have minimum temperatures that are considerably higher than those of the ab-type variables. This problem was noted by Kemper (1982). Butler et. al. (1982) have used a correction, so that the corrected ΔS

is $0.7\Delta S_m + 3.0$, where ΔS_m is the uncorrected ΔS. This correction has been applied in this work. Column 4 in Table 3.2 shows the value of ΔS for each observation of the RR Lyrae stars of this survey. Column 5 shows the corresponding value of [Fe/H] obtained from Butler's (1975) relation:

$$[Fe/H] = -0.16\Delta S - 0.23 \qquad (3.7)$$

3.4 RADIAL VELOCITY MEASUREMENT

The radial velocities of the RR Lyrae stars were measured by finding the wavelengths of the centers of the hydrogen and the CaII K lines. These lines are several pixels wide, and their positions can therefore be determined to reasonable accuracy. In some cases, where the star is very metal poor and the CaII K line is not appreciably wider than a pixel, velocities measured from it can be quite erroneous. In such cases the CaII K line has not been used for velocity determination.

An obvious approach to determining radial velocities from these low dispersion spectra is to use the method of cross-correlation. J. R. Pier kindly made available his programs that perform cross-correlation in the Fourier domain. The spectra are rebinned so that the abscissa is log of wavelength (i.e. the abscissa is linear in velocity units) and the shift in the abscissa between two spectra gives the velocity difference between the two stars. The subdwarfs mentioned in section 3.1 served very well as templates. The region of

the spectrum from 3890Å to 5020Å, where the signal to noise is best and where the wavelength scales are best determined, was used for cross-correlation. Further details of the method have been discussed by Pier (1982). Cross correlating the various templates among each other indicated that velocities accurate to 25 km/s could be obtained. The spectra of the object RR Lyrae stars are very much noisier than the spectra of the templates, so the expected accuracy is less.

The cross-correlation technique is applied to entire regions of spectra, not merely to individual lines. Weak lines that are otherwise not very prominent add their contributions to the velocity determination. In the case of well sampled spectra this is a gain, but in undersampled spectra this is a severe problem since it is necessary to rebin the spectra to a logλ scale. In rebinning an undersampled spectrum, there is no estimation of noise, and the rebinned spectrum does not inspire very much confidence. The situation gets worse with increase in noise. The rebinning process can amplify noise in a way that affects the cross-correlation process.

An alternative process is to fit model profiles to the hydrogen and CaII K lines. This can be done without rebinning the spectrum. The profiles described in section 3.2 (on equivalent width measurement) are very well-suited for the purpose. One of the free parameters for fitting these hybrid profiles is the wavelength of the center of the line. The best fit to this parameter is denoted by λ_o, and the rest wavelength is denoted by λ_r. The observed velocity v'_o is then given by:

$$v_o' = (\lambda_o/\lambda_r - 1)c - v_{hel} \qquad (3.8)$$

where c is the velocity of light, and v_{hel} is the correction due to the Earth's motion around the Sun.

The internal accuracy of this measurement is easily estimated from the spread in the values obtained from the four lines (Hβ, Hγ, Hδ and CaII K). For the subdwarfs and the bright RR Lyrae stars used for ΔS calibration, the internal accuracy was typically around 10 km/s (1 σ) for the average from the four lines, and hence around 20 km/s for an individual line. For the faint RR Lyrae spectra the corresponding accuracy depends on the quality of the spectrum, and is typically about 25 km/s.

The external errors can be random or systematic. Systematic errors can be corrected by comparing the values of v_o' for the subdwarfs with the "true" values v_t determined for them by coude spectroscopy (J. L. Greenstein, priv. comm.), which are accurate to about 2 km/s.

$$\text{Define } v_d = v_t - v_o' \qquad (3.9)$$

The average value of v_d from all the measurements of the subdwarfs is denoted by v_{corr}. Non-zero values of v_{corr} arise when the comparison lamps and stars illuminate the spectrograph's entrance slit in systematically different ways. It can also happen when CCD's are used, since charge transfer inefficiencies may occur, which affect the

emission lines from arc lamps differently from absorption lines from these stars. The value of v_{corr} was found to be +17 ($\pm$4) km/s. When the spectra were smoothed over 3 pixels, v_{corr} was found to be +46($\pm$6) km/s. This difference in v_{corr} indicates that charge transfer inefficiency is the source or the problem. The corrected observed velocity is given by v_o, where

$$v_o = v_o' + v_{corr}$$

The standard deviation for v_d is a measure of the random errors in the velocity measurement. This was found to be about 22 km/s for unsmoothed spectra and 30 km/s for spectra smoothed over 3 pixels. These values are significantly larger than the internal errors stated in the previous paragraph. Since the subdwarfs observed have the best signal to noise or all the observations in this study, these represent the best possible accuracy.

The internal random errors, denoted by σ_i, are due to the noise in the spectra and the extent to which that limits the determination of line centers. On the other hand, the 22 km/s error estimate, denoted by σ_b, includes all other random errors (e.g. if the seeing was comparable to the slit width and the star "leaned" to one or other edge of the slit during the exposure, a noticeable change is produced in the measured velocity — yet this is a random error, since the star could lean to either edge). In other words, σ_i denotes the error in finding the line center because of noise in the spectrum, whereas σ_b denotes the total error incurred when the signal to noise is very

high. We can estimate the external random errors, i.e. those that are incurred regardless of the noise in the spectrum, and denote them by σ_s.

$$\sigma_s^2 = \sigma_b^2 - \sigma_i^2 \qquad (3.10)$$

Taking the typical values of σ_b and σ_i for the bright subdwarfs to be about 22 km/s and 10 km/s respectively, we get a value of about 20 km/s for σ_s.

We are interested in the center of mass velocity v_γ of the RR Lyrae stars. The observed hydrogen and CaII line velocities must be suitably corrected to obtain this. This is a complicated problem, because the lines are formed in different mass layers at different phases. Hγ and CaII K line velocities for X Arietis and SU Draconis as a function of phase are available from the works of Oke, Giver and Searle (1962), and Oke (1966), respectively, and that for SW Andromedae is known from Oke (priv. comm.). In these works the γ-velocities of the respective stars are derived accurately from the weaker metallic lines and detailed consideration of the mass layers from which the lines arise. The hydrogen and CaII K line velocities differ from the γ-velocity by amounts that depend on the phase. These phase dependent corrections are very nearly the same for all the above stars (in the phase interval .15 to .85) and so may be assumed to be the same for all ab-type stars. Using these, v_γ may be derived from the observed velocity of any ab-type RR Lyrae star, provided the phase at which the observation was made is known and lies

between 0.15 to 0.85. For the c-type RR Lyrae stars, the corrections are different because their velocity amplitudes are much smaller. The work on VZ Cancri (Oke and Danziger) , which is on the same lines as the above-mentioned works, unfortunately does not report hydrogen line velocities, although an accurate determination of the γ-velocity is available. It was assumed that the hydrogen and CaII line velocity amplitudes are 40 percent higher than the weaker metallic lines at all phases, and so the metallic line velocities for VZ Cancri were used to infer the hydrogen and CaII line velocities at all phases. The error σ_c in applying these corrections is estimated at about 10 km/s. The total estimated error σ in the γ-velocity is then given by

$$\sigma^2 = \sigma_i^2 + \sigma_s^2 + \sigma_c^2 \qquad (3.11)$$

$$\text{or, } \sigma^2 = \sigma_i^2 + (22.4)^2 \text{ (km/s)}^2 \qquad (3.12)$$

Columns 7 and 8 of Table 3.2 list the γ-velocity and the estimated error in the γ-velocity for all the RR Lyrae stars for which velocity determinations have been made. The interpretation of the velocities in the context of the dynamics of the Galaxy is the subject of another chapter.

3.5 SPECTROPHOTOMETRIC OBSERVATIONS AND DERIVATION OF INTERSTELLAR EXTINCTION

From a systematic study of field RR Lyrae stars, Sturch (1966) has shown that the (B-V) colors or all ab-type RR Lyrae stars remains constant to within 0.03^m during the phase interval 0.5 to 0.85. Further, he showed that if line blanketing and extinction corrections are applied, the corrected color $(B-V)_{o,c}$ in this phase interval is the same for all ab-type RR Lyrae stars. This is equivalent to saying that during the indicated phase interval, all RR Lyrae stars are at the same effective temperature. Oke and Bonsack (1960), Oke, Giver and Searle (1962), and Oke (1966) made detailed spectrophotometric measurements of RR Lyrae, SU Draconis and X Arietis. They found for all of the above stars, θ_e in the phase interval 0.5 to 0.85 is between 0.82 and 0.83, i.e. T_e stays between 6000 and 6150 ^oK. Unpublished work by Oke (priv. comm.) gives the same result for SW And. These four stars, although a small sample, cover the entire range or metallicity, and corroborate the findings of Sturch. This gives us the confidence to extend this to all ab-type RR Lyrae stars. It is asserted that all ab-type RR Lyraes have T_e = 6100^oK, and log g = 2.0 (from the above mentioned works of Oke and collaborators). Actually log g varies between 1.5 and 2.5, and can vary somewhat from star to star, but this does not affect the output flux between 4000Å and 7000Å for stars with temperatures near 6000^oK. It is now possible to derive the reddening of a star by comparing its energy distribution between 4000Å and 7000Å with the model energy distribution for a star with the same values of T_e and log g, and the

appropriate value of [Fe/H] (in this case the values obtained from spectroscopy and ΔS measurement were used).

McDonald (1977) has discussed a somewhat similar way of deriving E(B-V) from the minimum temperatures of RR Lyrae stars, and Burstein and Heiles (1978) have used his formulae to obtain E(B-V) for many brighter field RR Lyrae stars in their studies of E(B-V) and neutral hydrogen column density correlation. McDonald's relations involve B and V photometry at minimum light, and the line blanketing phenomena are accounted for by adopting different relations for different metallicity domains. The method outlined here is much more general. By using spectrophotometry, all wavelength regions are exposed simultaneously, and the result is free of many systematic errors associated with two-color photometry. The method described here can use much larger wavelength domains and hence obtain more accurate results.

The spectrophotometry was done with the SIT Vidicon detector digital spectrograph on the 60 inch telescope at Palomar mountain. A 300 lines/mm grating was used and the wavelength range from 3700Å to 7100Å was covered. The entrance slit was 6 arc-seconds, so that all the light would enter the spectrograph. Observations were made during the phase interval 0.5 to 0.85 (using the ephemeris in Table 2.2), and only when the seeing was 3 arc-seconds or better. All observations were made at airmass less than 1.5 to minimize complications due to atmospheric dispersion and higher order effects in atmospheric extinction. For each observation, the spectrograph slit was oriented

in the optimum manner (Filippenko 1982) so that atmospheric dispersion would be along the slit and not across it. Standard stars for the purpose of flux calibration were observed several times a night at various values of the airmass. The star X Arietis, which is an RR Lyrae star with a known reddening, was also observed to confirm the success of this procedure for deriving reddening.

Initial reduction to one-dimensional spectra, wavelength fitting, atmospheric extinction corrections, and flux calibration using the observed standards was performed using a program by T. Boroson. The reduced spectra were then compared to appropriate model-atmosphere fluxes calculated by Kurucz (1979). Fig. 3.4 shows the plot of AB(star) - AB(model) + C vs. $1/\lambda$,

where $AB = -2.5\log f - 48.60$ (3.13)

and where 'f' is the flux in ergs/cm^2/s/Hz, and C is an arbitrary number that scales the model fluxes. The figure shows considerable scatter about the straight line that has been fitted through it. However, the scatter is due to noise, and is random. Since there are so many points, the line of regression is quite accurately determined, even though there is large scatter in the individual points. The slope of the line of regression furnishes the reddening through Whitford's (1959) reddening law.

The limited dynamic range of the SIT detector is a major inconvenience. For the faint objects the night sky contribution to the spectrum is very high, and to be able to properly subtract its effect it would be preferable to have a detector with larger dynamic range. Also, only the spectral range from 4000Å to 6700Å could be utilized, because of the poor response above 6700Å. Longer exposures would saturate the spectra near 4500Å. The stronger night sky emission lines (4358Å, 5460Å, 5577Å and 5890Å) were saturated in the spectra of faint stars, and the intensities at these wavelengths were reconstructed by interpolation from neighboring wavelength points. The spectrum in a 200Å wide region around 5900Å is also poor because of the high-pressure sodium lamp glow from the cities.

Four separate spectra of X Ari were examined and E(B-V) for X Ari were derived from each of them. The values obtained are: 0.17, 0.19, 0.20 and 0.20. Oke (1966) has derived 0.19, Sturch (1966) gives 0.222, and Burstein and Heiles (1978) give 0.16.
Burstein and Heiles (1978) have pointed out that Sturch's values of E(B-V) are too high by about 0.03. At any rate, the values obtained by a single measurement using the method presented here has no definite systematic difference from other values in the literature.

Table 3.3 shows the derived values of E(B-V) for the stars for which this measurement was made. In addition there are observations of II V6, II V601 and IV V105, but ΔS is not yet known for these stars, so values of E(B-V) for them have not been derived.

There are errors in the determination of E(B-V) if the stars are not at T_e = 6100°K and log g = 2.0, or if the metallicity has been incorrectly determined. An error of 100°K in temperature produces an error of 0.015 in E(B-V). The effect of misjudging log g by 0.5 introduces an error of .008 in E(B-V), and an error of 0.5 in [Fe/H] at [Fe/H] = 1.5 results in an error of 0.015 in the same. A fiducial temperature T_e = 6100°K has been used in the calculations. This figure is known to within about 100°K. The minimum temperatures of individual stars may differ from one another by about 100°K. The surface gravities are known to within 0.5, and the accuracy in [Fe/H] is about 0.4. Consequently we should expect the accuracy in E(B-V) from the measurement of any one star to be only about 0.04. Errors in flux calibration deteriorate the result further. If a larger range of spectrum is observed the results may be improved, particularly if part of the Balmer continuum is included. By observing fluxes from 3100Å to 10,000Å, it will be possible to determine T_e, log g and E(B-V) separately, so that we no longer have to depend on assumptions about a fiducial minimum temperature.

It seems appropriate to take the average value for all measurements of E(B-V) for stars in any given field, and adopt this average as the reddening in that field. Since all the objects are very far out in the halo, it is presumed that the extinction is not affected by how far away they are, since essentially all of the extinction takes place within a few kpc. For field III the mean extinction obtained in this way corresponds to an E(B-V) of 0.06. For fields II and IV (for which there are admittedly an unsatisfactory

number of observations), the average values for E(B-V) are 0.07 and 0.06 respectively.

Using the cosecant formula by Sandage (1973), E(B-V) of .044 is obtained for fields III and IV, while E(B-V) of .064 is obtained for field II. The reddening maps of Burstein and Heiles (1981) indicate E(B-V) of .03 to .06 for fields III and IV, and .06 to .09 for field II. These maps are not patchy in these regions of interest. Kinman and Mahaffey (1982) have used a combination of methods to determine E(B-V) for their fields. Their fields VI and VII lie partially over fields II and III respectively of this work. They have found E(B-V) to be .06 and .05 for their fields VI and VII respectively, which are in agreement with what is obtained here for the corresponding fields II and III of this work. E(B-V) values or .07, .06 and .06 are adopted for fields II, III and IV respectively.

While determining E(B-V) in the manner described here, it has been seen that a few stars, e.g. II V104 and III V102 do not reach minimum temperatures as low as 6100°K. Their flux distribution at the minimum light phase resembled that from a star at 6500°K or so. The chances that this is due to an error in the ephemerides is small, since the value of B indicated by the observed flux at 4500Å corresponds to the value of B expected for the star when it is at minimum light. It is possible that some RR Lyrae stars do not get to as low as 6100°K at minimum temperature, and it is of interest to investigate whether this tells us anything of significance. It is necessary to confirm this anomalous behavior, and further observations

with better signal and wider wavelength coverage are in order.

REFERENCES

Burstein, D. and Heiles, C. 1978, Ap.J., 225, 40.

Burstein, D. and Heiles, C. 1981, A.J., 87, 1165.

Butler, D. 1975, Ap.J. 200, 68.

Butler, D., Kraft, R. P., Miller, J. S., and Robinson, L. B. 1973, Ap.J., 179, L73.

Butler, D., Kemper, E., Kraft, R. P., and Sumtzeff, N. B. 1982, A.J., 87, 353.

Filippenko, A. V. 1982, Pub.A.S.P., 94, 715.

Griffin, R., and Griffin, R. 1979, A Photometric Atlas of the Spectrum of Procyon.

Kinman, T. D., Mahaffey, C. T., and Wirtanen, C. A. 1982, A.J., 87, 314.

Kemper, E. 1982, A.J. 87, 10.

Kurucz, R. L. 1979, Ap.J. Supp., 40, 1.

McDonald, L. H. 1977, Ph. D. Thesis, University of California, Santa Cruz.

Oke, J. B. 1966, Ap.J., 145, 468.

Oke, J. B., and Bonsack, S. J. 1960, Ap.J., 132, 417.

Oke, J. B., and Danziger, I. J. 1967, Ap.J., 147, 151.

Oke, J. B., Giver, L. P., and Searle, L. 1962, Ap.J., 136, 393.

Oke, J. B., and Gunn, J. E. 1982, Pub.A.S.P., 94, 586.

Oke, J. B., and Gunn, J. E. 1983, Ap.J., 266, 713.

Pier, J. R. 1982, Ph. D. Thesis, California Institute of Technology.

Preston, G. W. 1959, Ap.J., 130, 507.

Sandage, A. R. 1973, Ap.J., 183, 711.

Sturch, C. 1966, Ap.J. 143, 744.

Van de Hulst, H. C., and Reesinck, J. J. M. 1947, Ap.J., 106, 121.

Whitford, A. E. 1959, A.J., 63, 204.

FIGURE CAPTIONS

Figure 3.1

Typical spectra of three of the survey RR Lyrae stars (II V306, II V401 and II V101) are shown. These have been taken with the blue camera of the double spectrograph at the Palomar 200 inch telescope. The y-axis represent AB magnitudes which are explained in the text.

Figure 3.2

This illustrates the multiple line profile fitting by non-linear least squares fitting. The data are shown as points, and the solid line is the profile that has been fit. The object is II V306.

Figure 3.3

ΔS contour map in the W(K) W(Hy) plane obtained by relating the line strength measurements of bright field RR Lyrae stars whose ΔS values are well known. The points mark the observed locations of the survey RR Lyrae stars in this diagram.

Figure 3.4

The points show residuals from comparison of flux spectrum and model atmosphere when plotted vs. $1/\lambda$. The line is the fit whose slope gives the reddening. See text for details.

TABLE 3.1

List of wavelength bands for continuum selection

Blue wavelength (Angstroms)	Red Wavelength (Angstroms)
3716	3717
3729	3730
3742	3743
3755	3756
3765	3766
3782	3785
3810	3813
3853	3874
4000	4040
4060	4075
4145	4170
4235	4255
4410	4450
4506	4530
4600	4636
4685	4722
4770	4795
4940	4970
5000	5020
5055	5077
5130	5154
5200	5220
5280	5295
5410	5430

TABLE 3.2

Abundances and Observed Velocities

OBJECT NAME (1)	JD at mid exposure 2,440,000+ (2)	Mean Phase (3)	DeltaS (4)	[Fe/H] (5)	Center of mass vel (km/s) (6)	Error in vel (km/s) (7)
II V3	4716.768	0.55	6.0	-1.2	+191	67
II V104	5327.934	0.32	10.3	-1.9	+48	23
II V208	5327.986	0.52	8.7	-1.6	-10	28
II V208	5434.665	0.56	6.3	-1.3	+15	34
II V306	4912.970	0.52	5.8	-1.2	-3	27
II V401	4962.822	0.51	2.5	-0.6	+33	39
II V501	5288.932	0.60	6.7	-1.3	-80	29
II V502	5324.940	0.69	6.0	-1.2	-179	46
II V504	4961.861	0.75	8.5	-1.6	+116	26
III V101	4962.886	0.74	11.6	-2.1	+87	33
III V102	4961.837	0.82	8.4	-1.6	+93	24
III V201	5328.010	0.77	10.1	-1.8	+255	54
III V202	5325.066	0.53	9.2	-1.7	-126	26
III V202	5050.826	0.12	-	-	-107	27
III V203	5434.722	0.57	10.0	-1.8	+96	45
III V206	5433.685	0.93	8.5	-1.6	+239	45
III V302	5286.892	0.52	6.0	-1.2	+58	33
IV V103	5324.704	0.90	9.4	-1.7	-272	25
IV V106	4914.623	0.73	1.0	-0.4	-293	51
IV V107	5324.733	0.71	7.7	-1.5	-74	36
IV V401	5324.625	0.85	6.9	-1.3	-207	34

TABLE 3.3

Derived Reddening Values

OBJECT	JD at mid exposure 2,444,000+	Mean Phase	E(B-V)
X Ari	5341.70	0.53	0.17
X Ari	5343.65	0.50	0.20
X Ari	5343.71	0.60	0.19
X Ari	5347.66	0.65	0.20
II V3	5343.72	0.62	0.04
II V3	5343.73	0.63	0.06
II V208	5348.95	0.67	0.11
III V101	5348.91	0.49	0.06
III V201	5348.85	0.77	0.01
III V202	5343.76	0.61	0.05
III V202	5347.95	0.78	0.05
III V206	5347.78	0.67	0.09
III V206	5348.88	0.77	0.10
IV V107	5343.63	0.83	0.12
IV V107	5348.64	0.56	0.06
IV V301	5348.61	0.81	0.07
IV V401	5343.67	0.54	0.00

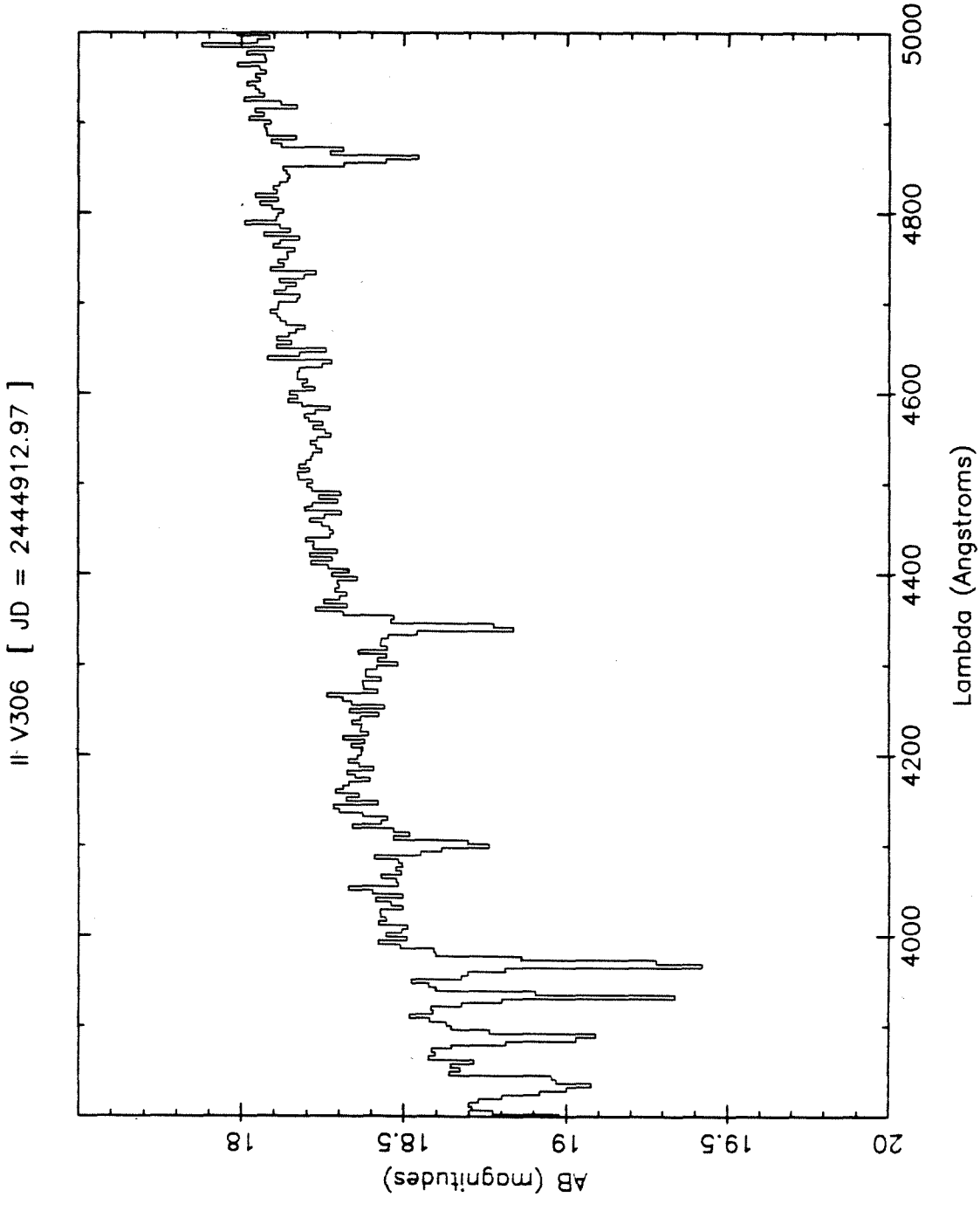
II V306 [JD = 2444912.97]
AB (magnitudes)
18
18.5
19
19.5
20
Lambda (Angstroms)
4000
4200
4400
4600
4800
5000

Fig. 3.1a

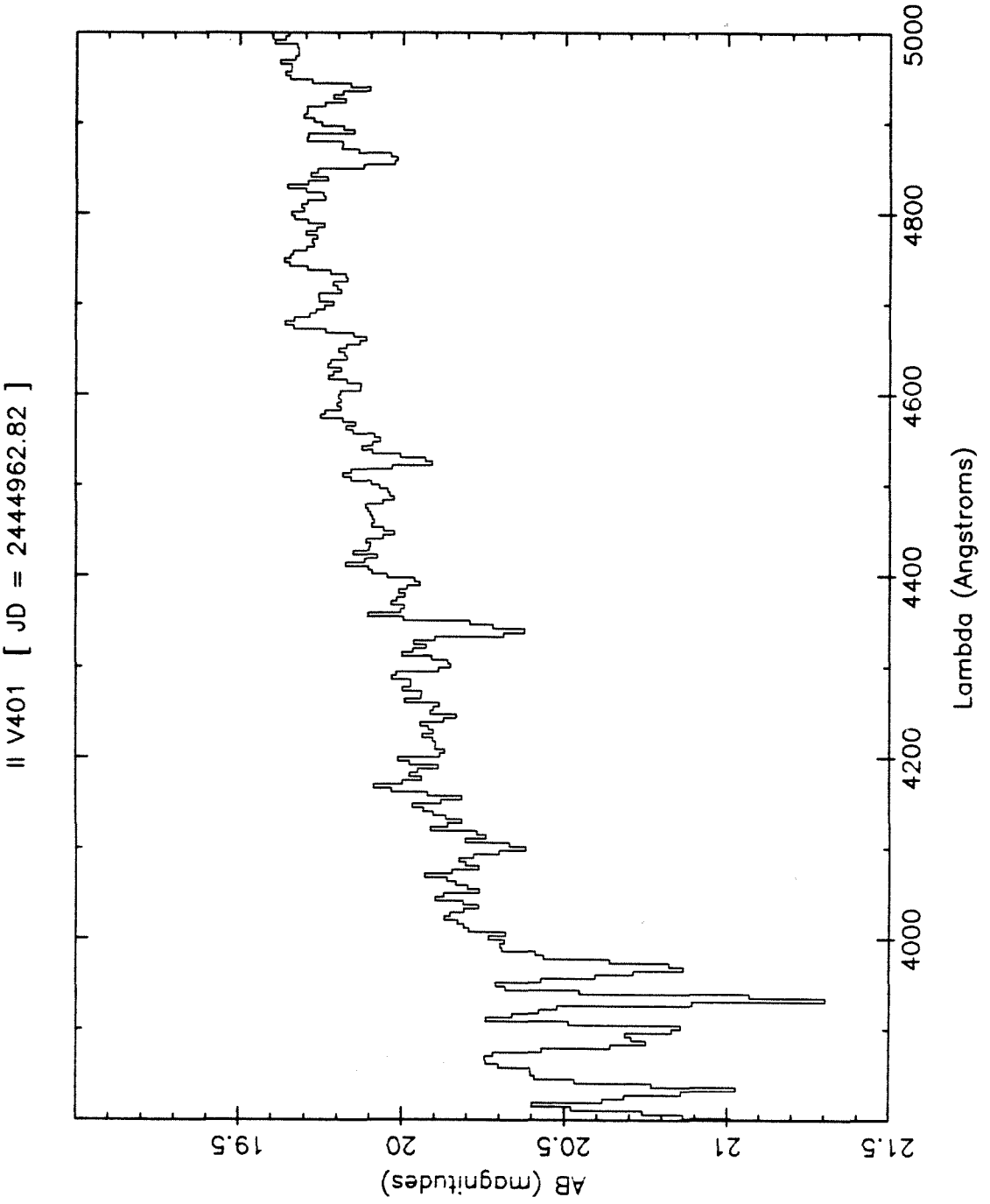
II V401 [JD = 2444962.82]
AB (magnitudes)
19.5
20
20.5
21
21.5
4000
4200
4400
4600
4800
5000
Lambda (Angstroms)

Fig. 3.1b

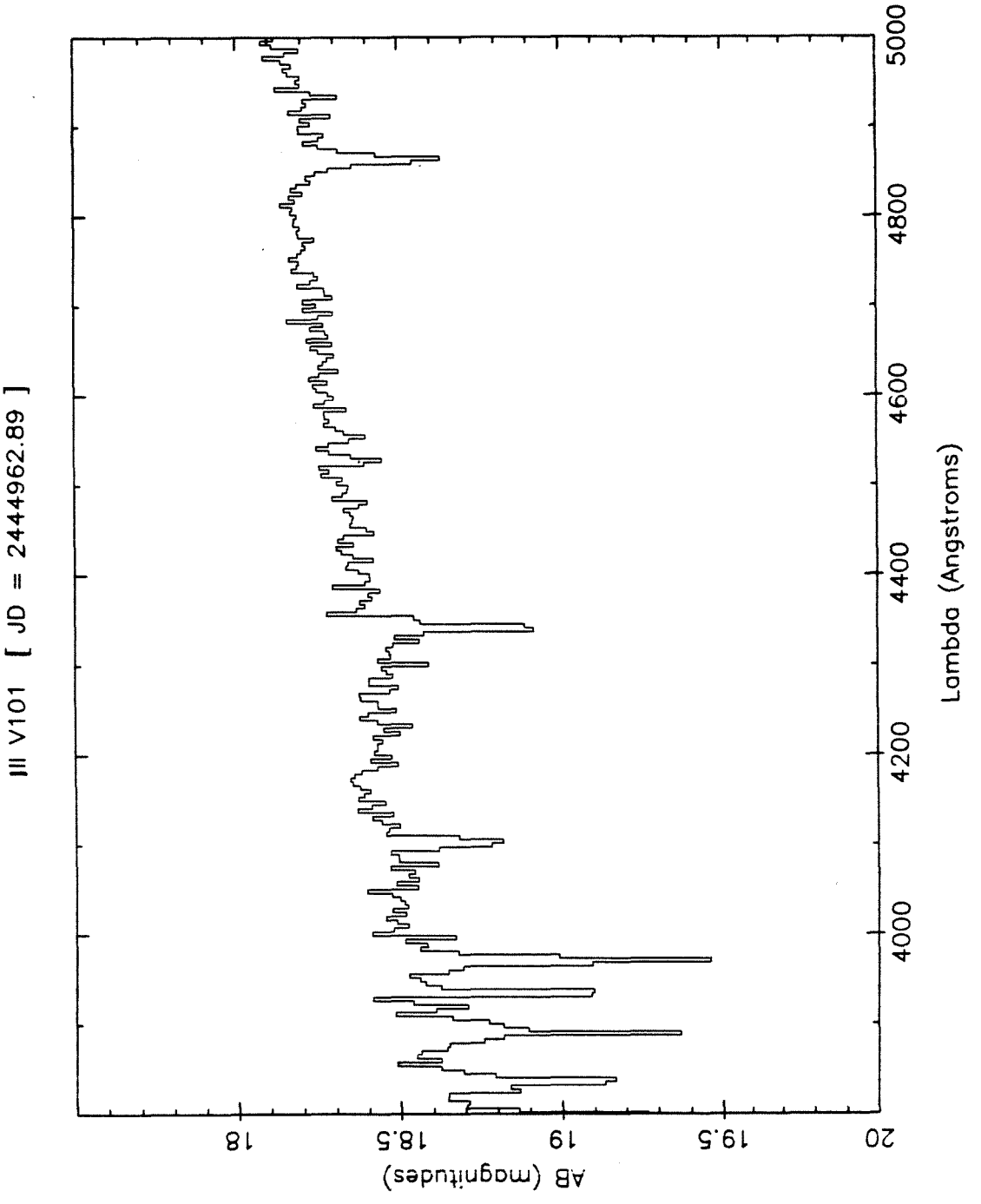
III V101 [JD = 2444962.89]
AB (magnitudes)
18
18.5
19
19.5
20
4000
4200
4400
4600
4800
5000
Lambda (Angstroms)

Fig. 3.1c

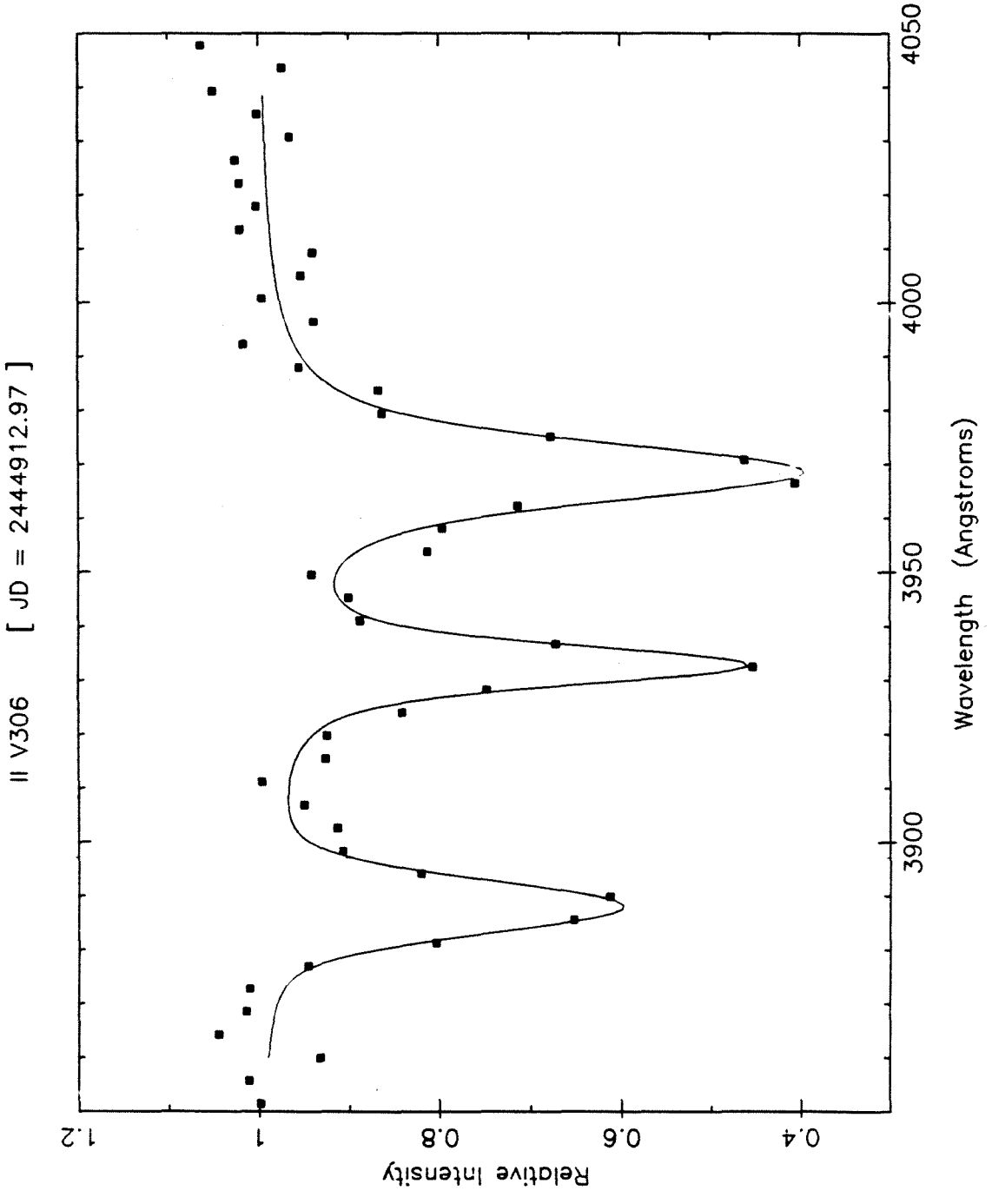
II V306 [JD = 2444912.97]
Relative Intensity
0.4
0.6
0.8
1
1.2
3900
3950
4000
4050
Wavelength (Angstroms)

Fig. 3.2

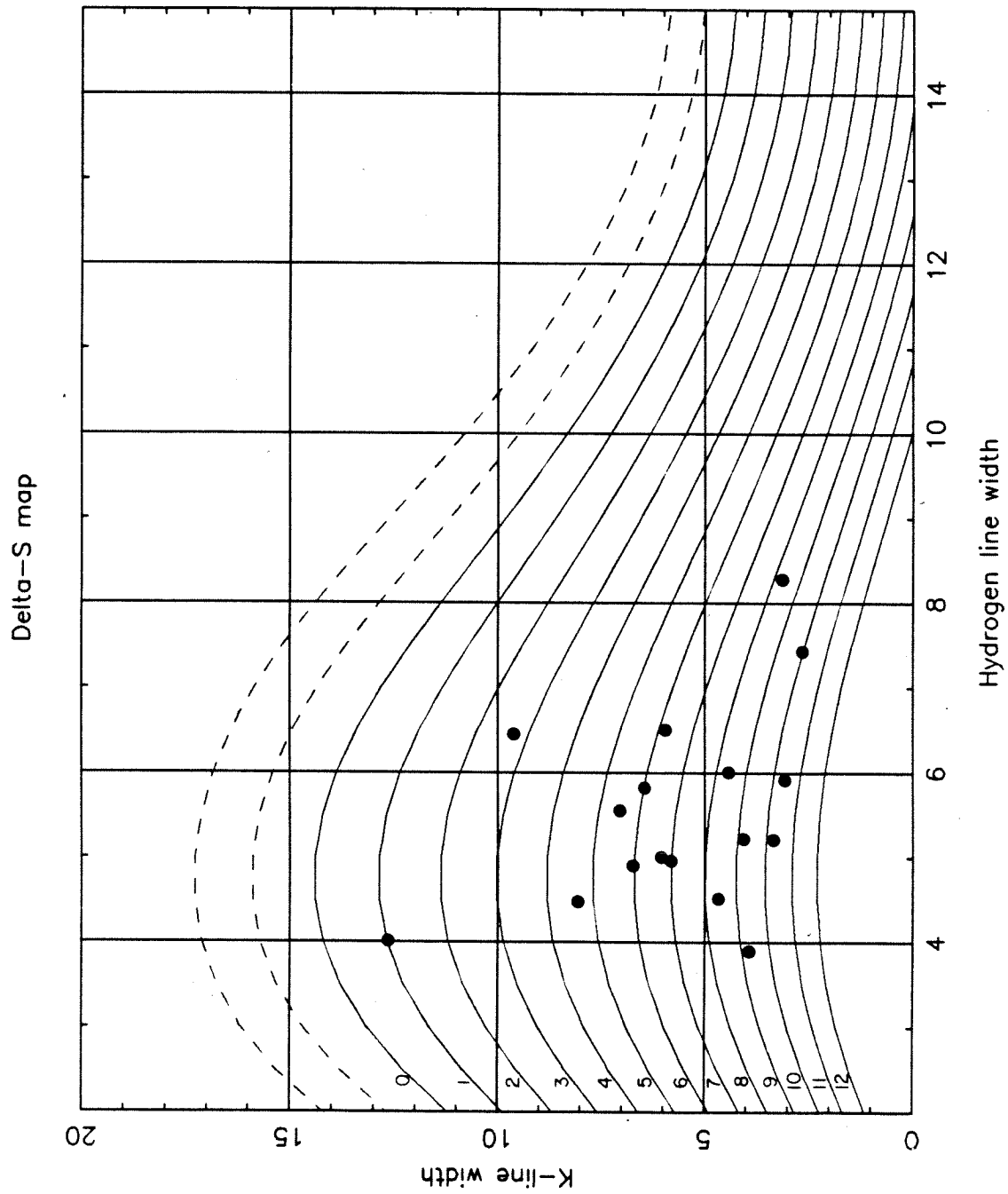
Delta-S map
K-line width
Hydrogen line width
0
5
10
15
20
4
6
8
10
12
14
0
1
2
3
4
5
6
7
8
9
10
11
12

Fig. 3.3

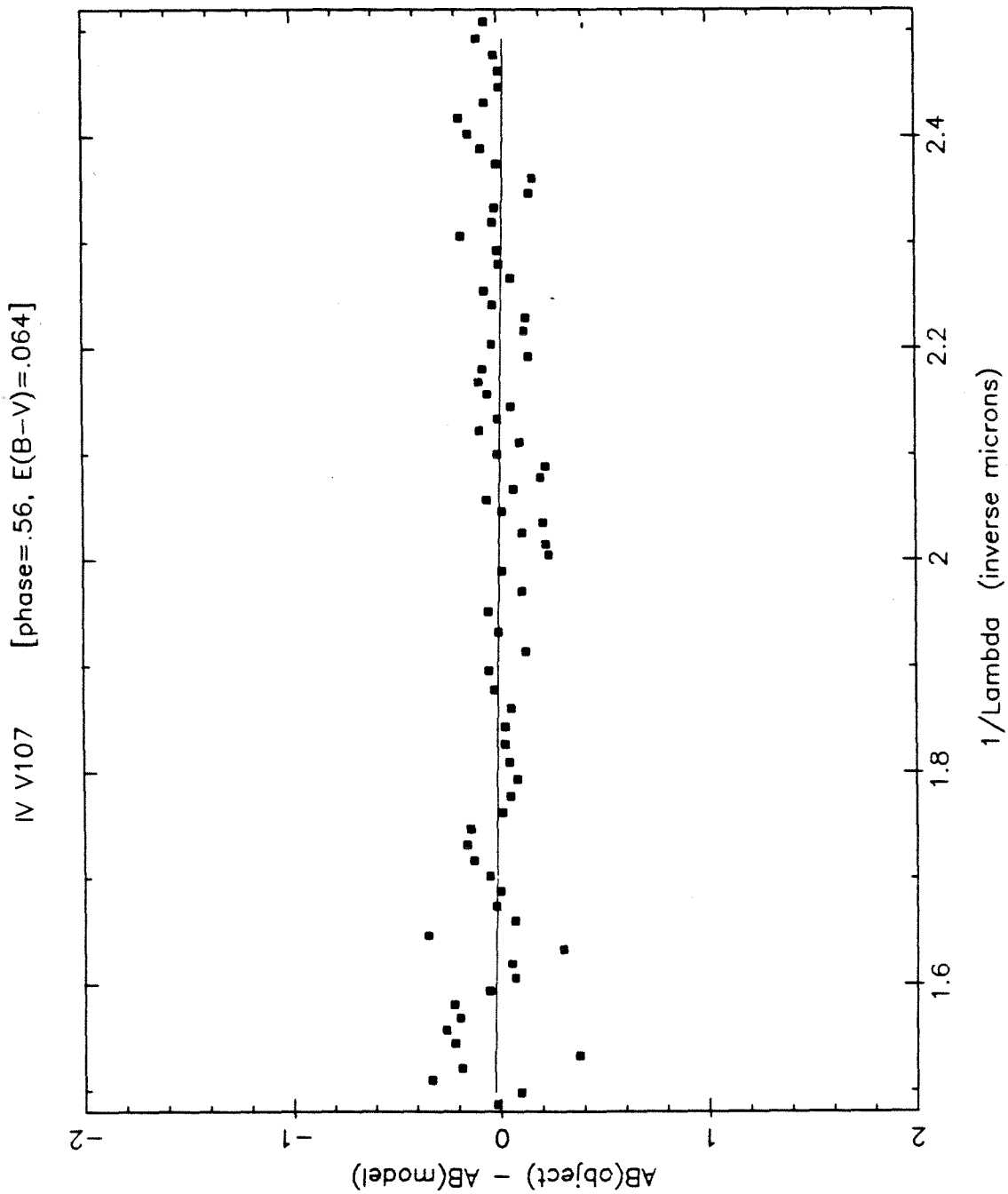
IV V107 [phase=.56, E(B-V)=.064]
AB(object) - AB(model)
-2
-1
0
1
2
1.6
1.8
2
2.2
2.4
1/Lambda (inverse microns)

Fig. 3.4

CHAPTER 4

NUMBER DENSITY AND ABUNDANCE DISTRIBUTION OF RR LYRAE STARS IN THE GALAXY

4.1 ABSOLUTE MAGNITUDES AND DISTANCES

RR Lyrae stars are perhaps the best calibrated astronomical standard candles, and distances obtained from individual objects are accurate to 20 percent or better. In a series of papers, Sandage et. al. (1981) and Sandage (1981a,b, and 1982a,b) have demonstrated the relationship between periods, luminosities and amplitudes of RR Lyrae stars in globular clusters and in the field, and have justified them on the basis of stellar evolution theory. A very elegant explanation of the "Oosterhoff effect" is put forward. The period, amplitude, luminosity (P-L-A) relation allows us to derive the luminosity of an individual RR Lyrae star with respect to a fiducial luminosity of the horizontal branch of the globular cluster M3. Equation (8) of Sandage (1981c) is the explicit form of the P-L-A relation, provided the mass of the RR Lyrae star under consideration is the same as that for the RR Lyrae stars in M3. Equation (9) of the same paper shows the dependence of zero age horizontal branch mass with metallicity. The general theoretical P-L-A relation, obtained by combining the above cited equations reads as follows :

$$M_{bol} = M_{bol}(M3) - 3.0(\log P + .129\,Amp(B) + .088) + .133([Fe/H] - [Fe/H](M3)) \qquad (4.1)$$

where M_{bol} is the mean bolometric absolute magnitude of an ab-type RR Lyrae star with period 'P' days, light amplitude in B of 'Amp(B)'

magnitudes, and metallicity index [Fe/H]. $M_{bol}(M3)$ is the mean bolometric absolute magnitude of an RR Lyrae star in the globular cluster M3 which has a mean apparent bolometric magnitude of 15.52. [Fe/H](M3) is the value of [Fe/H] for M3. From an inspection of Fig. 3 of Sandage (1982a), it is reasonable to conclude that (4.1) is valid for c-type RR Lyrae stars as well, provided we replace log P by (log P + .3).

Notice that the effect or changing [Fe/H] by 1.0 in equation (4.1) changes M_{bol} by $.13^m$. Sandage was not able to see this effect in his data, and in any case the effect is small enough to be negligible. The relations used in this work are :

$$M_{bol} = M_{bol}(M3) - 3.0(\log P + .129\,Amp(B) + .088) \qquad (4.2)$$

for ab-type stars, and

$$M_{bol} = M_{bol}(M3) - 3.0(\log P + .129\,Amp(B) + .388) \qquad (4.3)$$

for the c-type stars.

Baade-Wesselink determinations for absolute magnitudes of field RR Lyrae stars can be used to determine $M_{bol}(M3)$ in the above equations. From the works or Oke and Bonsack (1960), Oke et. al. (1962), Oke (1966), McDonald (1977), and Manduca et. al. (1981), the value of 0.63 is obtained for $M_{bol}(M3)$. An uncertainty of about 0.30 in this quantity is the major source or uncertainty in

distances. Bolometric corrections from Rabin (1980) were used in the above determinations.

The periods and B amplitudes of the RR Lyrae stars of this survey were read from chapter 2 and used in eqn. (4.2) or (4.3) (as the case may be), to derive absolute bolometric magnitudes M_{bol}. To obtain the absolute 'B' magnitude M_B, ($\langle B \rangle - \langle V \rangle$) was taken to be 0.26^m and a bolometric correction of −0.08 was adopted. Thus,

$$M_B = M_{bol} + 0.34 \tag{4.4}$$

The extinction A_B in the 'B' wavelength band is given from Whitford's law (Whitford (1959)):

$$A_B = 4.0E(B-V) \tag{4.5}$$

and E(B−V) values adopted in chapter 3 were used. The heliocentric distance "r" to an RR Lyrae star whose mean apparent 'B' magnitude is $\langle B \rangle$ is then given by

$$\log_{10} r = 0.2(\langle B \rangle - M_B - A_B + 5) \tag{4.6}$$

where r is in pc.

Column 2 of Table 4.1 gives the values of r derived in the above manner for each of the RR Lyrae variables of this survey. Columns 3 and 4 of Table 4.1 give the new galactic coordinates l^{II} and b^{II} respectively.

4.2 A GALACTOCENTRIC SPHERICAL COORDINATE SYSTEM

A major portion of the discussion of the distribution, chemical abundances, and kinematic behavior of the RR Lyraes from this survey will assume spherical symmetry in the far halo of the Galaxy. It is convenient, therefore to adopt a spherical polar coordinate system centered on the Galactic center. Fig. 4.1 illustrates the system to be used. An arbitrary spatial point 'S' is defined by the three quantities R, Θ, and ϕ, where R is the distance from the Galactic center, Θ is the angle away from the North Galactic Pole, and ϕ is the azimuthal angle whose zero is along the line from the Galactic center to the Sun, and in the sense that (R,Θ,ϕ) forms a right handed system.

The transformation equations are derived in an appendix (Appendix I) to this chapter. The Galactocentric coordinates (GCC) of the RR Lyrae stars of this survey are listed in columns 5 to 7 of Table 4.1 . Column 8 of Table 4.1 lists the height Z above the Galactic disc, where positive values indicate departures towards the Galactic north.

4.3 SPACE DENSITIES OF THE SURVEY RR LYRAE STARS AND THE RADIAL DENSITY DISTRIBUTION IN THE GALACTIC HALO

The present survey probes the halo out to 40 kpc. Apart from a very few globular clusters, there is no other class of objects that has been studied that far out in the halo. Although any attempt to infer the stellar density distribution from the density distribution of RR Lyrae stars is severely frought with selection effects, it is nevertheless worth an attempt since these stars are the only known probes that are known out to large distances in the halo.

Kinman's technique of obtaining space densities (Kinman et. al. 1965), where the volume element is the volume that contains four stars (consecutively arranged in distance), may not be sound at the extremely low densities encountered here. At very low densities, the distance intervals in each volume element become large enough that this non-linearity introduces large errors in the derived space densities.

The method applied here uses the following relation:

$$N = \int \omega \rho(r) r^2 dr \qquad (4.7)$$

where N is the total number of objects found in a solid angle ω along a given direction, r is the line of sight distance (in this case the heliocentric distance), and ρ is the number density of RR Lyrae stars. Equivalently,

$$\rho(r) = \omega^{-1} r^{-2} \, dN/dr \qquad (4.8)$$

The total number of objects N is plotted versus r and the slope of the smooth curve that best fits these points (by eye) can be found at any desired value of r. The slope is the value of dN/dr at that value of r, and the density at that point is given by equation (4.8). The densities obtained in this way were corrected for selection effects by dividing by 0.8, which is a mean correction for incompleteness (see Fig. 2, Chapter 1); finer discrimination (i.e. variation of discovery probability with period and from one field to another) seems meaningless in the light of so many other uncertainties. The Galactocentric distance R of this point is calculated, since we are interested in the run of ρ versus R, and not versus r.

Fig. 4.2(a) is the N versus r diagram for (the anti-center fields) FII and FIII taken together. Fig. 4.2(b) is the same diagram for (the apex field) FIV, and since it has only about half the objects, is more poorly defined. Fig. 4.3(a) is a plot of log ρ versus log R for RR Lyrae stars. The densities derived from Fig. 4.2(a) are shown in Fig. 4.3(a) by filled circles, and those from Fig. 4.2(b) by open circles. The errors in the density measurement come mainly from the uncertainty of the slopes in the N vs. r diagram, and errors were estimated from a comparison of the most extreme allowable slopes and the best fit slopes. For comparison, Fig. 4.3(b) shows log ρ versus log R, where ρ is derived from the data from this survey, but using the method of Kinman et. al. (1965). There is no significant difference, and the two methods give results that are

consistent within the estimated errors.

Fig. 4.3(a) also shows the RR Lyrae densities obtained by previous investigators. The triangles represent space densities derived by Kinman et. al. (1965), and Kinman et. al. (1966) from their RR Lyrae surveys of the region near MWF 361 and the North Galactic Pole (NGP) respectively. Their density values have been corrected by a factor of 7/6 to roughly account for the fact that they excluded the c-type RR Lyraes. The crosses represent Oort and Plaut's (1975) values for the region in the Galactic bulge and inner halo. All the points in this figure, except perhaps the higher of the two triangles at log R ~ 0.7 (from Kinman et. al.'s MWF 361 field), are clear of the Galactic disk, and represent densities in the Galactic bulge and halo.

In interpreting Fig. 4.3(a) two things must be kept in mind:
a) The density distribution need not be spherical, and
b) Abundance gradients will affect the number of RR Lyrae star density. The fraction of the total stellar density that the RR Lyrae density represents, varies by up to two orders of magnitude depending on the age, metallicity and the enigmatic "second parameter" of the relevant stellar population. Thus the only instances when the RR Lyrae densities indicate the general stellar densities are:
(1)when we have a homogeneous population, or
(2) when we have a uniformly mixed population.
In the following section (4.4), it will be shown that there is a very large range of abundances for these RR Lyrae stars, and that they are clearly not drawn from a homogeneous population. By case (2) we mean

that the population mix is the same everywhere, or that no gradients are seen in the features that characterize differences of population.

The crosses in Fig. 4.3(a) (from Oort and Plaut) and the lower of the two triangles at log R ~ 0.7 (from Kinman et. al.'s MWF 361 survey), all have altitudinal angles θ that are within 20 degrees of the rotation axis. The triangle at log R ~ 1.3 has $\theta \sim 35^{o}$, and all the other points are more than 60^{o} away from the rotation axis. Even if the density distribution is not spherical, the crosses and the lower of the two triangles at log R ~ 0.7 should lie along a roughly continuous curve. This is indeed the case, and these data points are consistent with an R^{-3} density variation. Similarly, all the remaining points (with the possible exception of the triangle at log R ~ 1.3) should lie along a smooth curve. This is also the case, and from log R ~ 0.7 to log R ~ 1.3, the observed densities are also consistent with an R^{-3} law. The break in these two lines at log R ~ 0.7 can then be explained by invoking an oblate spheroidal density distribution model, with axial ratio ~ 0.5, which is the result obtained by Kinman et. al. (1965).

The above argument is not without contradictions. Oort and Plaut (1975) have shown that their data is not in agreement with an axial ratio of 0.5. Also, Kinman et. al.'s density at log R ~ 1.3 (from the NGP survey) shows a striking agreement with the densities at that radius derived in this work for the anti-center. This is not possible if the axial ratio is 0.5. These are arguments against an oblate spheroidal model.

In the following section it will be seen that the average value of [Fe/H] in the outer regions of the halo is ~ -1.5, with a large spread ranging from -1 to -2, and that there is no detectable abundance gradient. However, for Galactocentric radii smaller than R ~ 10 kpc, this result is not valid. In fact, abundance measurements by Butler et. al. (1976) show that the average [Fe/H] of RR Lyrae stars in Baade's window (close to the Galactic center) is ~ -0.5. As will be discussed in section 4.4, this difference in average metallicity is a reason why fewer (than expected) RR Lyrae stars are found in the regions closer to the Galactic center, which can qualitatively explain the observed drop in RR Lyrae star density near the Galactic center. To test this hypothesis, the average abundance of the stars that are associated with the lower of the two triangles at log R ~ 0.7 in Fig. 4.3(a) should be compared to the average abundance of the stars associated with the higher triangle at the same Galactocentric radius.

Consider the data points in Fig. 4.3(a) beyond log R ~ 1.0. The lack of a density gradient beyond 10 kpc may be taken to mean that case (2) (discussed above) prevails, and that the populations are well mixed, unless the "second parameter" shows a radial gradient. If case (2) is valid, the run of RR Lyrae star density with Galactocentric radius will be the same as that of the general stellar population. Thus metallicity gradients play no role in in the observed density distribution beyond log R ~ 1.0. With the exception of the triangle at log R ~ 1.3, all the other points have θ greater than 60^{o} but less than 120^{o}, so for these points, the effects of oblateness in the

density distribution are relatively small. Thus Fig. 4.3(a) indicates that beyond R ~ 20 kpc, the density falls off faster than R^{-3}. It has been tacitly assumed in chapter 1, that all RR Lyrae stars with mean magnitudes in the interval 16^m to 19^m are equally likely to be found, when this may not be correct. This can introduce selection effects that produce spurious densities, most probably in the sense that the efficiency of discovery falls at the fainter end. However, to put the data in accordance with an R^{-3} law by adjusting the discovery probability would mean that the discovery probability at a mean magnitude of 18^m is 10 percent or less. Since 18^m is still two magnitudes above the plate limit, such a proposition cannot be entertained, and the change of slope at R = 20 kpc is most likely to be real, at least qualitatively.

It appears that at this time there is insufficient data to model the RR Lyrae star density quantitatively. The results from future surveys should help to clarify the issues, and make a more detailed analysis possible.

4.4 ABUNDANCE GRADIENTS

Figs. 4.4(a) and (b) show the distribution of observed [Fe/H] (as derived in chapter 3) with Galactocentric distance R, and with the distance from the Galactic plane |Z|. It is seen that there is a wide range of abundances at all R and |Z|. All the stars are far enough away from the disk that we may assume that this is a sample of purely

halo stars. No net abundance gradient with R or |Z| is seen.

The results are not surprising. Butler et. al. (1982) have obtained similar results from their abundance measurements of RR Lyrae stars from Kinman's (Kinman et. al. (1982),(1966)) survey. Searle and Zinn (1978) have found the same qualitative result for the globular clusters. Both these works show that [Fe/H] for halo objects ranges from -1 to -2 with no indication of an abundance gradient. However, neither of the above works has found metal rich objects ([Fe/H] $>$ -.6) at R greater than 10 kpc, but II V401 and IV V106 from this survey appear to be metal rich. The spectrum of II V401 is shown in Fig. 3.1 (chapter 3). It is important to confirm the results on these two stars, since only one spectrum of each of these objects has been examined. If these two stars are excluded, the mean abundance is [Fe/H] = -1.52, which is in agreement with what Butler and co-workers have found for stars from the survey by Kinman and co-workers and with the mean from Searle and Zinn.

The abundance distribution is a vital key to an understanding of the origin and evolution of the halo. The lack of an abundance gradient is inconsistent with the galaxy formation models of Larson (1975). Searle and Zinn (1978) and Searle (1977) examined possible scenarios of star formation in the halo that are consistent with the lack of a net abundance gradient and with the wide abundance distribution that they obtained for the globular clusters. Although the data in Butler (1982) and in this work corroborate the findings of Searle and Zinn, the abundance distribution in a sample of RR Lyraes

is not a faithful representation of the abundance distribution in the parent stellar population (Kraft et. al. (1978)). Very metal poor ([Fe/H] < -2.2) stars map the horizontal branch blueward of the instability strip. Similarly (Kraft (1977)), metal rich stars tend to map the horizontal branch redward of the instability strip. Thus there are strong selection effects at both extremities of the metallicity range. Also as pointed out by Kraft et. al. (1978), the extremely metal poor RR Lyrae stars have the longest periods and smallest amplitudes, making them the hardest to find. Unless these selection effects are understood quantitatively, inferences drawn from the observed abundance distribution of RR Lyrae stars must be viewed with appropriate caution.

If II V401 and IV V106 are confirmed to be metal rich stars, it will be a major discovery. According to the selection effects just mentioned, the odds for finding an RR Lyrae star with [Fe/H] greater than -0.6 to that for finding a metal poor star are about 1:200 (Kraft (1977)), so even a single metal rich RR Lyrae star represents a sizable metal rich parent population. The confirmed existence of such a population would place stringent constraints on theoretical models of galaxy formation.

APPENDIX I

The transformation equations from heliocentric to galactocentric coordinates are derived.

Define $\lambda = (l-\pi)$, where l is the Galactic longitude. Referring to Fig. 4.1, the following relationships are apparent:

$SP = r.\sin b$

$CP = r.\cos b$

$CQ = CP.\cos\lambda$

$OQ = R_0 + CQ$

$PQ = CP.\sin\lambda$

$OP^2 = OQ^2 + PQ^2$

$R^2 = OP^2 + SP^2$

$\sin\phi = PQ/OP$

$\tan\phi = PQ/OQ$

$\sin\theta = OP/R$

$\tan\theta = OP/SP$

Note that R and OP are always positive. The above relations define (R,θ,ϕ) uniquely in terms of (r,l,b).

REFERENCES

Butler, D., Carbon, D., and Kraft, R. P. 1976, Ap.J. 210, 120.

Butler, D., Kemper, E., Kraft, R. P., and Sumtzeff, N. B. 1982, A.J. 87, 353.

Kinman, T., Wirtanen, C., and Janes, K. 1965, Ap.J. Suppl. 11, 223.

Kinman, T., Wirtanen, C., and Janes, K. 1966, Ap.J. Suppl. 13, 379.

Kinman, T., Mahaffey, C. T., and Wirtanen, C. A. 1982, A.J 87, 314.

Kraft, R. P. 1977, IAU Colloquium 42, 521.

Kraft, R. P., Trefzger, C. F., and Sumtzeff, N. 1978, IAU Symposium 84, 463.

Larson, R. B. 1975, M.N.R.A.S., 173, 671.

Manduca, A., Bell, R. A., Barnes, T. G., Moffet, T. J., and Evans, D. S. 1981, Ap.J. 250, 312.

McDonald, L. H. 1977, Ph.D. thesis, Univ. of California, Santa Cruz.

Oke, J. B. 1966, Ap.J. 145, 468.

Oke, J. B., and Bonsack, S. J. 1960, Ap.J. 132, 417.

Oke, J. B., Giver, L. P., and Searle, L. 1962, Ap.J. 136, 393.

Oort, J. H., and Plaut, L. 1975, Astron. and Astroph. 41, 71.

Rabin, D. M. 1980, Ph.D. thesis, California Institute of Technology.

Sandage, A. 1981(a), Ap.J. (Letters) 244, L23.

Sandage, A. 1981(b), Ap.J. 248, 161.

Sandage, A. 1982(a), Ap.J. 252, 553.

Sandage, A. 1982(b), Ap.J. 252, 574.

Sandage, A., Katem, B., and Sandage, M. 1981, Ap.J. Suppl., 46, 41.

Searle, L. 1977, in The Evolution of Galaxies and Stellar Populations,
ed. B. M. Tinseley and R. B. Larson (New Haven: Yale University Observatory), p. 219.

Searle, L., and Zinn, R. 1978, Ap.J., 225, 357.

Whitford, A. E. 1959, A.J., 63, 204.

FIGURE CAPTIONS

Fig. 4.1

Illustration of the elements of the Galactocentric coordinates described in section 4.2, and of angles and distances pertinent to the transformation from heliocentric to galactocentric coordinates.

Fig. 4.2(a)

Shows the increase in the total number of RR Lyrae stars found as a function of increasing heliocentric distance, for the anticenter fields FII and FIII taken together.

Fig. 4.2(b)

Shows the increase in the total number of RR Lyraes found as a function of increasing heliocentric distance, for the apex field FIV.

Fig. 4.3(a)

Variation of RR Lyrae star density with Galactocentric distance. Filled circles are for FII and FIII, and open circles are for FIV. Triangles are from Kinman's surveys (see text), and the crosses are from Oort and Plaut (1975).

Fig. 4.3(b)

Variation of RR Lyrae star density with Galactocentric distance, as derived for FII and FIII (filled circles) and for FIV (open circles) using Kinman's method.

Fig. 4.4(a)

The observed values of [Fe/H] for the survey RR Lyrae stars are plotted against their Galactocentric distance R.

Fig. 4.4(b) The observed values of [Fe/H] for the survey RR Lyrae stars are plotted against their distance |Z| from the Galactic disk.

TABLE 4.1
Galactic and Galactocentric Coordinates

OBJECT	r (kpc)	l (deg)	b (deg)	R (kpc)	θ (deg)	ϕ (deg)	Z (kpc)
II V3	5.3	180.06	+25.85	13.7	80.23	0.02	2.3
II V6	23.1	180.44	+23.60	31.3	72.78	0.31	9.3
II V104	17.4	179.74	+24.14	25.6	73.84	-0.71	7.1
II V208	14.3	179.83	+24.87	22.5	74.48	-0.10	6.0
II V306	17.0	182.02	+22.49	25.3	75.07	1.30	6.5
II V401	20.2	179.17	+27.02	28.2	71.02	-0.56	9.2
II V501	10.7	179.30	+26.82	18.9	75.17	-0.37	4.8
II V502	32.5	178.02	+26.28	40.5	69.17	-1.52	14.4
II V504	14.5	177.57	+23.59	22.7	75.20	-1.47	5.8
II V601	19.9	180.33	+22.76	28.1	74.10	0.22	7.7
III V101	13.4	177.58	+30.76	21.3	71.26	-1.38	6.9
III V102	11.1	176.55	+29.76	19.1	73.26	-1.81	5.5
III V103	33.1	181.08	+29.41	40.9	66.57	0.83	16.3
III V201	11.0	182.33	+27.25	19.2	74.74	1.23	5.0
III V202	13.0	176.86	+29.10	21.0	72.49	-1.78	6.3
III V203	28.2	177.89	+28.05	36.1	68.44	-1.56	13.3
III V204	14.7	181.24	+28.37	22.7	72.09	0.74	7.0
III V206	18.1	177.74	+31.85	25.9	68.34	-1.44	9.6
III V208	16.0	179.56	+29.83	23.9	70.57	-0.27	8.0
III V302	16.7	177.64	+30.93	24.6	69.54	-1.47	8.6
IV V103	11.7	110.44	-31.60	16.5	111.77	-37.47	-6.1
IV V104	22.9	108.56	-32.15	26.6	117.27	-51.02	-12.2
IV V105	24.1	106.17	-30.52	27.5	116.41	-54.01	-12.2
IV V106	15.3	106.62	-30.97	19.4	113.99	-45.27	-7.9
IV V107	21.6	109.54	-29.77	25.5	114.85	-49.73	-10.7
IV V108	12.5	112.06	-29.90	17.4	110.98	-38.18	-6.2
IV V201	14.2	111.93	-30.45	18.9	112.39	-40.55	-7.2
IV V301	13.5	112.92	-31.24	18.3	112.45	-38.86	-7.0
IV V401	11.1	111.21	-32.52	16.1	111.83	-35.83	-6.0

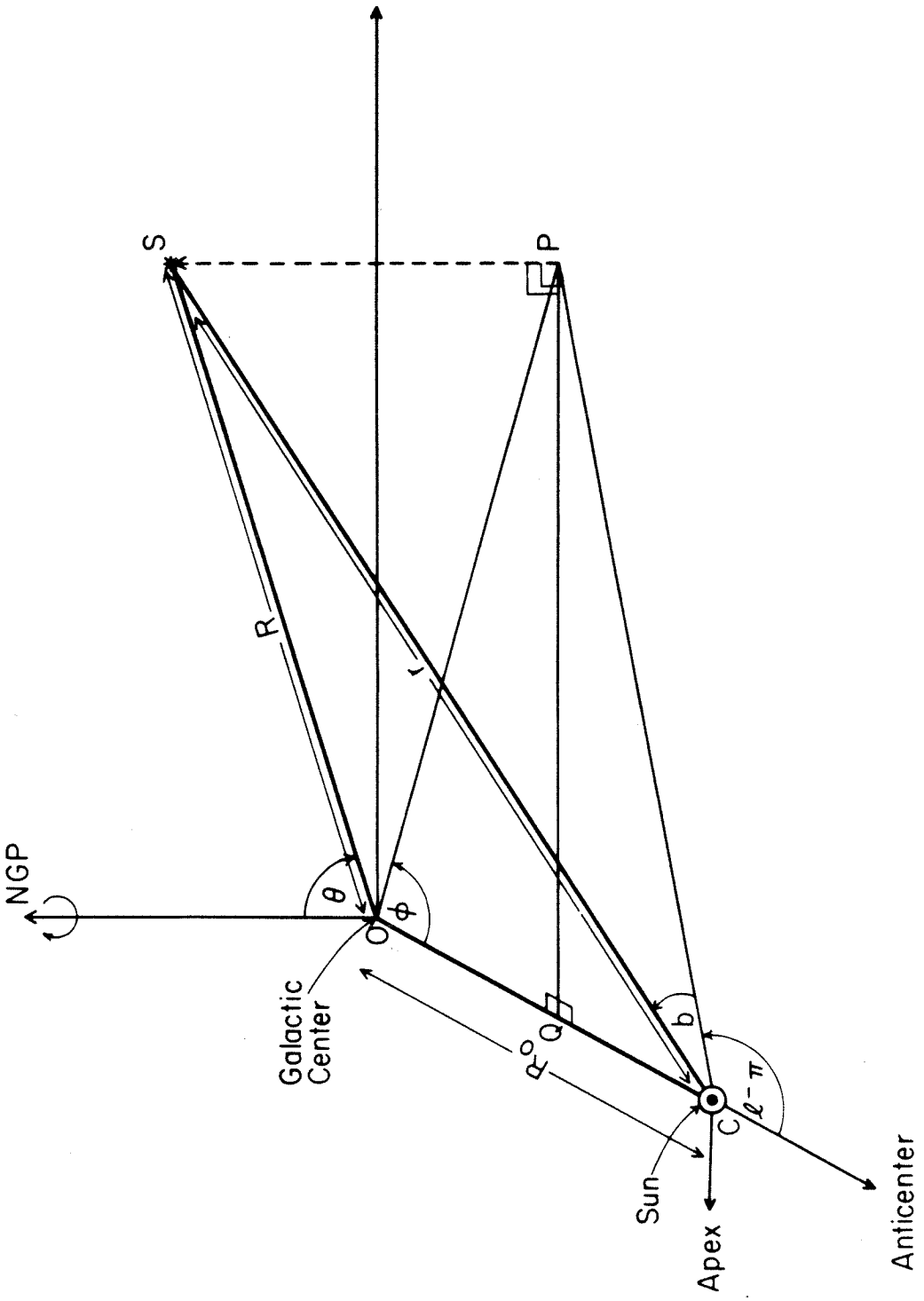

Fig. 4.1

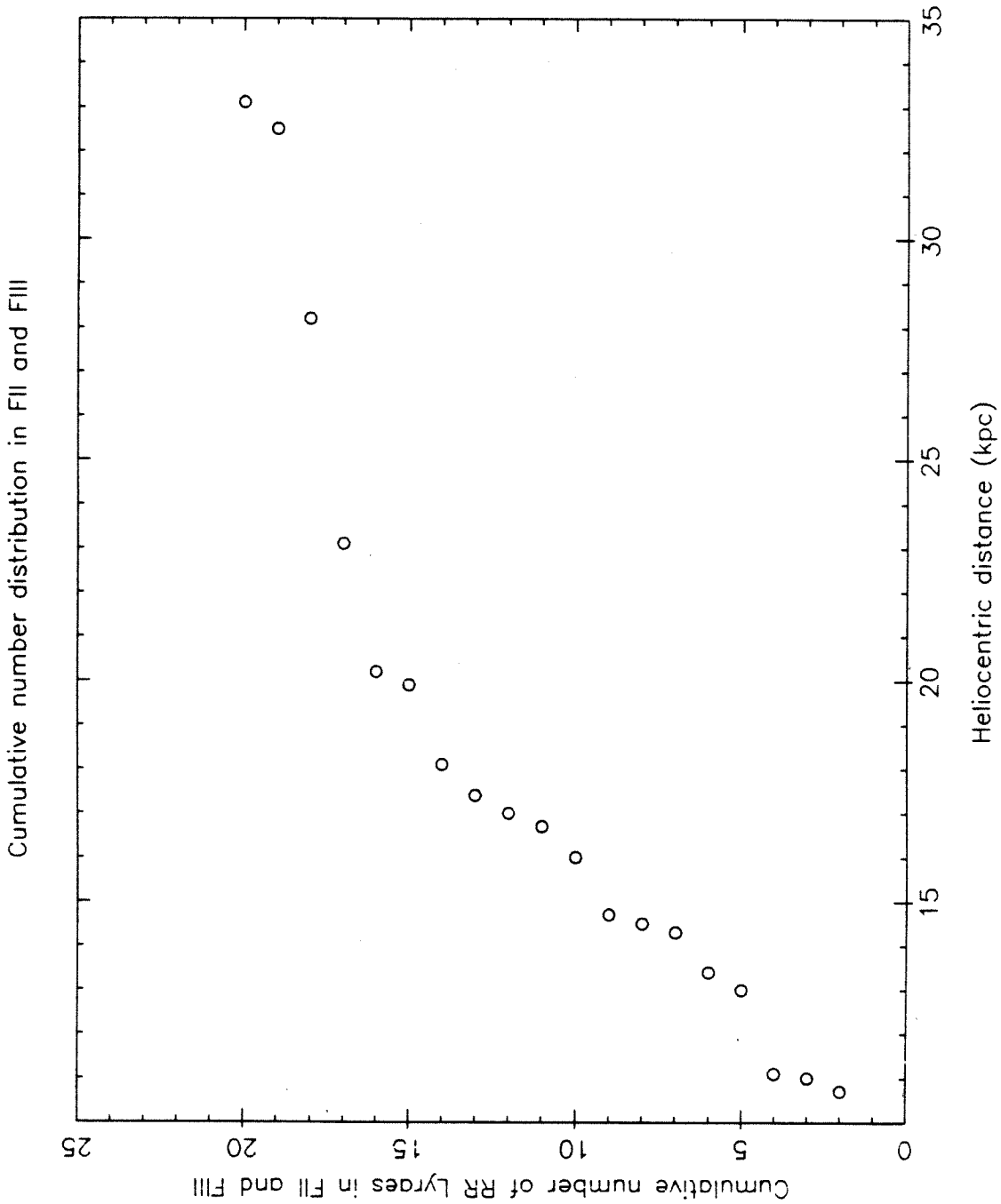
Cumulative number distribution in FII and FIII
Heliocentric distance (kpc)
Cumulative number of RR Lyraes in FII and FIII
0
5
10
15
20
25
15
20
25
30
35

Fig. 4.2(a)

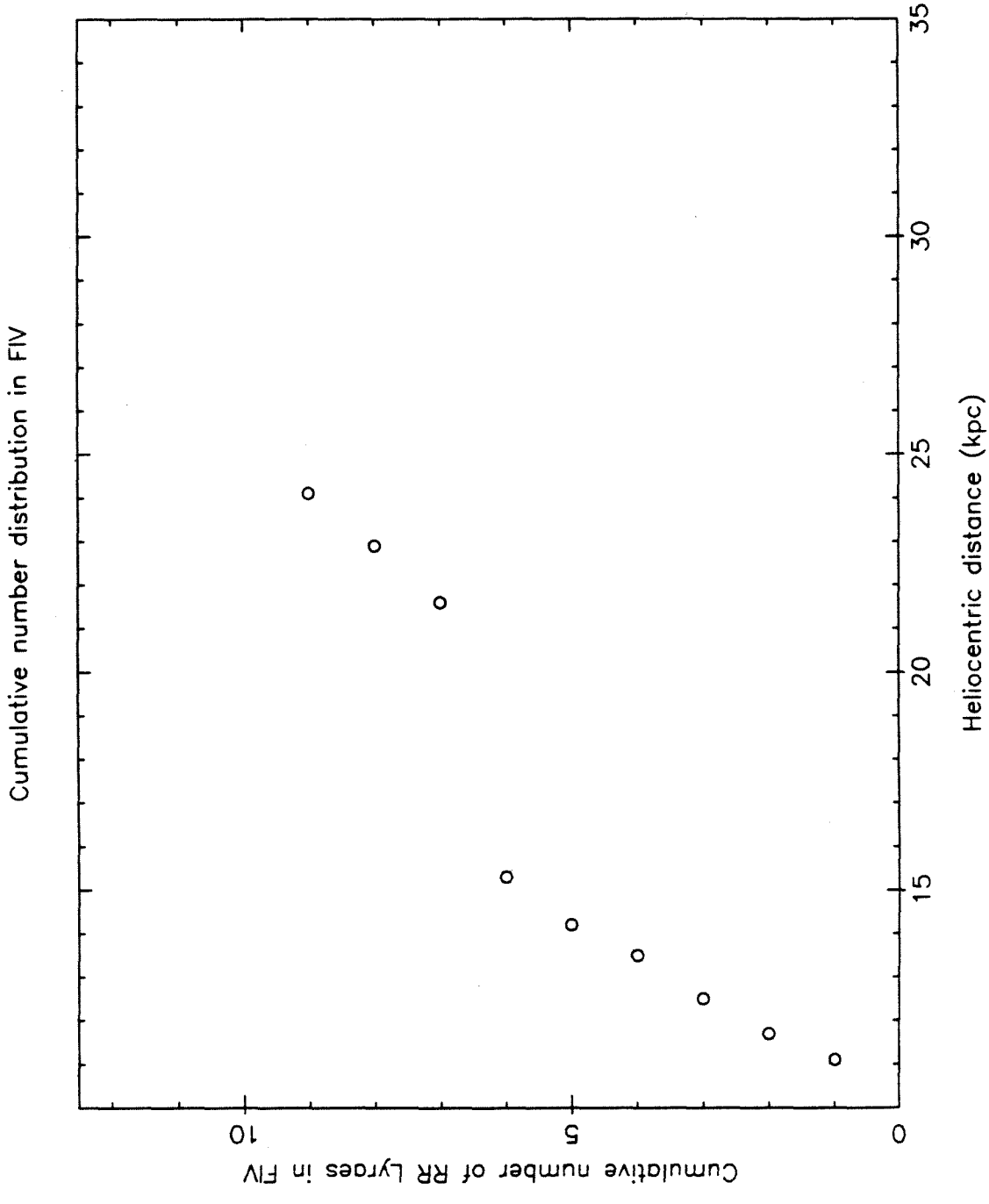
Cumulative number distribution in FIV
Heliocentric distance (kpc)
Cumulative number of RR Lyraes in FIV
0
5
10
15
20
25
30
35

Fig. 4.2(b)

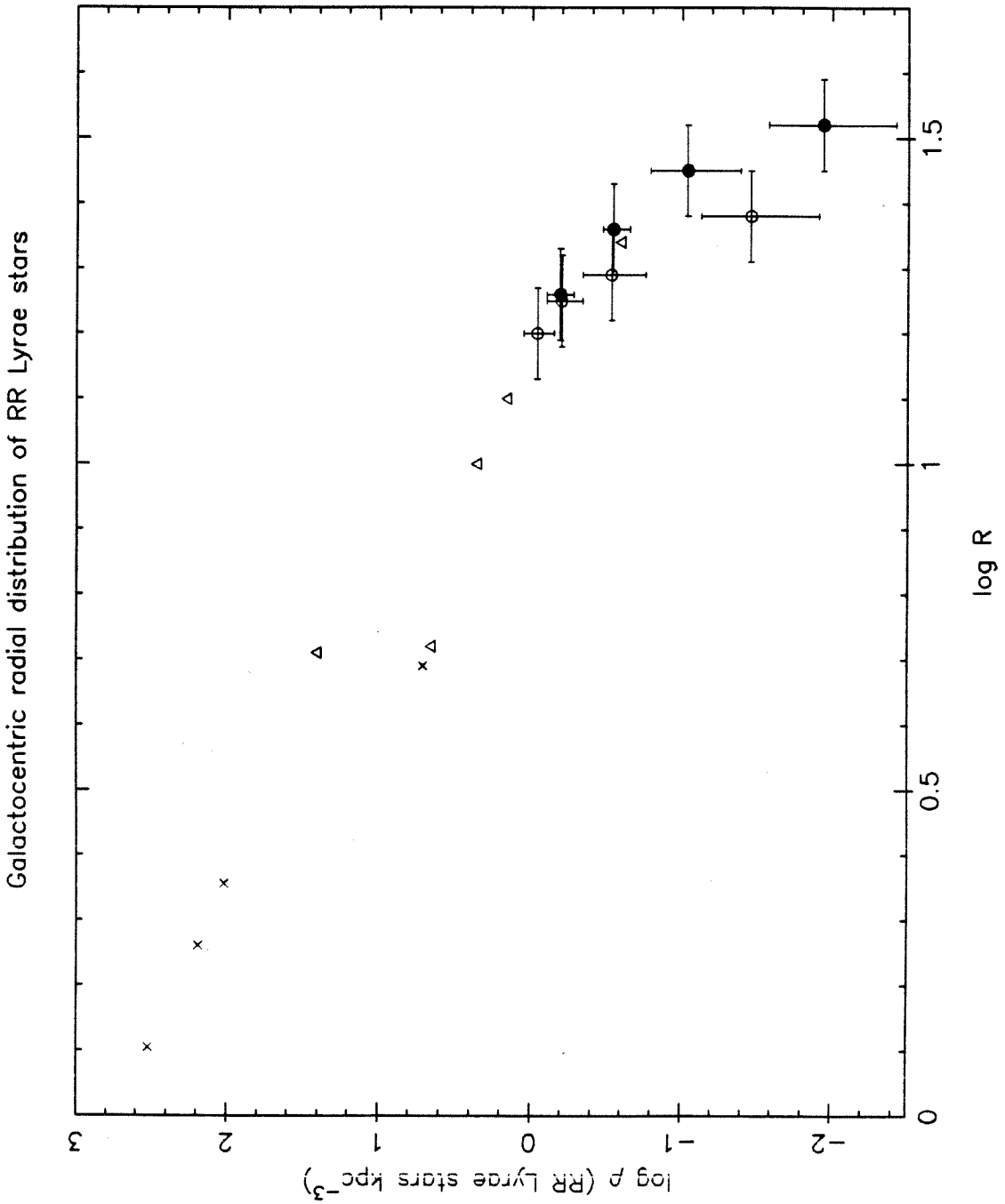
Galactocentric radial distribution of RR Lyrae stars
log ρ (RR Lyrae stars kpc⁻³)
log R
3
2
1
0
-1
-2
0
0.5
1
1.5

Fig. 4.3(a)

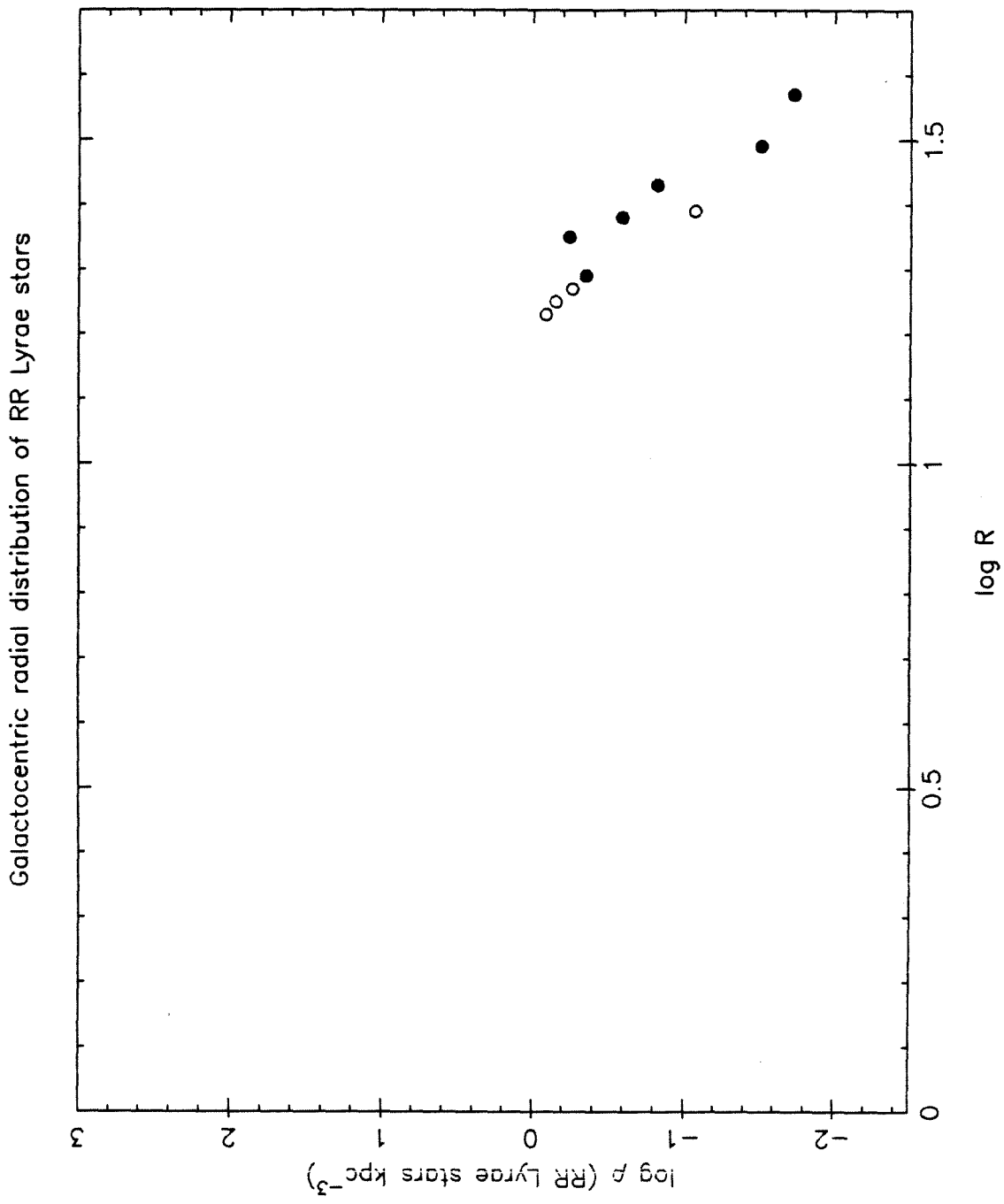
Galactocentric radial distribution of RR Lyrae stars
log ρ (RR Lyrae stars kpc^{-3})
log R
3
2
1
0
−1
−2
0
0.5
1
1.5

Fig. 4.3(b)

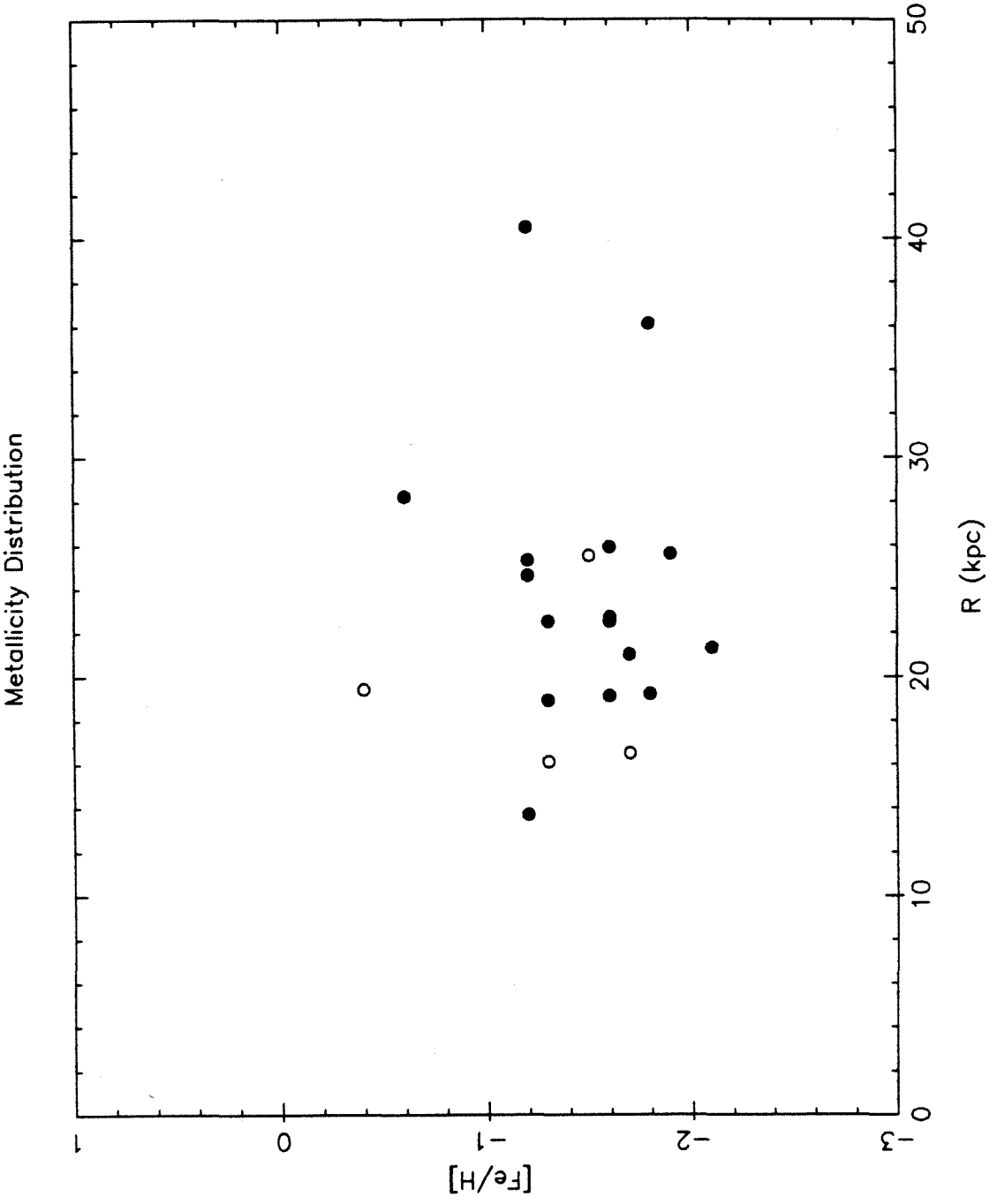

Fig. 4.4(a)

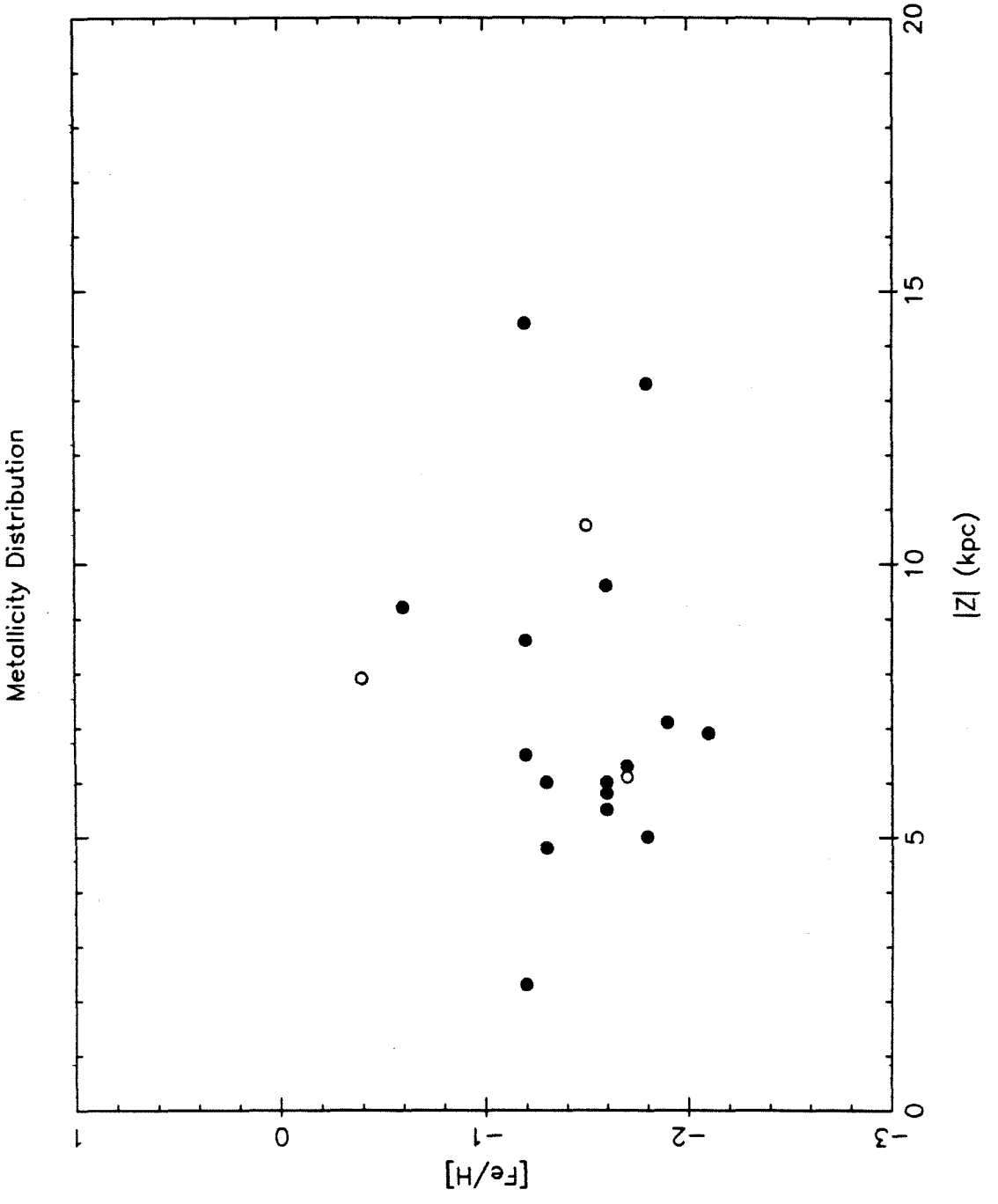

Fig. 4.4(b)

CHAPTER 5

KINEMATICS OF THE HALO RR LYRAES AND THE MASS OF THE GALAXY

5.1 SYSTEMIC MOTION

In analyzing the motions of the survey RR Lyrae stars, spherical symmetry will be assumed. The velocity ellipsoid at any point in the halo is assumed to have one of its axes along the line to the galactic center and the other two axes are assumed to be along the altitudinal and azimuthal directions. In other words, in the coordinate system defined in section 4.1, the axes lie along R, Θ and ϕ. The observer sees the velocity ellipsoid projected along the line of sight. Define the angle ϕ such that $\cos\phi$ is the projection of a unit line of sight vector $\tilde{r}$ along $\tilde{R}$ (see Fig. 5.1). Define the angle ξ (see Fig. 5.1) such that $(\sin\phi.\cos\xi)$ is the projection of the unit line of sight vector in the Θ direction, and $(\sin\phi.\sin\xi)$ is the projection of the same in the ϕ direction. For convenience, denote $(l-\pi)$ by λ, where l is the Galactic longitude.

$$\cos\phi = (r^2+R^2-R_0^2)/(2rR) \qquad (5.1)$$

$$\text{and } \sin^2\phi = 1 - \cos^2\phi \qquad (5.2)$$

Since ϕ can take values from 0 to π, $\sin\phi$ is always positive or zero.

$$\sin\xi = (\cos b.\sin\lambda.\cos\phi - \cos\lambda.\cos b.\sin\phi)/\sin\phi \qquad (5.3)$$

$$\cos\xi = (\cos\lambda.\cos b.\cos\theta.\cos\phi + \cos b.\sin\lambda.\cos\theta.\sin\phi - \sin b \sin\theta)/\sin\phi \qquad (5.4)$$

Let the systemic velocity along R, θ and ϕ be denoted by U, W and V respectively, Assume U, W and V to be constant everywhere in the halo. Since nothing is definitely known about the halo systemic motion, this assumption will suffice unless it becomes apparent that it is wrong. Let the random or peculiar velocity components of a star along R, θ and ϕ be u, w and v respectively. Note that V is in the opposite sense of galactic rotation in the right-handed coordinate system used here. All velocities will be expressed in units of km/s, unless otherwise stated. The peculiar velocity of the Sun with respect to the LSR is $-9\tilde{e} + 7\tilde{f} - 12\tilde{g}$, where $\tilde{e}$, $\tilde{f}$ and $\tilde{g}$ are the local unit vectors along R, θ and ϕ respectively (Mihalas and Binney (1981)). The velocity of the LSR is taken to be $-220\tilde{g}$ (Gunn, Knapp and Tremaine (1979)).

The observed velocity of a star, V_{obs} is given in terms of the above defined quantities by the following relation:

$$V_{obs} = (U+u).\cos\phi + (W+w).\sin\phi.\cos\xi + (V+v).\sin\phi.\sin\xi - [-9\cos b.\cos\lambda - 232\cos b.\sin\lambda + 7\sin b] \qquad (5.5)$$

Define $V_{corr} = [\,-9\cos b.\cos\lambda - 232\cos b.\sin\lambda + 7\sin b]$

V_{corr} is the projection along the line of sight (to an object) of the

velocity of the Sun in a non-rotating frame comoving with the Galactic center.

Also define $V_f = V_{obs} + V_{corr}$

so that V_f is line of sight projection of the velocity of the observed object as seen from a non-rotating frame that is comoving with the Galactic center, and we have:

$$V_f = (U+u).\cos\phi + (W+w).\sin\phi.\cos\xi + (V+v).\sin\phi.\sin\xi \qquad (5.6)$$

Table 5.1 lists $\sin\phi$, $\cos\phi$, $\sin\xi$ and $\cos\xi$ for all the objects for which radial velocities have been obtained. Notice that in the anticenter fields FII and FIII, all the objects (with the exception of II V3 which is a relatively nearby object) have $\cos\phi$ of 0.98 or 0.99. Also, for these objects, $\sin\xi$ is essentially zero. We assume that any systemic halo rotation is about an axis coincident with the rotation axis of the disk, i.e. that $W = 0$. The mean value $\langle V_f \rangle$ for the anticenter objects (denoted by $\langle V_f \rangle_{a-c}$) is then given by:

$$\langle V_f \rangle_{a-c} = U\langle\cos\phi\rangle = 0.99U \qquad (5.7)$$

This gives the systemic expansion velocity of the halo. From the stars in the anticenter for which we have radial velocities, a value of 46 $\pm$32 km/s is obtained for the systemic expansion velocity U. There have been attempts to discern systemic expansion or contraction

in the system of globular clusters. Kinman (1959), derived a systemic contraction proportional to galactocentric distance with a rate of $1.48 \pm .85$ km s^{-1} kpc^{-1}. Clube and Watson (1979) obtained a systemic velocity of ~60 km s^{-1} for 29 globular clusters. Frenk and White (1980) have noted that the the apparent systemic motions are linked to cluster position and that the significance of these results is not clear. Pier (1982) found no statistically significant expansion velocity from a sample of 171 relatively nearby halo A type horizontal branch stars. It is clear from this work that radial velocity measurements of additional RR Lyrae stars along $l = 180^{o}$ from Kinman et. al.'s (1982) survey should give more statistically meaningful results. Further surveys at other points along the meridional plane of $l = 180^{o}$ are also desirable.

$\langle V_f \rangle$ for the FIV field (or apex field) is given by :

$$\langle V_f \rangle_{apex} = U\langle \cos\phi \rangle + V\langle \sin\xi . \sin\phi \rangle \qquad (5.8)$$

Since U is known from the previous analysis, the systemic rotation velocity V can be obtained from (5.8). $V\langle \sin\xi . \sin\phi \rangle$ was found to be -71 ± 60 km s^{-1}, so that V is 178 ± 148 km s^{-1}, which is of no statistical significance. When radial velocities from all the RR Lyrae stars in this survey are obtained, it will be possible to determine V to an accuracy of 90 km s^{-1}. A large part of the uncertainty in this result is because the uncertainty in U propagates through the determination of V. The projected survey of RR Lyrae stars in field FV (see Table 1.1) will eliminate U in the calculation

of V, and an accuracy of ~40 km s^{-1} in V can be attained from a sample of 20 stars from fields FIV and FV. The solar motion with respect to these distant halo stars can be obtained to an accuracy of ~20 km s^{-1} when such a survey is completed.

5.2 VELOCITY DISPERSIONS

Define

$$V_s = V_f - U\cos\phi - W\sin\phi.\cos\xi - V\sin\phi.\sin\xi \qquad (5.9)$$

Thus V_s is the line of sight projection of the peculiar velocity of an object (this is independent of the frame of reference). From equations (5.6) and (5.9),

$$V_s = u\cos\phi + w\sin\phi.\cos\xi + v\sin\phi.\sin\xi \qquad (5.10)$$

Since $\langle u\rangle = \langle w\rangle = \langle v\rangle = 0$ by definition, $\langle V_s\rangle = 0$. Also, since u, w and v are mutually independent, we can write

$$\langle V_s^2\rangle = \langle u^2\cos^2\phi\rangle + \langle w^2\sin^2\phi.\cos^2\xi\rangle + \langle v^2\sin^2\phi.\sin^2\xi\rangle \qquad (5.11)$$

Assume that the two transverse axes of the velocity ellipsoid (i.e. perpendicular to $\tilde{R}$) are equal, so that $\langle w^2\rangle = \langle v^2\rangle = \sigma_t^2$, and denote $\langle u^2\rangle$ by σ_R^2. Then,

$$\langle V_s^2\rangle = \sigma_R^2\langle\cos^2\phi\rangle + \sigma_t^2\langle\sin^2\phi\rangle \qquad (5.12)$$

For FIV we find:

$$\langle V_s^2 \rangle^{1/2}_{apex} = 93 \pm 33 \text{ km s}^{-1},$$

and at the anticenter,

$$\langle V_s^2 \rangle^{1/2}_{a-c} = 112 \pm 21 \text{ km s}^{-1}.$$

The random errors associated with the measurement of individual velocities makes a contribution to the dispersion. The above values have been corrected for such a contribution. Using (5.12) and the appropriate direction terms, we can estimate $\sigma_t^2/\sigma_R^2 = q$. It is seen that q lies between 0 and 4.75 to within the ninety-five percent confidence limit generated by the errors in the $\langle V_s^2 \rangle^{1/2}$'s. This rules out the possibility of circular orbits, but it does not allow us to pinpoint a value for q within the expected interval from 0 (radial orbits) to 1 (isotropic orbits). Determination of the velocity ellipsoid at large galactocentric distances is difficult because the $\cos^2\phi$ term in equation (5.12) is never small, and we get no leverage on the transverse axes of the ellipsoid. The two directions used in this analysis are the best suited for this calculation, yet even they yield no useful answers.

5.3 THE MASS OF THE GALAXY

The mass distribution in the Galaxy can be deduced from the kinematical data derived above. The line of analysis that Hartwick and Sargent (1978) used for the globular cluster system is particularly appropriate for this purpose. Following Hartwick and Sargent, it is assumed that at the large galactocentric radii under consideration, the gravitational potential is spherically symmetric. The system of RR Lyrae stars is considered to be a collisionless fluid, to which the collisionless Boltzmann equation may be applied. Their expression for the mass M(R) within a galactocentric radius R has been modified to allow for streaming motions in the radial direction, and reads as follows:

$$M(R) = \frac{R}{G}\left[\{(\overline{U^2}+\sigma_R^2)\}.\{-d\ln\rho/d\ln r - d\ln(\overline{U^2}+\sigma_R^2)/d\ln r\}\right.$$

$$\left. + \{\overline{V^2} + (2q-2)\sigma_R^2 - 2\overline{U^2}\}\right] \qquad (5.13)$$

where ρ is the number density distribution of RR Lyrae stars.

The anticenter RR Lyrae stars were split into two groups, those with R less than 22 kpc, and those that are more distant. No significant difference was seen in the velocity dispersions of these subsamples. Also, we have no information on the run of $\overline{U^2}$ with radial

distance, and so ignore it, so that $d\ln(U^2+\sigma_R^2)/d\ln R$ is taken to be zero. Fig. 4.3 supplies $d\ln\rho/d\ln R$. U and V have been derived in section 5.1. σ_R^2 depends formally on the value of q. Since q cannot be determined, two cases are considered: one where the peculiar velocities are radial, and the other where they are isotropic. These cases correspond to q=0 and q=1 respectively.

Define V_d so that

$$V_d^2 = V_s^2 - \varepsilon^2 \tag{5.14}$$

where ε is the standard error in the measurement of V_{obs}. $\langle V_d^2 \rangle$ then gives the true line of sight velocity dispersion.

In the case of radial orbits, σ_R^2 is calculated using the following expression:

$$\sigma_R^2 = \langle V_d^2/\cos^2\phi \rangle \tag{5.15}$$

From the combined data from both the anticenter and apex fields, it is seen that σ_R is 107 $\pm$17 km s^{-1} if radial orbits are assumed. For the isotropic case, σ_R^2 is simply equal to $\langle V_d^2 \rangle$, and the result for σ_R is 104 $\pm$17 km s^{-1}.

For the case of isotropic orbits (q=1), $M_G(25)$ the mass of the Galaxy within 25 kpc is found from the above to be 3.9(+3.4 or -2.2) $\times 10^{11} M_\odot$. While estimating errors, care was taken to account for terms in equation (5.13) where the errors correlate. For example, U

and u are always interdependent, and U, V and u are all interlinked for the objects in FIV. A major contribution to the errors arises from the uncertainty in V. Since |V| can never be negative, the lower and upper error bounds are different. For the case of radial orbits, $M_G(25)$ is $2.6(+3.1 \text{ or } -1.9) \times 10^{11} M_\odot$. From the rotation curve at R_0, Schmidt (1965) has obtained $M(R_0) = 0.9 \times 10^{11} M_\odot$ for a model where all the mass is in the disk. This is the minimum possible mass at R_0 (ellipsoidal or spherical mass distributions require a higher mass to explain the rotation curve). The lower limit of the estimate of $M_G(25)$ for the case of radial orbits lies well below the minimum allowable mass at R_0, so the lower limit is disallowed although the most probable value of $2.6 \times 10^{11} M_\odot$ is perfectly acceptable. Since the lower limit corresponds to the case where |V| is zero, the argument can be inverted to say that |V| cannot be zero and must be at least 34 km/s if the orbits are radial.

The results obtained here are consistent with the results of Hartwick and Sargent (1978) and of Frenk and White (1980). For the case of isotropic orbits, Hartwick and Sargent obtained $d\ln M_G(R)/d\ln R \sim 1$. The value of $M_G(25 \text{ kpc})$ obtained in this work for isotropic orbits agrees very well with their values of M_G at 5.6, 11 and 61 kpc and the above-mentioned logarithmic slope.

In the above calculations it has been assumed that at large Galactocentric distances the gravitational potential is spherical. The results can be expressed instead in terms of an "equivalent circular velocity" i.e. the velocity an object would have if it were

moving in a circular orbit. Of course, objects that are off the plane of the Galaxy cannot move in strictly circular orbits if the potential is non-spherical, but we ignore this for the present. The equivalent circular velocity Θ_C is the total of the terms within the square brackets in equation (5.13). The value of Θ_C corresponding to the case of isotropic orbits is 260 (+225 or -145) km/s, and that corresponding to the case of radial orbits is 150 (+178 or -110) km/s.

It is tempting to compare these results against recent mass models and test their predictions about a massive halo. However, the uncertainties in the results of this work are too large to admit any definitive conclusions. These uncertainties can be significantly reduced by a better determination of the rotation velocity V. Further surveys for halo RR Lyrae stars should address this problem. The proper determination of this quantity alone will improve the mass estimates significantly. As mentioned before, it is virtually impossible to derive a useful estimate of q for distant halo objects because of the geometry involved, unless an extremely large number of objects (several hundred) are studied. This is unfortunate, since the estimate of M_G depends rather heavily on the assumed value of q. The axial ratio estimates for the velocity ellipsoids of relatively nearby halo objects differ. Woolley (1978) noted a marked anisotropy in the velocity ellipsoid of the brighter halo RR Lyrae stars. These are all within a few kpc of the Galactic disk. Woolley's results show no statistically significant difference between $\langle u^2 \rangle$ and $\langle v^2 \rangle$, but $\langle w^2 \rangle$ is significantly smaller ($\langle u^2 \rangle$:$\langle w^2 \rangle$ of 3:1). Pier (1982) has noted a milder anisotropy ($\langle u^2 \rangle$:$\langle w^2 \rangle$ of 3:2) in his sample of blue halo

horizontal branch stars. Frenk and White (1980) have seen no evidence for unequal axes in the velocity ellipsoid of globular clusters, which are at larger distances than Woolley's RR Lyrae stars or Pier's blue horizontal branch stars. They are able to rule out the possibility of radial orbits for globular clusters. The anisotropy seen by Woolley and by Pier may be a local effect, perhaps due to the gravitational influence ot the disk, or it may be global. This is one uncertainty that will not be resolved unless several hundreds of distant halo stars are observed, and sets a limit on how accurately the mass of the Galaxy is likely to be determined in the foreseeable future.

REFERENCES

Clube, S. V. M., and Watson, F. G. 1979, M.N.R.A.S., 187, 863.

Frenk, C. S., and White, S. D. M. 1980 M.N.R.A.S., 193, 295.

Gunn, J. E., Knapp, G. R., and Tremaine, S. D. 1979, A.J., 84, 1181.

Hartwick, F. D. A., and Sargent, W. L. W. 1978, Ap.J, 221, 512.

Kinman, T. D. 1959, M.N.R.A.S., 119, 559.

Kinman, T. D., Mahaffey, C. T., and Wirtanen, C. A. 1982, A.J., 87, 314.

Mihalas, D., and Binney, J. 1981, Galactic Astronomy, (2d ed.; San Francisco: W. H. Freeman).

Pier, J. R. 1982, Ph.D. Thesis, California Institute of Technology.

Schmidt, M. 1965, in Galactic Structure, ed. A. Blauw and M. Schmidt (Chicago: University of Chicago Press), p.513.

Woolley, R. 1978, M.N.R.A.S., 184, 311.

FIGURE CAPTION

Fig. 5.1

The angles ϕ and ξ are defined with respect to the Galactocentric coordinates R, Θ and ϕ.

TABLE 5.1

Projection Angles for Determination of Velocity Components

OBJECT	R (kpc)	$\sin\phi$	$\cos\phi$	$\sin\xi$	$\cos\xi$
II V3	13.7	.28	.96	0.00	-1.00
II V104	25.6	.14	.99	-.01	-1.00
II V208	22.5	.16	.99	-.01	-1.00
II V306	25.3	.13	.99	.09	-1.00
II V401	28.2	.14	.99	-.03	-1.00
II V501	18.9	.21	.98	-.03	-1.00
II V502	40.5	.10	1.00	-.08	-1.00
II V504	22.7	.15	.99	-.10	-0.99
III V101	21.3	.21	.98	-.08	-1.00
III V102	19.1	.23	.97	-.11	- .99
III V201	19.2	.21	.98	.08	-1.00
III V202	21.0	.20	.98	-.10	- .99
III V203	36.1	.11	.99	-.07	-1.00
III V206	25.9	.18	.98	-.07	-1.00
III V302	24.6	.18	.98	-.07	-1.00
IV V103	16.5	.50	.87	-.90	.44
IV V106	19.4	.44	.90	-.93	.37
IV V107	25.5	.33	.95	-.94	.34
IV V401	16.1	.52	.86	-.89	.46

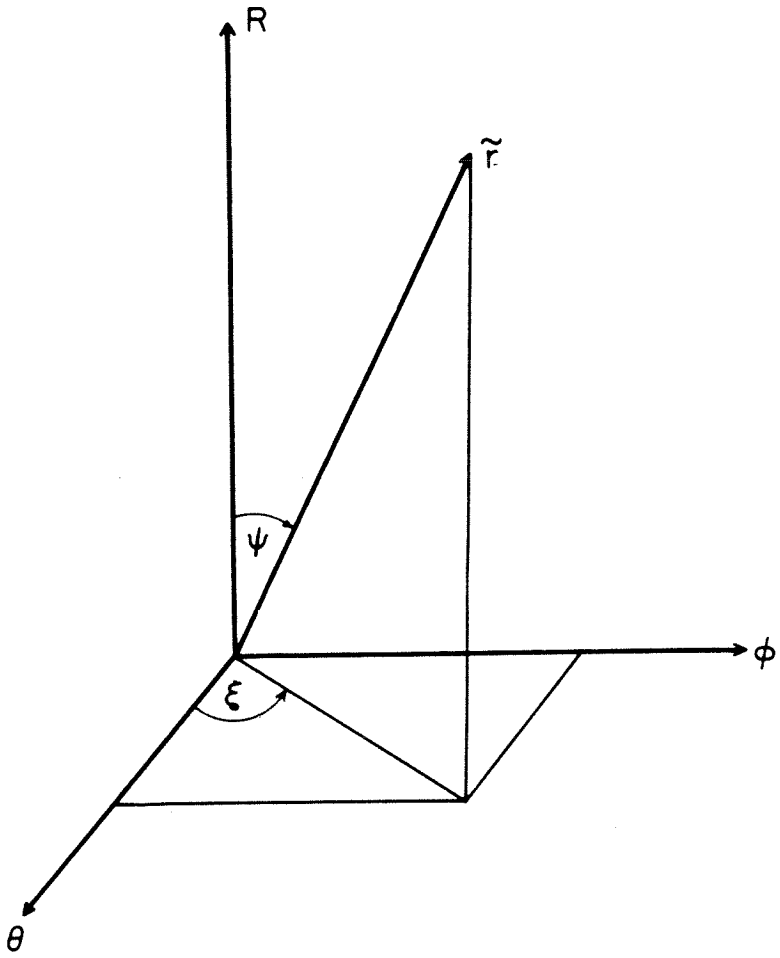

Fig. 5.1

CONCLUSIONS AND SUMMARY

From this survey, 29 RR Lyrae stars were found in the Galactocentric distance range of 13 to 41 kpc. More than two-thirds of these are at Galactocentric distances greater than 20 kpc. Aside from a very few globular clusters, these stars are the most distant known probes of the outer halo.

Photoelectric photometry has been used to obtain accurate light curves and ephemerides for these stars. Chemical abundances and radial velocities of many of them have been derived from spectroscopy. Up-to-date methods of data analysis have been developed and used.

Space densities of RR Lyrae stars out to 33 kpc from the Galactic center have been derived. Using this information in conjunction with similar data obtained by others in the relatively nearby halo and in the Galactic bulge, we obtain a view of the run of space densities over a very wide range of Galactocentric radius R.

The data on abundances show that there is no discernible abundance gradient in the halo from 10 to 40 kpc, but that there is a very wide range of abundances to be found. These results corroborate the findings of other investigators who have studied globular clusters and other halo RR Lyrae stars. Two RR Lyrae stars with [Fe/H] ~0.5 have been found. These are 7 or 8 kpc away from the Galactic disk, and at Galactocentric distances of 20 and 28 kpc. Such high metallicity is unprecedented for halo objects at these Galactocentric

distances. Their presence indicates a sizeable population of moderately metal rich stars in the outer halo.

The observed radial velocities have been used to obtain systemic and random motions (velocity dispersion) of the system of RR Lyrae stars in the distant halo. Although these results should be improved by finding and studying more such stars, it has been possible to obtain an estimate of the mass of the Galaxy within 25 kpc, which indicates that the Galactic mass continues to increase out to this distance. The results obtained here are consistent with those obtained by others from the system of globular clusters.

It is possible to find many more RR Lyrae stars, and at even greater distances, whereas the globular clusters are nearly all known. Further work in this direction holds great promise. A better understanding of abundance distribution in the halo will be forthcoming, as will more accurate estimates of the mass and density distribution in the outer regions of the Galaxy.